PUBLICATION NO. 48 2/2013

NORDIC CONCRETE RESEARCH

EDITED BY
THE NORDIC CONCRETE FEDERATION

CONCRETE ASSOCIATIONS OF: DENMARK
FINLAND
ICELAND
NORWAY
SWEDEN

PUBLISHER: NORSK BETONGFORENING
POSTBOKS 2312, SOLLI
N - 0201 OSLO
NORWAY

VODSKOV, DECEMBER 2013

Preface

Nordic Concrete Research is since 1982 the leading scientific journal concerning concrete research in the five Nordic countries, e.g., Denmark, Finland, Iceland, Norway and Sweden. The content of Nordic Concrete Research reflects the major trends in the concrete research.

Nordic Concrete Research is published by the Nordic Concrete Federation which also organizes the Nordic Concrete Research Symposia that have constituted a continuous series since 1953 in Stockholm. The Symposium circulates between the five countries and takes normally place every third year. The next symposium, no. XXII, will be held Reykjavik, Iceland 13 - 15 August 2014, in parallel with the ECO-CRETE conference. More information on the research symposium can be found on the webpage of the Nordic Concrete Federation; www.nordicconcrete.net as well as on www.rheo.is. Deadline for submitting papers for the Symposium is 1st of March 2014.

Since 1982, 401 papers have been published in the journal. Since 1994 the abstracts and from 1998 both the abstracts and the full papers can be found on the Nordic Concrete Federation's homepage: www.nordicconcrete.net. The journal thus contributes to dissemination of Nordic concrete research, both within the Nordic countries and internationally. The abstracts and papers can be downloaded for free.

The high quality of the papers in NCR are ensured by the group of reviewers presented on the last page. All papers are reviewed by three of these, chosen according to their expert knowledge.

Since 1975, 76 Nordic Miniseminars have been held – it is the experience of the Research Council of the Nordic Concrete Federation, that these Miniseminars have a marked influence on concrete research in the Nordic countries. In some cases, the information gathered during such Miniseminars has been used as Nordic input to CEN activities. The latest Miniseminar concerning Alkali Silica Reactions was held in Riga in an attempt to involve the Baltic countries in our Nordic activities.

We look forward to welcome You to the XXII Nordic Concrete Research Symposium in Reykjavik 13. - 15. August 2014.

Vodskov, December 2013

Dirch H. Bager
Editor, Nordic Concrete Research

Reykjavik, December 2013

Olafur H. Wallevik
Chairman, Research Council of the Nordic Concrete Federation &
Chairman of the Organizing Committee for the XXII Research Symposium

PUBLICATION NO. 48 2/2013

CONTENTS

Influence of curing temperature and maturity on chloride permeability of concrete containing fly ash or slag

Martin Kaasgaard
M.Sc., Consultant
Concrete Centre
Danish Technological Institute
Gregersensvej
DK-2630 Taastrup
mkaa@teknologisk.dk

Claus Pade
M.Sc., Team Leader
Concrete Centre
Danish Technological Institute
Gregersensvej
DK-2630 Taastrup
cpa@teknologisk.dk

ABSTRACT

The resistance to chloride ingress of concrete with water to cement ratio equal to 0.40 was investigated. Concretes containing fly ash or blast furnace slag were compared to pure Portland cement concrete. The concretes were cured immersed in water at different temperatures ranging from 10 to 60 °C. Chloride migration and diffusion coefficients were determined at similar maturities, ranging from 28 to 180 maturity days. It was found that the resistance to chloride ingress of blast furnace slag cement concrete was generally very good at all temperatures and maturities. For the ordinary Portland cement concrete, the resistance to chloride ingress decreased as a function of curing temperature for temperatures above 30 °C. For the fly ash concrete, the resistance to chloride ingress increased as a function of curing temperature throughout the temperature range investigated. The chloride migration coefficient at 28 maturity days was a factor 10 lower for the fly ash concrete cured at 60 °C compared to the fly ash concrete cured at 10 °C.

Keywords: concrete maturity, curing temperature, chloride permeability, fly ash, slag

1. INTRODUCTION

Durability of concrete structures is an area of constant focus and the demands for service life, and hence durability, of new concrete structures increases constantly. For reinforced concrete structures exposed to marine environment or de-icing salts, resistance against chloride ingress is a key property with regards to durability [1]. Chloride induced reinforcement corrosion is fundamentally related to the reinforcement steel, but the effects on the concrete structure are critical with resulting delamination and loss of mechanical properties. The governing factors

concerning chloride induced reinforcement corrosion are related to the concrete properties and the exposure environment (chloride concentration, temperature, humidity, oxygen availability), and furthermore the thickness of the concrete cover to reinforcement is an important factor.

The most common approach to prevent or rather delay the deterioration due to chloride induced reinforcement corrosion is to prevent the chlorides from reaching the reinforcement. This is achieved through specifying an appropriate cover to reinforcement and by using a relatively impenetrable concrete [1]. The latter is related to the permeability of the concrete, which is fundamentally governed by the porosity. However, permeability is not only determined by the total porosity, but also pore size distribution and interconnectivity of pores. Furthermore, permeability is not a property that is constant in time, but a dynamic property, that changes as the concrete hydration proceeds and the hydration products fill the space originally occupied by water. Hence, the permeability is governed by the powder combination used, i.e. Portland cement and supplementary cementitious materials (SCM) such as fly ash, silica fume and blast furnace slag, the water/cement ratio, the degree of hydration and the curing conditions of the concrete. Finally, the capacity of the hydration products to bind chlorides can also affect the resistance against chloride ingress, as only "free" chlorides in the pore solution can move [1].

In both [2] and [3] the influence of fly ash, silica fume and slag on chloride ingress in concrete cured at room temperature and 37/38 °C respectively and at different humidity was investigated. It was found that both moist curing and addition of SCM improved the resistance towards chloride ingress. Furthermore it was found that curing at 38 °C and 65 % relative humidity decreased the resistance towards chloride ingress compared to moist curing at room temperature.

In [4] the microstructure of ordinary Portland cement (OPC) paste hydrated at 5, 20 and 50 °C to 30 and 70 % degree of hydration was investigated. It was found that the elevated curing temperature resulted in a coarser, more continuous pore structure. Tests on comparable concrete indicated a decreased resistance towards chloride ingress at the elevated curing temperature in line with the microstructure results [5]. Earlier it has been deduced that hydration at lower temperature allows for the hydrates to diffuse and precipitate more uniformly throughout the matrix, resulting in a less continuous pore system, while at elevated temperature, and accelerated reaction rate, there is less time for such diffusion [6].

In [7] the microstructure of ordinary Portland cement paste and cement pastes with silica fume and slag respectively cured at temperatures of 23 and 70 °C to 30 and 70 % hydration was investigated. Also here it was found, that generally the elevated curing temperature resulted in a coarser, more continuous pore structure for all pastes compared to curing at 23 °C. The use of silica fume or slag resulted in a refined pore structure and a more homogenized distribution of hydrates. The results were generally in agreement with the investigations of chloride diffusion on comparable concretes [8].

In [9] the chloride permeability at 28 and 91 days of ordinary Portland cement concrete and concrete with fly ash or slag cured at 23 and 71 °C was investigated. It was found that for the OPC concrete, the chloride permeability was higher for the elevated curing temperature, while the opposite was observed for the concretes containing fly ash and slag respectively.

In the referred earlier investigations, the testing of chloride permeability of concrete cured at different temperature was carried out either at similar age or similar degree of hydration. In the current study a different approach was used, where concrete cured at different temperatures was tested for chloride permeability at similar maturity according to the maturity function. The

purpose was to verify if the maturity function applies to chloride permeability, i.e. will the chloride permeability be the same for concrete cured at different temperatures when tested at similar maturity. This was investigated for both OPC concrete and concrete containing respectively fly ash and slag. The current study is part of a larger test program in connection with the Danish Expert Centre for Infrastructure Constructions, where also strength of similar concretes cured at different temperatures was tested at different maturities.

2. EXPERIMENTAL

Five types of concrete were selected for investigation of the influence of curing temperature on resistance towards chloride ingress. The concretes were mixed using an industrial scale mixing station and subsequently cylinders were cast and immersed in temperature controlled water curing tanks at 10, 20, 30, 45 and 60 °C respectively until testing. The chloride migration coefficient (NT Build 492) of the concrete was determined at 28, 56, 90 and 180 maturity days and chloride diffusion coefficient (NT Build 443) of the concrete was determined at 28 and 180 maturity days.

The real time ages of testing for the different curing temperatures and maturities were calculated using the maturity function:

$$H(\theta) = \exp(\frac{E(\theta)}{R} \times (\frac{1}{293} - \frac{1}{273 + \theta}))$$

H is the relative rate
θ is the temperature
E is the activation energy (θ ≥ 20 °C: E = 33500 J/mol, θ < 20 °C: E = 33500 + 1470 (20-θ))
R is the gas constant (R = 8.314 J/mol°C)

The maturity concept assumes that concrete samples of similar maturity will have similar strength. In that way the strength of a concrete can be estimated based on its temperature history and for a given temperature and age the maturity can be expressed in terms of an equivalent age at 20 °C. It should be noted that the maturity concept is based on experiences with pure OPC concrete and the applicability to cementitious systems containing fly ash or slag requires further documentation. As mentioned, a parallel study was conducted to investigate the influence of curing temperature on compressive strength for the same concretes. Some of these results will also be presented in this article for comparison.

The calculated real time ages of testing for the different curing temperatures and the age factors applied can be seen in Table 1.

Table 1 – Real time ages of testing.

Curing temp.	10 °C	20 °C	30 °C	45 °C	60 °C
Age factor	0.497	1.000	1.574	2.948	5.217
Maturity days			Real time days		
28	56.3	28	17.8	9.5	5.4
56	112.7	56	35.6	19.0	10.7
90	181.1	90	57.2	30.5	17.3
180	362.2	180	114.3	61.1	34.5

2.1. Materials and mix proportioning

Two types of Portland cement produced by Danish Aalborg Portland were used in pure Portland cement concrete as well as in fly ash concrete; a belite rich sulphate resistant CEM I 42.5 N (LAVALKALI) typically used for infrastructure projects as well as a more general purpose CEM I 52.5 N (RAPID). The fly ash was Emineral B4, a silicious ASTM class F fly ash from the Avedøre power plant near Copenhagen. The slag cement was a CEM III/B 42.5 N from CEMEX produced at the Schwelgern plant in Germany.

Concretes were proportioned as pure Portland cement concrete based on both RAPID and LAVALKALI cement, as fly ash concrete where each of the two cement types were combined with fly ash (25 wt% of binder – calculated as fly ash content divided by fly ash plus cement content) and a slag cement concrete. All concretes were proportioned with a water/cement ratio of 0.40 (calculated using activity factors of 0.5 and 1 for fly ash and slag respectively), air content of 4.5 % and a target slump of 160 mm. Air entraining agent (Amex SB 22) and superplasticizer (Glenium SKY 532-SU) from BASF were used. The fine aggregate used was sea dredged 0/2 mm sand from Rønne Banke in the Baltic Sea, and the coarse aggregate was crushed granite from Rønne on the Danish island of Bornholm in the fractions 4/8 mm, 8/16 mm and 16/22 mm. The mix proportions are shown in Table 2.

Table 2 – Concrete mix proportions in kg/m^3 SSD.

	A LAVALKALI	B LAVALKALI/FA	C RAPID	D RAPID/FA	E Slag cement
Cement	365	300	365	300	360
Fly ash	-	100	-	100	-
Sand 0/2	695	642	693	641	689
Rønne 4/8	377	367	376	366	373
Rønne 8/16	266	271	265	270	263
Rønne 16/22	529	541	528	540	525
Water total	146	140	146	140	144
Total	2378	2361	2373	2357	2354
w/c	0.40	0.40	0.40	0.40	0.40
Air content	4.5 %	4.5 %	4.5 %	4.5 %	4.5 %

2.2. Batching and mixing

The mixing of the concretes was performed in a 375 litre counter-current mixer with a capacity of 250 litre ready mixed concrete and equipped with 5 aggregate silos and 4 powder silos. The industrial mixing station ensures the applicability of the results to actual full scale concrete production. In order for the concretes to be produced with precisely the desired water to cement ratio, a special batching procedure was adopted, involving accurate determination of moisture content of aggregates. Each aggregate was weighed separately onto the conveyor belt, and samples were taken for determination of moisture content using microwave ovens, before the aggregate was transferred to the mixer. After determination of moisture content, the precise amount of water needed was calculated and batched to into a tank. The mixer, already containing the aggregates, was started and the powder was added followed by the water, air entraining agent and finally superplasticizer. The superplasticizer was added with a delay of 30 seconds from addition of the water. The final mixing time after dosage of all materials was 2 minutes. After mixing, the concrete was discharged to a crane bucket and samples were taken for determination of slump, air content and density.

2.3. Casting, curing and testing

If the fresh concrete properties were acceptable, Ø100 mm cylinders were cast using a vibration table. The cylinder moulds were immediately immersed in the temperature controlled water curing tanks with typical time from mixing to immersion of around 1 hour. All samples were demoulded the following day and immersed in the respective water curing tanks again until testing.

When reaching the required respective maturities, the concrete cylinders were taken from the water tanks and prepared for testing according to NT Build 492 and NT Build 443.

3. RESULTS AND DISCUSSION

An overview of the results from testing according to NT Build 492 and 443 of the 5 different concretes are found in Table 3. Furthermore results from testing of density and compressive strength at 28 maturity days are shown for completeness.

Table 3 – Overview of test results.

ID	Temp.	Density	Strength	CMC (*10^{-12} m^2/s)				CDC (*10^{-12} m^2/s)	
	°C	kg/m^3	MPa	28 md	56 md	90 md	180 md	28 md	180 md
A	10	2434	58.9	18.2	14.0	10.8	8.7	23.7	6.7
A	20	2420	58.5	17.4	11.5	9.4	7.1	10.5	12.7
A	30	2396	55.7	18.2	11.7	12.4	9.6	15.2	10.8
A	45	2393	49.3	16.7	11.3	11.7	11.9	17.0	18.9
A	60	2370	41.8	24.9	17.8	18.0	21.7	24.8	37.8
B	10	2387	49.9	24.1	11.4	8.3	2.2	8.7	2.3
B	20	2375	48.4	19.7	10.4	4.5	3.6	7.8	2.7
B	30	2406	58.7	10.3	4.1	3.0	0.9	5.1	-
B	45	2370	53.9	3.4	1.0	0.5	0.4	2.3	1.3
B	60	2362	46.6	2.2	1.2	0.7	0.6	1.9	1.6
C	10	2377	72.1	8.7	6.6	6.2	4.7	9.2	4.7
C	20	2362	64.1	7.1	6.4	5.4	5.7	11.1	4.6
C	30	2375	62.8	7.9	6.3	6.2	6.4	6.4	6.3
C	45	2348	52.4	13.4	11.4	11.3	10.7	13.9	23.2
C	60	2346	45.3	20.2	19.7	>23.4	>24.4	16.4	62.3
D	10	2388	67.9	6.6	4.3	3.2	1.0	4.0	9.2
D	20	2389	68.5	6.1	2.7	1.6	0.6	3.4	0.6
D	30	2390	70.7	2.8	1.3	0.8	0.4	3.3	0.5
D	45	2379	65.4	1.2	0.7	0.5	0.5	1.9	1.0
D	60	2361	56.6	0.8	0.8	0.6	0.6	1.3	0.9
E	10	2386	61.6	2.2	1.3	1.2	0.6	1.6	1.1
E	20	2407	66.1	1.3	1.2	1.1	0.5	1.7	1.9
E	30	2397	64.4	0.8	0.6	0.9	0.4	2.0	1.8
E	45	2409	55.2	0.8	1.0	0.6	0.5	2.1	1.2
E	60	2383	47.0	0.5	0.6	0.6	0.3	2.6	1.1

3.1. Chloride migration coefficient as function of maturity

The results from testing of chloride migration coefficient as a function of maturity for curing at 20 °C are presented in Figure 1.

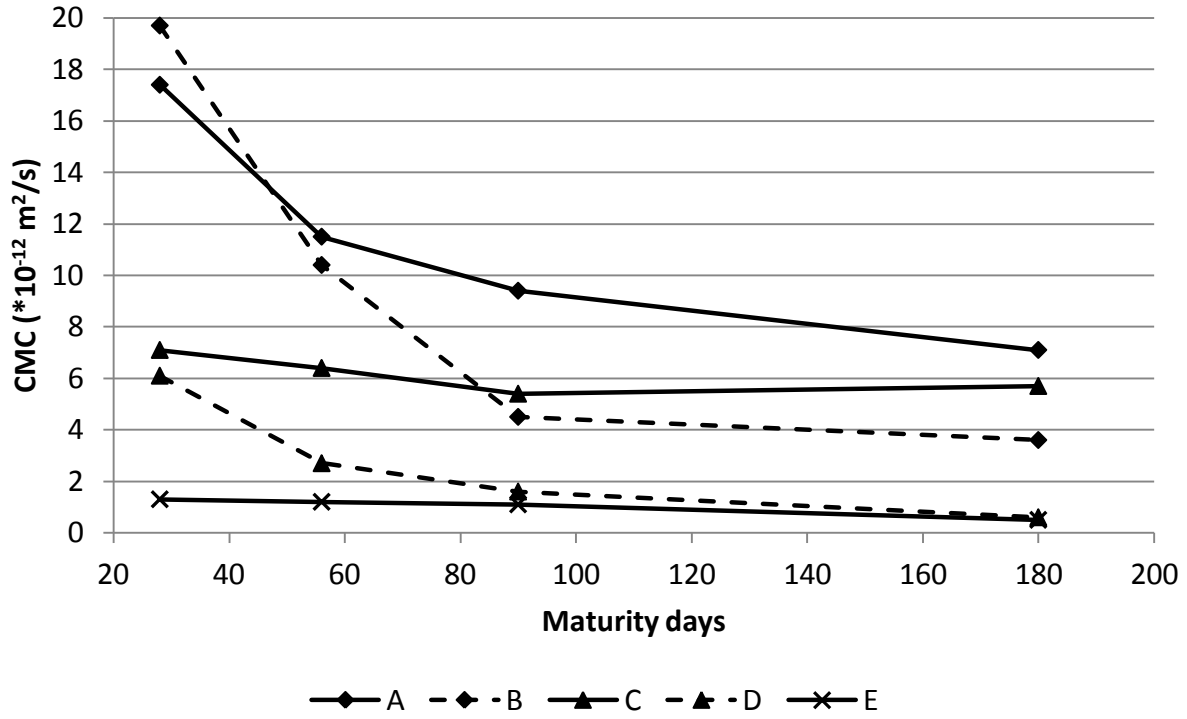

Figure 1 – Chloride migration coefficient as function of maturity for curing at 20 °C.

For the curing temperature of 20 °C the chloride migration coefficient becomes lower with increased maturity. This can be attributed to the reduction in permeability as the hydration process progresses and the hydration products fill the pores. The levels of chloride migration coefficient at 28 maturity days are as expected, as the LAVALKALI based concretes (A and B) has the highest chloride migration coefficients and the RAPID based concretes (C and D) has intermediate chloride migration coefficients, probably due to the faster reaction rate of RAPID compared to LAVALKALI. The slag cement concrete has very low chloride migration coefficient at all maturities, which may be attributed to the slag reacting to refine the pore structure and thereby reducing the permeability. The LAVALKALI/FA concrete has a higher chloride migration coefficient compared to the LAVALKALI concrete at 28 maturity days. However, at the higher maturities, and especially beyond 90 maturity days, the LAVALKALI/FA concrete has a significantly lower chloride migration coefficient than the pure Portland cement concrete, and also lower than the RAPID concrete (C). This can be explained by the effect of the pozzolanic fly ash reaction, which occurs later compared to the cement hydration reactions. For the RAPID based concretes, the addition of fly ash results in a lower chloride migration coefficient at all maturities, i.e. the pozzolanic reaction of fly ash is better "driven" by the RAPID cement than the LAVALKALI cement. Comparing concrete C and D again shows an increased effect of the fly ash at higher maturities.

The results from testing of chloride migration coefficient as a function of maturity for curing at 45 °C are presented in Figure 2.

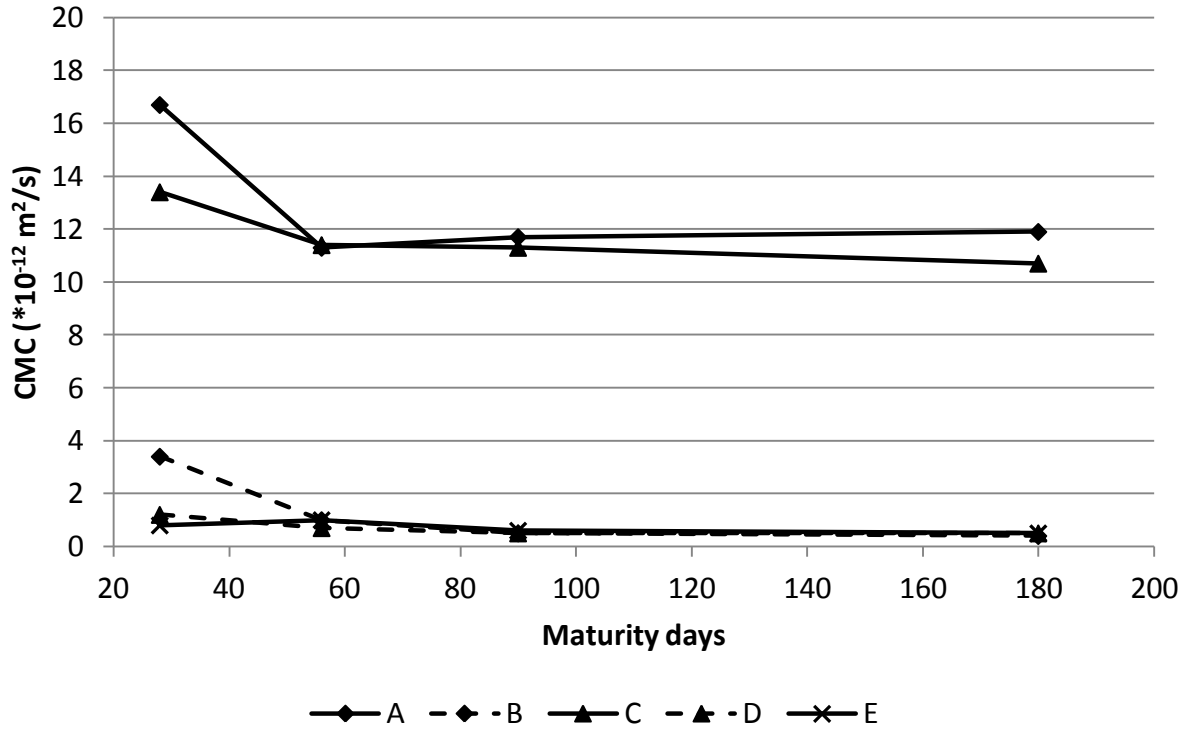

Figure 2 – Chloride migration coefficient as function of maturity for curing at 45 °C.

For the curing temperature of 45 °C, the reduction in chloride migration coefficient over time is less pronounced and beyond 56 maturity days there is no change for any of the concretes. There are clearly two levels of chloride migration coefficients with the pure Portland cement concretes having significantly higher chloride migration coefficients than the fly ash and slag cement concretes that have rather similar very low chloride migration coefficients. The more pronounced difference between pure Portland cement concrete and the fly ash and slag concretes could be the result either of a positive effect of temperature on the pozzolanic reaction or a negative effect of temperature on the pure Portland cement concretes.

3.2. Chloride migration coefficient as function of curing temperature

The results from testing of chloride migration coefficient at 28 maturity days are presented in Figure 3 as a function of curing temperature. The tendencies observed at the other maturities (56, 90 and 180) of testing are similar, as it appears from Table 1.

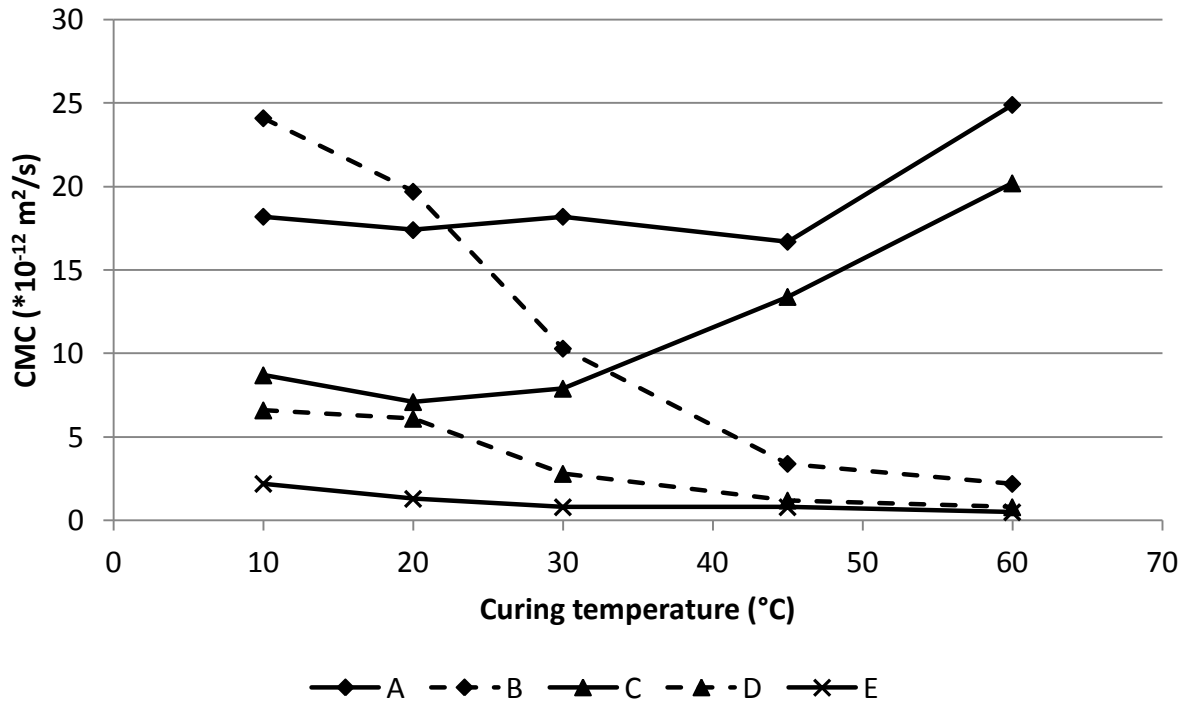

Figure 3 – Chloride migration coefficient at 28 maturity days as function of curing temperature.

For the pure OPC concretes, the chloride migration coefficient is more or less unaffected by the curing temperature up to 30 °C for the RAPID concrete and up to 45 °C for the LAVALKALI concrete. At higher temperatures, the chloride migration coefficient increases. This correlates well with the observations in [4] and [5], which report that elevated curing temperatures results in a coarser, more continuous pore structure and a decreased resistance against chloride ingress. Furthermore a decrease in strength at 28 maturity days as a function of temperature is observed for the pure Portland cement concretes (see Table 1). This suggests not only a coarser pore structure, but also a lower degree of hydration and hence higher porosity. Thus, the used maturity function may be overestimating the effect of temperature on the hydration process, at least when the concrete is cured at high temperatures for prolonged time as in this study.

For the fly ash concretes, the trend is the opposite of the pure Portland cement concretes. The chloride migration coefficient decreases as a function of curing temperature throughout the investigated temperature range (10 to 60 °C). The effect is most pronounced for the LAVALKALI/FA concrete (B), with the chloride migration coefficient being more than a factor 10 lower at 60 °C compared to at 10 °C. It has been reported, that generally addition of supplementary cementitious materials (silica fume and slag) will improve the resistance towards chloride penetration, when comparing concretes cured at similar elevated temperature and to similar degree of hydration [8]. This was attributed to the curing at elevated temperature resulting in a coarser, more continuous pore structure and the supplementary cementitious materials mitigating this effect by refining the pore structure. However, contrary to the current study, it was also found that the chloride permeability still increased at elevated temperature for the concretes containing supplementary cementitious materials. In another study, lower chloride permeability was observed for concrete containing fly ash or slag cured at 71 °C compared to the same concretes cured at 23 °C, while the opposite trend was observed for pure Portland cement concrete [9]. These results therefore show the same trend as found in the current study,

even though the chloride permeability was tested at similar real time age (28 days), whereas in the current study the testing was carried out at similar maturity.

When comparing the strengths of the fly ash concretes cured at the different temperatures (see Table 1), there is no clear indication of a lower strength as a function of increasing curing temperature as was observed for the pure Portland cement concretes. This could indicate that the fly ash concretes cured at the different temperatures reach a similar overall porosity and that the effect of elevated curing temperature is a reduction in the continuity of the pore structure and/or an increase in tortuosity of the pore system. Another potentially contributing factor could be that the resulting hydration product phase assemblage is different when curing at elevated temperature and that the chloride binding capacity may therefore be different/higher.

The slag cement concrete has a low chloride migration coefficient at all temperatures. A slight reduction is observed as a function of temperature up to 30 °C, while at higher temperatures, the chloride migration coefficient is unaffected by curing temperature. This correlates well with previous observations [10], where slag cement concrete cured at respectively 23 and 50 °C had similar low chloride permeability. However, at 70 °C an increase in chloride permeability was reported. In the current study, the strength results at 28 maturity days might indicate a higher porosity as a function of curing temperature, as the strength decreases with higher curing temperature from 20 to 60 °C (see table 1). This does however not affect the chloride migration coefficient.

3.3. Chloride diffusion coefficient as function of curing temperature

The results from testing of chloride diffusion coefficient (NT Build 443) at 28 maturity days are presented in Figure 4 as a function of curing temperature.

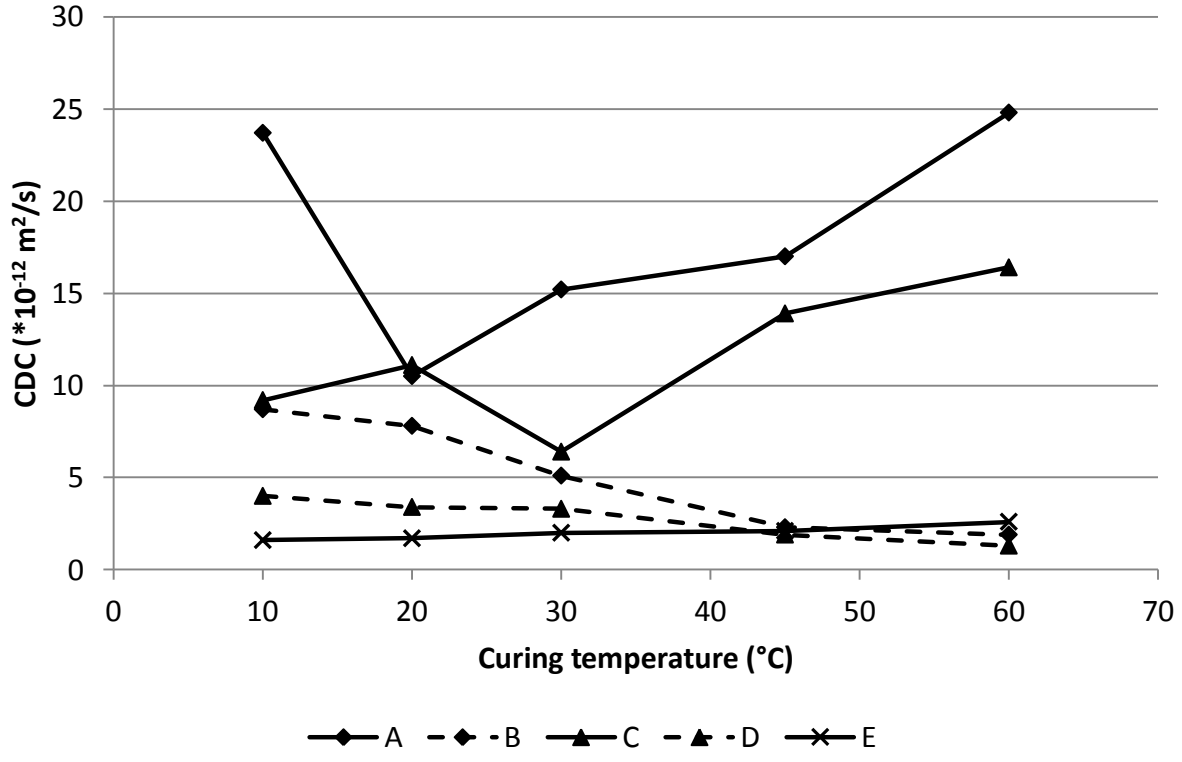

Figure 4 – Chloride diffusion coefficient at 28 maturity days as function of curing temperature.

The general trends in diffusion coefficient are the same as observed for the chloride migration coefficient. However, the relatively high value for the LAVALKALI concrete at 10 °C and low value for the RAPID concrete at 30 °C does not correlate with the results from testing of chloride migration coefficient. For the fly ash concretes, especially the LAVALKALI/FA concrete, the chloride diffusion coefficient decreases as a function of curing temperature, even though the effect is not quite as pronounced as for the chloride migration coefficient.

4. CONCLUSION

The pure Portland cement concretes and fly ash concretes investigated in this study show opposite trends in resistance towards chloride ingress as a function of curing temperature. The pure Portland cement concretes show a significantly reduced resistance towards chloride ingress as measured by NT Build 492 and 443 testing when cured at higher temperatures, while the fly ash concretes exhibit an increased resistance to chloride ingress as a function of curing temperature. Slag cement concrete has a high resistance towards chloride ingress at all temperatures investigated.

REFERENCES

1. Loser, Roman; Lothenbach, Barbara; Leeman, Andreas; Tuchschmid, Martin: “Cloride resistance of concrete and its binding capacity – Comparison between experimental results and thermodynamic modeling”, *Cement & Concrete Composites*, vol. 32, 2010, pp. 34-42

2. Ramezanianpour, A.A.; Malhotra, V.M.: “Effect of Curing on the Compressive Strength, Resistance to Chloride-Ion Penetration and Porosity of Concretes Incorporating Slag, Fly Ash or Silica Fume”, *Cement and Concrete Composites*, vol. 17, 1995, pp. 125-133

3. Khatib, J.M.; Mangat, P.S.: “Influence of high-temperature and low-humidity curing on chloride penetration in blended cement concrete”, *Cement and Concrete Research*, vol. 32, 2002, pp. 1743-1753

4. Kjellsen, Knut O.; Detwiler, Rachel J.; Gjørv, Odd E.: ”Development of Microstructures in Plain Cement Pastes Hydrated at Different Temperatures”, *Cement and Concrete Research*, vol. 21, 1991, pp. 179-189

5. Detwiler, Rachel J.; Kjellsen, Knut O.; Gjørv, Odd E.: ”Resistance to Chloride Intrusion of Concrete Cured at Different Temperatures”, *ACI Materials Journal*, vol. 88, 1991, pp. 19-24

6. Verbeck, George J.; Helmuth, Richard H.: “Structures and Physical Properties of Cement Paste”, *Proceedings of the 5th International Symposium of the Chemistry of Cement*, Tokyo, 1968, pp. 1-32

7. Cao, Yajuan; Detwiler, Rachel J.: ”Backscattered Electron Imaging of Cement Pastes Cured at Elevated Temperatures”, *Cement and Concrete Research*, vol. 25, 1995, pp. 627-638

8. Detwiler, Rachel J.; Fapohunda, Chris J.; Natale, Jennifer: ”Use of Supplementary Cementing Materials to Increase the Resistance to Chloride Ion Penetration of Concretes Cured at Elevated Temperatures”, *ACI Materials Journal*, vol. 91, 1994, pp. 63-66

9. Acquaye, Lucy; Chini, Abdol; Danso-Amoako, Mark: “Green options for high temperature cured concrete through the use of fly ash and blast furnace slag”, *33rd Conference on Our World in Concrete and Structures*, Singapore, 2008

10. Fapohunda, Chris A.: “Effects of blast furnace slag on chloride permeability of concrete cured at elevated temperatures”, *Journal of Life and Physical Sciences*, vol. 3, 2010, pp. 119-123

Disturbed Regions in Dapped-End Beams – Numerical Simulations of Strengthening Techniques

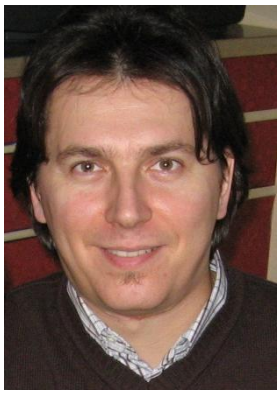

Cosmin Popescu
M.Sc., Ph.D. Student
NORUT Narvik, N-8504, P.O. Box 250, Norway
Department of Infrastructure Structures and Materials
E-mail: cosmin.popescu@norut.no

Cosmin Dăescu
Ph.D., Assistant Lecturer
Politehnica University of Timisoara
Department of Civil Engineering
2nd T. Lalescu, 300223 Timisoara, Romania
E-mail: cosmin.daescu@ct.upt.ro

Nagy-György Tamás
Ph.D., Lecturer
Politehnica University of Timisoara
Department of Civil Engineering
2nd T. Lalescu, 300223 Timisoara, Romania
E-mail: tamas.nagygyorgy@ct.upt.ro

Gabriel Sas
Ph.D., Assistant Lecturer
Luleå University of Technology
Department of Structural Engineering
SE – 971 87 Luleå, Sweden
E-mail: gabriel.sas@ltu.se

ABSTRACT

This paper investigates the effectiveness of strengthening reinforced concrete (RC) dapped-end beams using carbon fiber reinforced polymers (CFRP). Parametric studies are performed by means of numerical simulations in which several types of composite materials as well as their orientation are combined. The primary objectives of this research were the evaluation of the strengthening systems in terms of ultimate capacities and the failure modes involved. Results show that only some of them provide significant load bearing capacity increase. The observed failure modes ranged from a sudden failure up to the desired progressive failure of the strengthening system.

Key words: Numerical analysis, dapped-end, strengthening, precast concrete, FRP, EBR, NSMR, full-scale tests.

1. INTRODUCTION

The abrupt change of cross-section in a RC structural element results in a complex flow of internal stresses. Such regions are disturbed regions (D-regions), so called dapped-ends for RC beams, and represent areas where severe reductions of the cross-section are created so that the beam is supported on other structural elements. The load carrying capacity (hereafter capacity, for convenience) of dapped-end beams may be insufficient for reasons such as design errors, code changes, increases in loads or structural damage. Fiber-reinforced polymers (FRP) applied using the externally bonded reinforcement (EBR) or near surface mounted reinforcement (NSMR) techniques have been proven to be reliable for strengthening RC structures. Several guidelines for strengthening RC structures with FRPs have been published [1-3]. However, these guidelines do not refer in detail to FRP strengthening of dapped-end beams due to insufficient experimental and theoretical investigations on the variations in geometry, material and loading conditions at their dapped-ends. To the authors' knowledge, only four experimental investigations on dapped-end beams strengthened with FRPs have been reported [4-7].

Gold et al. [4] strengthened with FRP several dapped-end beams of a three-story parking garage that were deficient in shear capacity. Due to the lack of design provisions at that time, they carried out a series of tests to verify the effectiveness of the FRP strengthening as well as the predictive performance of their design approach. The FRP strengthening systems doubled the capacity of the beams, confirming their effectiveness.

Taher [5] assessed the effectiveness of the following techniques for improving the capacity of dapped-end beams: externally bonding steel angles; anchoring unbonded steel bolts in inclined, pre-drilled holes; externally applying steel plate jackets; and wrapping carbon fiber around the beam stem. Tests with 50 small-scale rectangular beams indicated that the FRPs were the most viable solution for strengthening/retrofitting applications. Using the strut and tie analogy, Taher [5] also derived a regression model to estimate the capacity of the FRP-strengthened dapped-end beams, which reportedly provided "reasonable predictions" [5], but he did not consider any possible scale effects of the beams tested for deriving the model.

Tan [6] experimentally investigated the efficiency of several FRP configurations for strengthening dapped-end beams with deficient shear resistance, varying both fiber types and mechanical anchorage systems for the FRPs. The results indicated that glass fiber reinforced polymers (GFRP) provided greater improvements in terms of ultimate capacity than CFRP plates and carbon fiber fabrics. He has also verified that the tested mechanical anchorage devices provided higher exploitation of the FRP systems' strengthening capacity by preventing their debonding. The empirically based strut and tie model he derived was applied to predict the shear capacity of the dapped-end beams and proved to be sufficiently accurate for the tested beam types.

In another series of tests, Huang and Nanni [7] verified if the FRPs can increase the capacity of dapped-end beams with "mild steel and no mild reinforcement" [7] and proposed a method for strengthening dapped-end beams with FRPs, which was found to be "satisfactory and conservative" [7].

The current study presents a parametric study of the FRP strengthening systems used for a real case application, previously presented in [8]. The analysis is carried out by means of FEM-based material nonlinear numerical simulations. In several dapped-end beams, diagonal cracks were observed starting at the re-entrant corner, see [8]. These damaged dapped-ends were retrofitted with CFRP plates. The aims of the strengthening solutions were to increase the capacity up to the design load and to delay the yielding initiation of the steel reinforcement. Three full scale laboratory tests and nonlinear numerical simulations of those tests were carried out to verify the capacity of the retrofitted dapped-ends. The results indicated that FRPs can be used successfully for rehabilitating dapped-ends. However, that study confirmed also that the capacity gain is influenced by the application direction and type of FRP material used. The present investigation aims to clarify the contributions of the individual components of the strengthening and identify the most effective FRP-based strengthening system for the retrofit of large dapped beams ends. The efficiency is discussed in terms of ultimate capacity and global failure mode of the strengthened elements.

2. THE FIELD APPLICATION

The field work was carried out in 2003. In an industrial hall, 20 m span identical precast/prestressed beams with dapped-ends were designed for a reaction force of 800 kN positioned 400 mm from the re-entrant corner. Due to a construction error, in seven beams the position of the reaction force was displaced by an additional 275 mm, thus diagonal crack formed starting from the re-entrant corner. Considering the new lever arm (675 mm), a deficit in capacity of 200 kN resulted. To increase the demanded capacity and prevent further cracking in service, a strengthening solution using EBR CFRP plates was applied. Based on the initial studies performed in 2003 using a linear FEM and strut-and-tie model, it resulted in the necessity to strengthen the dapped-ends with the $0^o/90^o$ layout (see Figure 1), since this layout provided the longest anchorage length and debonding could have been avoided. In the design of the retrofitting, the strains in FRP were limited to 4 ‰, according to *fib* Bulletin 14 [1]. However, in the real field application, in some cases, the dapped-ends were arranged head-to-head and the purlins obstructed the application of this layout, hence for these situations the $45^o/90^o$ layout was adopted (as shown in Figure 1).

3. EXPERIMENTAL PROGRAM

To verify the efficiency of the applied strengthening configurations, two beams were casted and tested in laboratory environment, each with two dapped-ends. The arrangement, spacing, diameter and strength class of the reinforcements were identical to those of the original beams. The dapped-end specimens were subjected to a monotonic force in increments of 50 kN.

The first element (denoted C1 in [8]) was tested up to failure, serving as reference specimen. The remaining three dapped-ends (denoted C2, C3 and C4 in [8]) were tested up to 800 kN, which corresponded to the design load of the original dapped-ends. These pre-cracked elements were strengthened in three different solutions. The test setup was identical for all the unstrengthened (C) and retrofitted (RC) specimens (see Figures 1 & 2).

Two strengthening systems were composed of CFRP plates, applied in $45^o/90^o$ (RC2 in Figure 1) and $0^o/90^o$ (RC4 in Figure 1) directions, respectively. The overall behaviour of the elements retrofitted with these two systems was similar. Both capacity and stiffness increased compared with C1, and crack formation was delayed. At a load of 800 kN, the maximum strains measured

in the steel reinforcements in RC2 and RC4 were 31%, respectively 15% less than the corresponding strains at this load in the reference specimen. The elements' failure occurred by successively deponding of the plates in both situations [8]. The load-displacement curves as determined from the experimental tests and the corresponding predictions from the numerical model are presented in Figure 3.

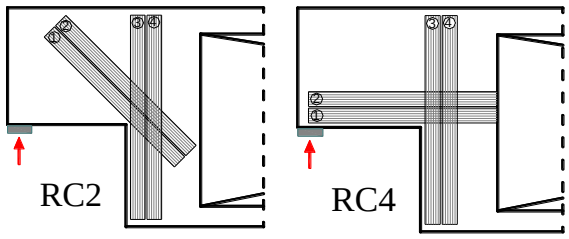

Figure 1 – Strengthening systems tested

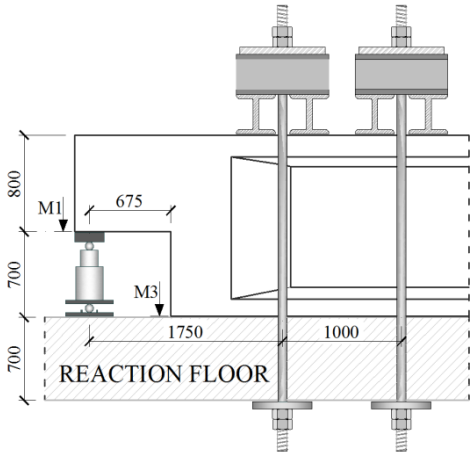

Figure 2 – Test set-up (mm)

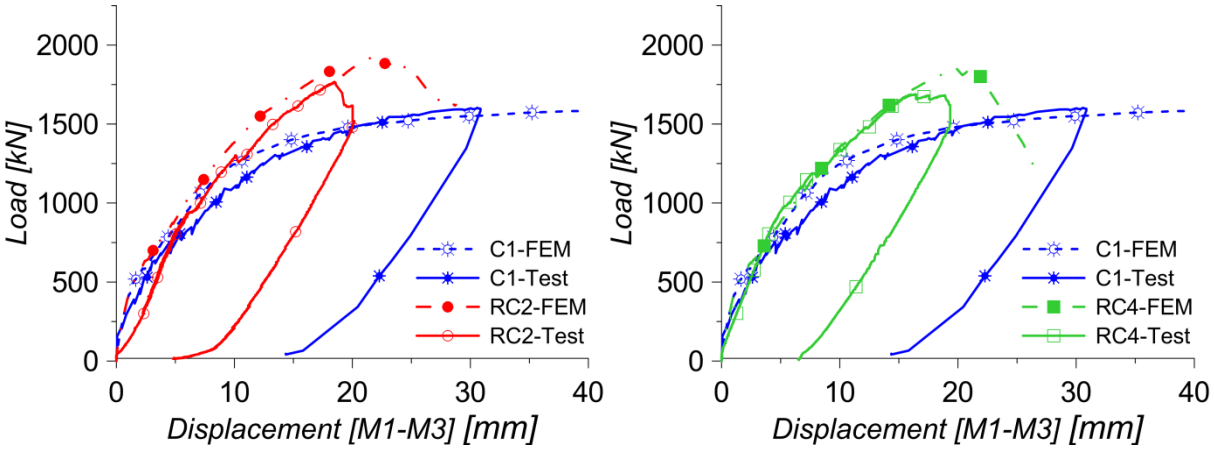

a) C1 and RC2 *b) C1 and RC4*

Figure 3 – Load – displacement diagram. Experimental vs. numerical systems tested

4. NUMERICAL ANALYSIS

The modelling strategy is identical to the one presented in [8], where a very good agreement was found between experimental and numerical results. The standard incremental and iterative Newton-Raphson method for material nonlinear structural analysis was used in the numerical simulations, based on the finite element method. The specimens were modelled with a mesh of 8-node serendipity plane stress finite elements. A Gauss integration scheme with 2x2 integration points was used for all the concrete elements. The steel bars, NSMR, CFRP plates and CFRP fabrics were modelled with 2-noded perfectly bonded embedded truss elements (one degree of freedom per node) [9]. Details regarding the geometry and layout of the reinforcement are given in [8]. Due to the fact that the whole element was modelled in 2D, the out-of-plane effects (such as lateral debonding of the CFRP plates or NSMR) could not be recorded. Although in ATENA software two models (Bigaj, 1999 and CEB-FIP 1990 Model Code) [10] of bond slip laws are

implemented to analyse interaction between discrete bars and concrete, full debonding (separation between the FRP and the concrete surface) cannot be properly captured by a model only considering axial slip. The above two bond models can be used for simulating uniaxial state of stress. For our tests the state of stress is biaxial, therefore using these models could produce to erroneous results. Moreover, in our tests, the debonding took the form of concrete rip-off, where all the concrete cover was separated from the surface of the stirrups. To the authors best knowledge there is only one model [11] that could capture such failure mode. However that model [11] is derived on empirical basis from uniaxial lap joint tests, thus not applicable to our case. For this reason, all the applied CFRP materials are considered to be mechanically anchored and the debonding process is disregarded.

4.1 Modelling strategy

The numerical analysis presented in this paper is a continuation of the analysis presented in [8] and aims to highlight the performance of the different FRP strengthening systems that have not been tested nor applied. To model the optimum strengthening system, the numerical modelling was carried out in two steps.

First, the individual components (P00, P45 and P90 in Figure 4) are modelled separately so that their efficiency is determined. The denomination used reflects the angle that the specific strengthening system makes with the longitudinal direction of the beam. For example: P00 means horizontally applied CFRP plates, F45 stands for 45^o applied CFRP fabrics and N90 indicates a vertically applied NSMR bars. The scope is to identify how individual CFRPs perform function of the: (1) applied inclination with respect to the horizontal axis and (2) type of the composite used, i.e. fabrics (F), plates (P) or NSMR (N). The inclinations of $0^o/45^o/90^o$ were chosen in such a way that they correspond to the real case application and to the experimental program carried out. Then, fabrics and NSMR components, designed to be equivalent in nominal strength along each direction with the P00, P45 and P90 components were modelled (see models F00, F45, F90, N00, N45 and N90 in Figure 4). The mechanical materials properties of the fabrics and NSMR were chosen so that they are similar to the ones used in the real application and experimental testing (see Table 1). Due to practical limitations, the resulted values of the nominal strength are not identical, however the difference is marginal (±4%). The results of the first step were evaluated and, in the second step, the individual components were combined so that strengthening systems were formed.

Table 1 – Mechanical properties of CFRPs (specified by the producer)

System	FRP	Tensile Modulus E [N/mm^2]	Strain at failure ε_u [‰]	Thickness t [mm]	Width b [mm]	No. of plates/ layers/ bars per side	Equivalent tensile strength [kN]
1	Plate (P)	165000	17	1.2	100	2	673
2	Fabric (F)	231000	17	0.17	340	3	680
3	NSMR (N)	165000	13	10	10	3	645

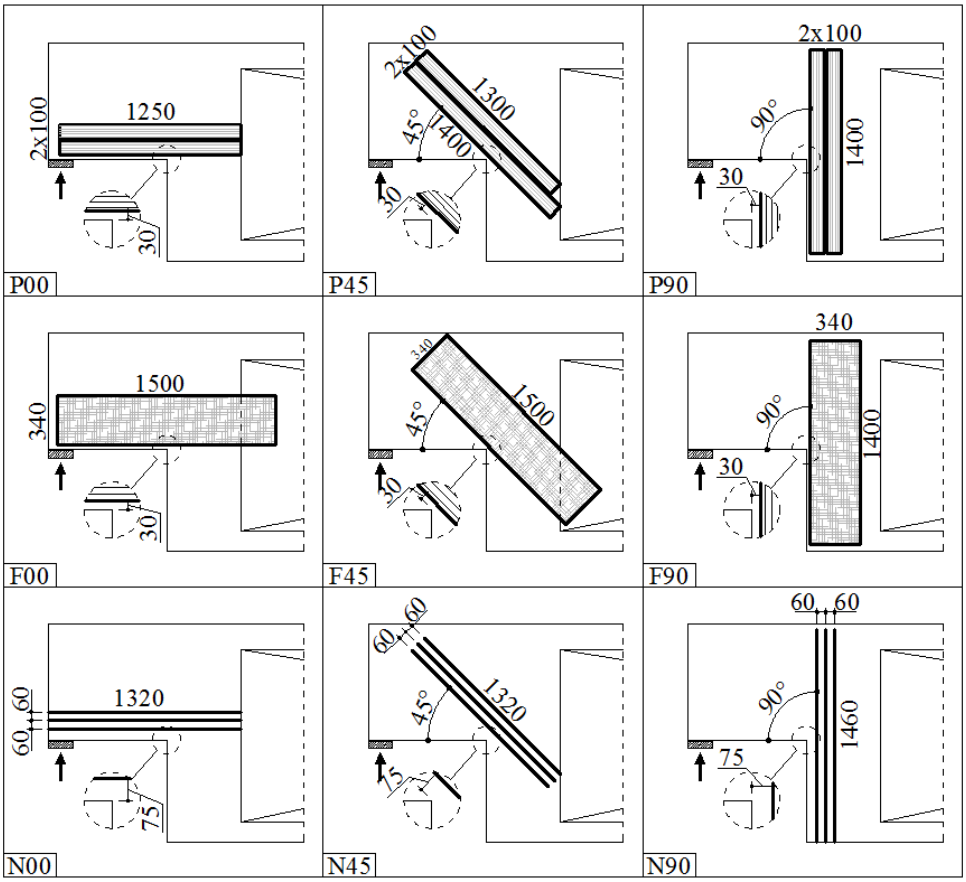

Figure 4 – Individual strengthening solutions

4.2 Material characteristics

Concrete

The constitutive model for concrete used in the analysis is a fracture-plastic model that combines constitutive sub-models for tensile and compressive behaviour, see ATENA user manual [9] for further details. This fracture model employs the Rankine failure criterion and exponential softening, with the hardening/softening plasticity component based on the Menétrei-William failure surface [12]. The concrete post-cracking tensile behaviour was simulated by the softening function illustrated in Figure 5, in combination with the crack band theory [12]. Crack band approach assumes that the crack spacing is larger than a finite element size. The program ATENA allows the user to manually define the crack spacing. For this work it was set at 50 mm based on laboratory observations. This user defined spacing is used as crack band size when the user defined crack spacing is smaller than the crack band size that would be implicitly determined by the software. According to [12] "The purpose of the failure band is to eliminate two deficiencies, which occur in connection with the application of the finite element model: element size effect and element orientation effect". The crack band size is calculated as a size of the element projected into the crack direction, taking into consideration also the angle between the direction of the normal to the failure plane and element sides.

The web area and the unloaded dapped end of the beams were not structurally damaged during testing. In order to reduce the computational time, these areas were discretized with 100 mm

element size mesh. For the loaded dapped end it was used a 50 mm mesh size. The material properties were determined from laboratory tests, in conformity with [13] for concrete and [14] for steel, respectively. In Figure 5, f_{ct} is the tensile strength of concrete, G_f is the mode I fracture energy of concrete determined based on equation (1) developed by Vos, 1983 [9] and w_c is the crack opening at the complete release of stress, as described in [12]. The concrete had a maximum aggregate size of 16 mm and the measured mean compressive cube strength was 56 N/mm^2 corresponding to a C35/45 concrete strength class according to [13]. Tension and compressive strength and elastic modulus of the concrete were determined as functions of the cube strength (see Table 2). The formulas for these functions were taken from the CEB-FIP Model Code 90 [15].

FRP and steel bars

Discrete bars were used to model the reinforcement; the characteristic material behaviour are presented in Figure 6.

Table 2 – Properties of the concrete material used in FEM analysis

Concrete class	Mean compressive strength f_{cm} [N/mm^2]	Compressive cylinder strength f_c [N/mm^2]	Tensile strength f_{ct}[N/mm^2]	Elastic modulus E_c[N/mm^2]	Crack spacing c_s [mm]
C35/45	56	47.6	3.513	38400	50

$$G_f = 0.000025 * f_t = 87.82 \text{ N/m} \quad (1)$$

After the peak tensile strength (f_u), the stress was reduced to 1% of f_u so that internal stress redistribution could be assured in the numerical computations. The values used for defining the stress-strain relationships are given in Table 1 and Table 3.

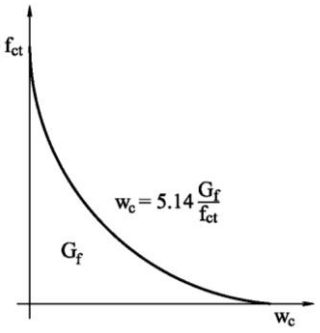

Figure 5 – Tensile softening diagram

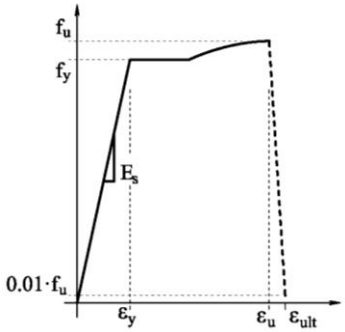

Figure 6 – Steel reinforcement model

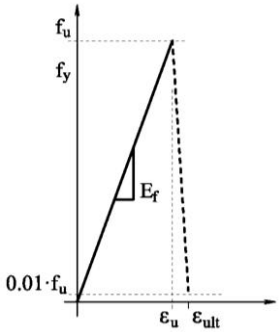

Figure 7 – CFRP tensile diagram

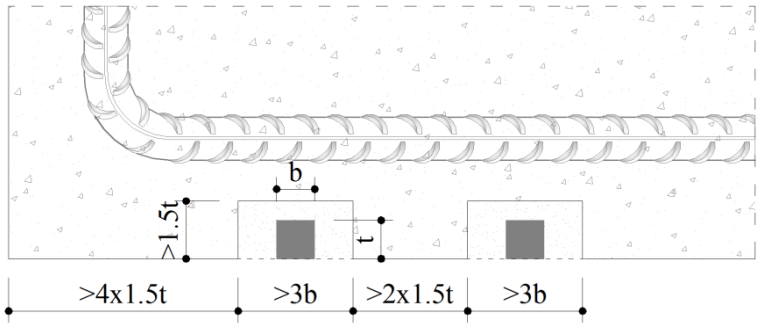

Figure 8 – NSMR layout rule according to [3]

The behaviour of the CFRP was modelled as linear elastic up to failure. In order to avoid numerical integration problems, the post-peak behaviour was modelled so that the residual stress is 1% of the maximum tensile strength, see Figure 7. For the NSMR, the thickness, as referred in Table 1, represents the depth embedded into the concrete cover, noted as "t" in Figure 8. The FRP fabrics were introduced using several discrete lines (modelled as bars perfectly bonded to the substrate), each equivalent to a 50 mm wide strip. The same procedure was used for the plates, except that the strips were 25 mm wide. In the case of the NSMR, each line was equivalent to the effective cross-section of each individual NSMR bar. The layout of the NSMR reinforcement respects the prescriptions presented in [3]; these rules are schematically presented in Figure 8. The predictive performance of the numerical simulations of the experimentally tested elements (see [8]) showed that this approach is reliable since it reproduced the relevant features recorded experimentally (i.e. maximum load, monitored displacements and monitored strains in both reinforcement and FRP). A general view of the finite element model is shown in Figure 9.

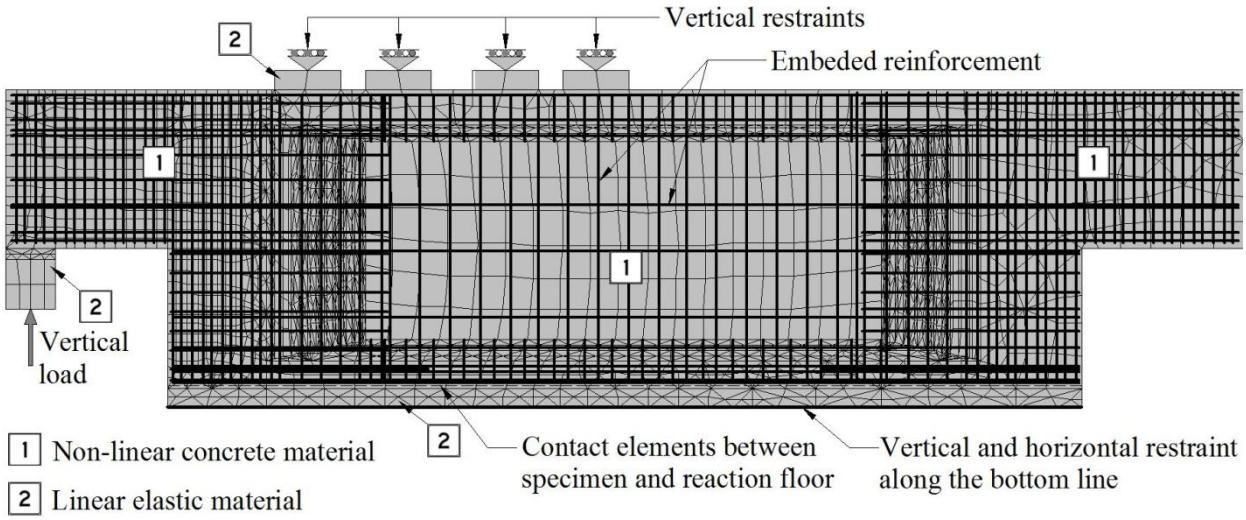

Figure 9 – FE model: material models and boundary conditions

Table 3 – Properties of the steel material determined from laboratory tests

Diameter Φ [mm]	Yield strength f_y [N/mm^2]	Tensile strength f_u [N/mm^2]	Yield strain ε_y [‰]	Ultimate strain ε_u [‰]	Strain at failure ε_{ult} [‰]
10	780	922	3.6	14.9	15.5
12	522	600	2.5	23.1	24.0
16/18/20	460	600	2.2	19.9	21.0
25	440	625	2.2	18.9	20.0

4.3 Boundary conditions

Contact elements without tensile capacity were adopted for the contact of the specimen with the supporting RC floor, thus allowing the eventual separation of the bottom surface. The elastic deformation of the test setup was calibrated based on the experimental results obtained for the reference specimen and then integrated in all numerical simulations (see [8]).

4.4 Utilization of the individual components

The notations in the Figure 10 are accompanied by the maximum force applied and their percentage increase with respect to the reference specimen C1. Note, diagram C1 represents the load displacement curve obtained from numerical analysis, also shown in Figure 3.

Figure 10 shows the load displacement response obtained from numerical analysis of the individual components applied at 0° (Figure 10a), 45° (Figure 10b) and 90° (Figure 10c). From here on, the "displacement" term in the load-displacement diagrams is defined as the difference in values recorded at points M1 (bottom part of the extended end) and M3 (bottom part of the beam in the undapped zone) (see Figure 1).

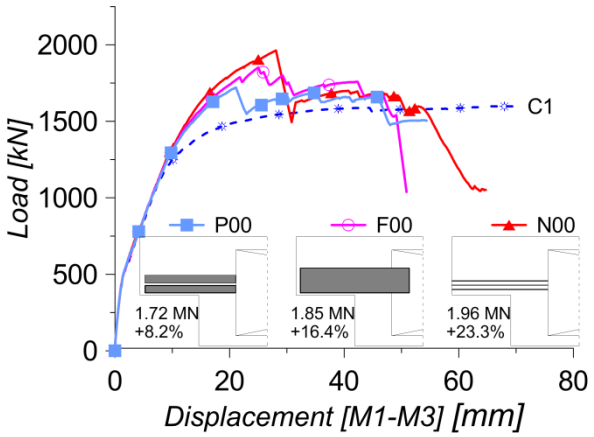

a) 0° angle

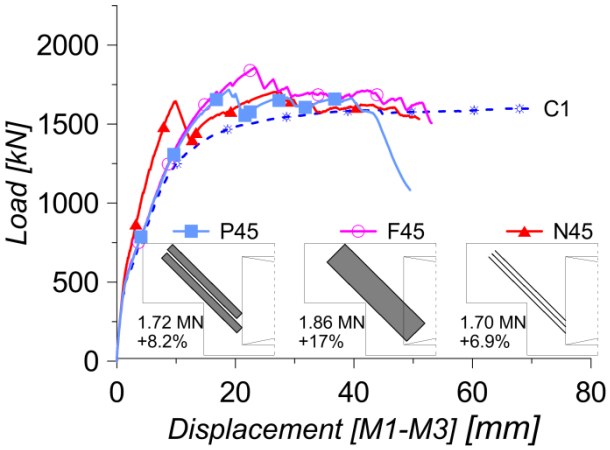

b) 45° angle

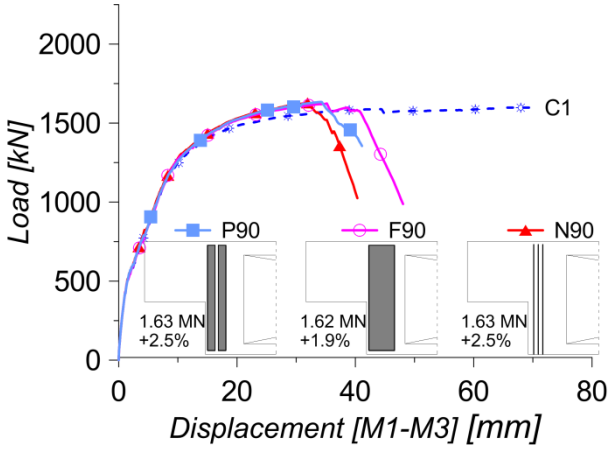

c) 90° angle

Figure 10 – Load displacement diagrams for individual components of the strengthening systems

For individual FRP components applied at 0° and 45°, the increase in load was in range of 6.9-23.3% compared to the reference specimen C1, which reached a maximum applied load of 1.59 MN (see [8]). However, the 90° strengthening systems does not provide significant improvement in the bearing capacity (around 2.0%, see Figure 10c). In the C1 specimen the yielding occurred at the same time in the horizontal and vertical reinforcement. Applying the

90° strengthening systems, yielding of the vertical steel reinforcement was delayed, while in the horizontal steel bars yielding was reached to a similar applied force as in reference C1. Thus only the strengthening systems made of individual components applied at 0° and 45° were considered further in the study.

In terms of ultimate capacity increase, for the components P00, F00 and N00 (see Figure 10a), the values varied between 8.2% up to 23.3%. At peak load, specimens P00 and F00 failed by rupture of the fibres closest to the re-entrant corner followed by a progressive failure of the adjacent fibres. Immediately after peak load, the fibres failed progressively for both systems P00 and F00, respectively. This less-brittle failure mode is attributed to the distribution of the fibres over a larger area, hence stresses are better redistributed. Opposed to this behaviour, in the N00 model, the 3 NSM bars have failed in a brittle manner, all at the same load level. However, in this case, it was obtained the highest capacity increase (23.3%) compared to the reference specimen (C1).

For the components P45, F45 and N45 (see Figure 10b) it was recorded an increase in ultimate capacity in the range of 6.9% up to 17%, compared to the reference specimen (C1). The P45 and F45 components failed progressively after the peak load, while all three NSM bars of the N45 component failed in a brittle manner immediately after the peak load had been reached. The N45 had provided a significant increase in the stiffness response of the structure due to an effective arrestment of critical crack propagation.

4.5 Assessment of the strengthening systems

Due to technological limitations imposed by the small concrete cover thickness, the NSM bars can only be used in combination with either plates or fabrics. The components applied at 90° did not provide any significant gain in capacity therefore those elements were not used in building up the strengthening systems. Considering these limitations, all possible combinations of strengthening are presented in Figure 11.

In Figure 12 are presented the numerical results of the systems components. The notations are accompanied by the maximum force applied and its percentage increase with respect to the reference unstrengthened specimen C1.

In Figure 12a-c are shown the load displacement responses for strengthening systems using:
a) Plates applied horizontally, in combination with 45° plates, fabrics or NSMRs;
b) Fabrics applied horizontally, in combination with 45° plates, fabrics or NSMRs;
c) NSMR applied horizontally, in combination with 45° plates or fabrics.

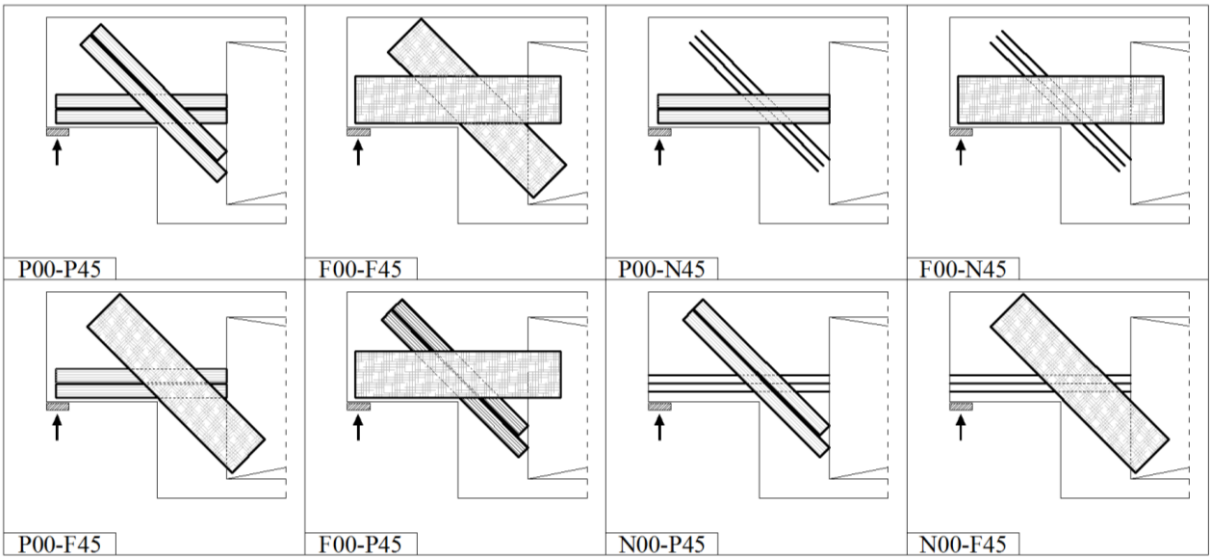

Figure 11 – Combined strengthening solutions

The increase of ultimate capacities of the P00-P45, P00-F45 and P00-N45 systems (Figure 12a) are in the range of 16.3% up to 32.7%. P00-P45 and P00-F45 have a progressive failure of the 45° components, followed by the failure in the first strip of the horizontal CFRP; for P00-F45, at the failure of all the strengthening systems, it was recorded also the failure of the first stirrup in the main part of the element, next to the re-entrant corner. All the NSMR bars in P00-N45 fail suddenly at the same maximum load.

All models using 00° fabrics (F00-P45, F00-F45 and F00-N45, in Figure 12b) reach maximum loads corresponding to an increase of 10.7% up to 37.7%. For F00-P45 and F00-F45, the failure modes are characterized by the progressive failure of the inclined components, followed by the initiation of the failure in the horizontal strengthening systems. For F00-N45 model, all the 45° NSMR failed suddenly together with 3 out of 8 horizontal CFRP strips.

N00-F45 and N00-P45 systems have similar maximum load capacities. The failure in the both models is brittle; at maximum load, all the NSMR bars fail simultaneously.

In all the strengthening systems including NSMR bars, the response up to peak load was higher than in the other strengthening configurations.

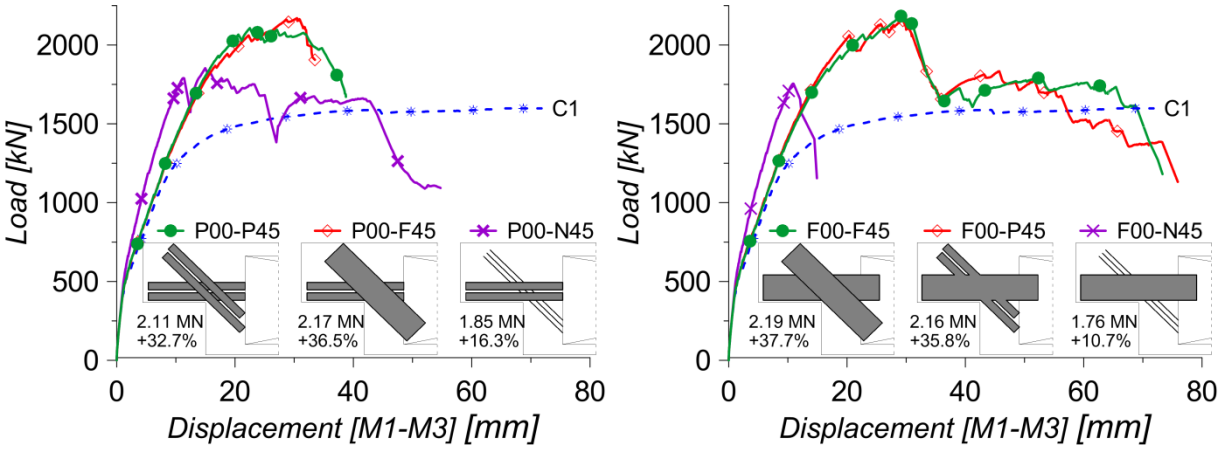

a) P00 as common component

b) F00 as common component

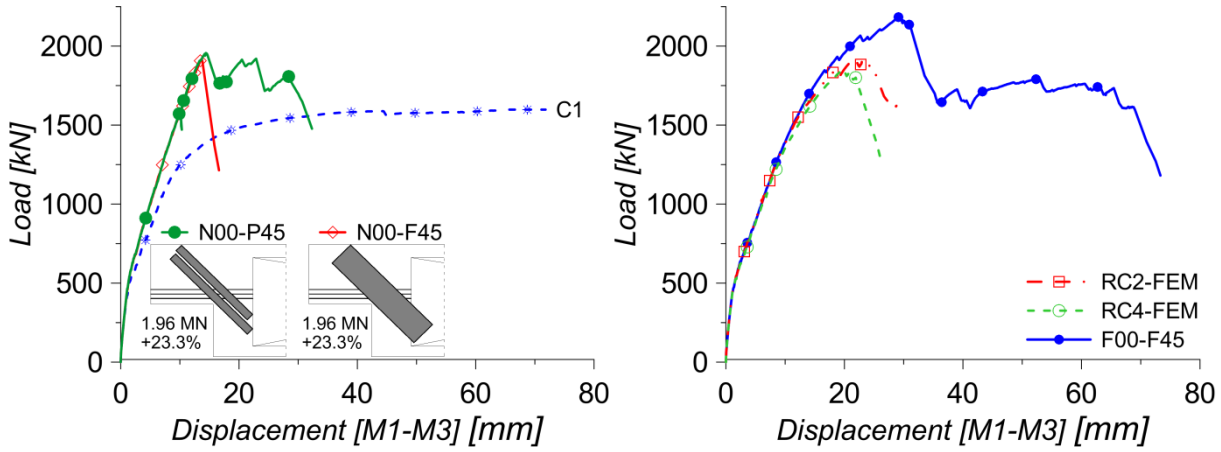

c) N00 as common component d) Optimum vs. tested systems

Figure 12 – Load displacement diagrams for strengthening systems

5. CONCLUSIONS

The research presented in this paper was prompted from a real case study. Several strengthening solutions could have been applied for that field application. However, the initial assessment of the capacity and the choice of the FRP materials available on the market at that time (2003) imposed the use of two different systems for strengthening the dapped-ends on site. To verify the efficiency of the applied systems, a series of tests and numerical simulations were carried out. Since only two strengthening systems were applied, the authors have decided to investigate if these two systems used were the best choice in terms of retrofitting efficiency. Therefore in this paper more practical strengthening configurations that could have been applied were investigated by means of numerical simulations. The modelling approach was first to obtain the individual influence for each component of the strengthening systems used and then to combine these components so that the most efficient strengthening system is determined. Individual models were studied using ATENA software [9], each one having only a part of the strengthening system applied. Then, based on the performance of the individual components, all feasible strengthening systems were built.

The results have showed that all the strengthening systems analysed provide an increase in the load bearing capacity. While some strengthening systems provided marginal increase with respect to the reference C1 specimen (about 2% for the systems with vertical fibres), many others have provided increased capacities ranging from 6.9 to 37.7% . The optimum solution for strengthening, which would have been chosen, is F00-F45 (fabrics with fibres at horizontal and at 45 degrees) that increased the capacity to about 37.7%. A similar increase was provided by P00-F45 (horizontal plate and fabrics with fibres at 45 degrees). However, the necessity for mechanical anchorages at the end-plates should be explored. The strengthening system F00-F45 outperforms the two systems used in the field application (Figure 11d). The test results for RC2 and RC4, presented in [8] (Figure 1), showed an increase of 20.7% and 16.1% respectively (Figure 3a and Figure 3b). In general a progressive failure mode is preferred to a brittle one (RC2 and RC4 in the laboratory tests). This aspect was not captured during the analyses, because the modelling was carried out in 2D. In a 3D analysis debonding could be modelled using a bond slip law or a cohesion-friction model. Nevertheless, the authors did not test these hypotheses due to lack of test information.

All the results presented above consider a perfect connection and anchorages between the strengthening systems and the concrete element. This limitation is aimed to be further studied and correlated with test results by means of strain distribution in the FRPs with regard to end-plates debonding and intermediate crack debonding.

The numerical analyses presented here indicate that the applied strengthening systems based on CFRP are viable solutions for improving the capacity of the dapped-end beams by concentrating a sufficiently strong material as close to the re-entrant corner as possible, which is good agreement with the results presented in [8].

The authors intend to improve their conclusions considering different material properties (i.e. high modulus vs. high strength) or various cross section dimensions for the NSMR, thus generating a future study subject.

REFERENCES

[1] *fib* Bulletin 14, Externally bonded FRP reinforcement for RC structures, International Federation for Structural Concrete, 2001.
[2] CNR 200-2004, Guide for the Design and Construction of Externally Bonded FRP Systems for Strengthening Existing Structures, Italian National Research Council, 2004.
[3] ACI 440.2R-08, Guide for the design and construction of externally bonded FRP systems for strengthening concrete structures, American Concrete Institute, 2008.
[4] Gold, W.J., Blaszak, G.J., Mettemeyer, M., Nanni, A., Wuerthele, M.D., "Strengthening Dapped Ends of Precast Double Tees with Externally Bonded FRP Reinforcement", ASCE Structures Congress, 9, CD version #40492-045-003, 2000.
[5] Taher, S., "Strengthening of reentrant corner zone in recessed RC beams", Eleventh International Colloquium on Structural and Geotechnical Engineering, 2005.
[6] Tan, K.H., "Shear Strengthening of Dapped Beams Using FRP Systems", FRPRCS-5, 2001, pp. 249-258.
[7] Huang, P.C. and Nanni, A., "Dapped-end strengthening of full-scale prestressed double tee beams with FRP composites", Advances in Structural Engineering, No. 9, 2006, pp. 293-308.
[8] Nagy-Gyorgy, T., Sas, G., Daescu, A.C., Barros, J.A.O., and Stoian, V., "Experimental and numerical assessment of the effectiveness of FRP-based strengthening configurations for dapped-end RC beams", Engineering Structures, Vol. 44, 2012, pp. 291-303.
[9] Cervenka, V., Jendele, L., Cervenka, J., ATENA Program Documentation. Part 1: Theory, Cervenka Consulting Ltd., 2012.
[10] Jendele, L., Cervenka, J., "Finite element modelling of reinforcement with bond", Computers & Structures, Vol. 84, No. 28, 2006, pp. 1780-1791.
[11] Aprile, A., Feo, L., "Concrete cover rip-off of R/C beams strengthened with FRP composites", Composites Part B-Engineering, Vol. 38, No. 5, 2007, pp. 759-771.
[12] Cervenka, J. and Papanikolaou, V.K., "Three dimensional combined fracture-plastic material model for concrete", International Journal of Plasticity, Vol. 24, No. 12, 2008, pp. 2192-2220.
[13] SR EN 12390-1-4:2002. Testing hardened concrete – Parts 1–4; 2002.
[14] SR EN 10002-1:2002. Metallic materials – Tensile testing – Part 1: Method of test at ambient temperature; 2002.
[15] Comité Euro-International Du Béton (CEB), "CEB-FIP model code for concrete structures", Lausanne, Switzerland; 1990.

Manufactured sand crushing process parameters: short review and evaluation for sand performance in fresh concrete

Rolands Cepurītis
B.Sc. Eng., M.Sc. Eng, PhD Candidate
Norcem AS, R&D Department
c/o NTNU, Department of Structural Engineering
Richard Birkelands vei 1A,
NO-7491 Trondheim, Norway
E-mail: rolands.cepuritis@norcem.no

ABSTRACT

Effect of manufactured sand crushing process parameters on performance of crushed fine aggregates in fresh concrete has been evaluated. Results indicate that the two most important parameters are the number of crushing stages used, reflecting the reduction ratio of the cone crushers, and the crusher type (cone or VSI) used for the last stage. VSI tip speed itself seems to be of a second order of importance; however, changes in fresh concrete rheology were observed when materials processed at high (45 m/s) and low (60 m/s) tip speeds were tested in concrete.

Key words: Crushed sand, manufactured sand, crusher, crushing process, fresh concrete, rheology, slump, plastic viscosity, yield stress.

1. INTRODUCTION AND BACKGROUND

For aggregate producers concrete aggregates are end products, while, for the concrete manufacturers, aggregates are raw material to be used for mix design and concrete production. Because of this, there is often lack of an "aggregate-concrete chain" in the research done so far. It is mostly either aggregate producers or researchers investigating the effect of crushing process variables on the properties of aggregate or experiments following the principle that is common for a lot of concrete producers – "*give us what you have, just make sure it is always the same*". However, such an approach is not driving the overall development in the right direction. It is therefore recommended to implement the full "*aggregate-concrete chain*" in order to see the issues connected to the production and use of crushed fine aggregate from a wider angle and thus gain maximum benefit for the society. Such an approach is attempted in the given study.

1.1 Effects of crushing process parameters on fine aggregate characteristics

Close to two decades ago one of today's recognised aggregate crushing process engineers Jarmo Eloranta has written in his Ph.D thesis [1]: "*In many instances rock crushing can be considered to be more art than science. One reason for that is that this industry on a global basis is such a*

small niche that the companies involved have not had the resources nor felt a real need to study what is happening inside their crushers."

After Eloranta's [1] statement the situation has been somewhat improved, both due to his own research efforts and following a global trend, when with the development of concrete technology the demand for high quality aggregates is steadily increasing. Already a little later after Eloranta [1], Mahonen [2] considers the crushing process variables important for coarse aggregate quality quite clear. However, he also emphasizes that factors affecting on the quality of crushed fine aggregate are not so distinct, the main reason being that there is hardly any research made for the sand size particles. He proposes a chart (Figure 1) based on the experience from the coarse aggregate particles that presents the parameters affecting the quality of crushed sand.

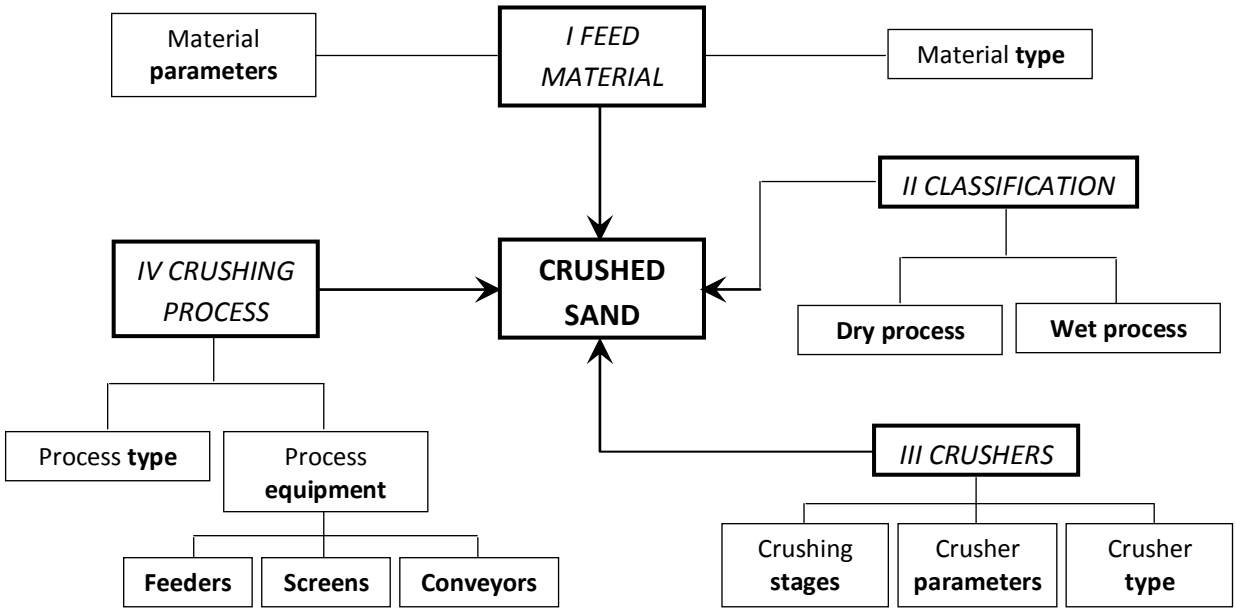

Figure 1 – Factors affecting the quality of crushed sand (reproduced and modified from [2])

It can be seen from Figure 1, that, in general, it is a complicated task to control the production process of crushed sand due to many variables involved. It is also obvious that investigation of all the many parameters is a very wide topic. Thus, the previous published research with respect to the influence of the processing techniques has mainly been narrowed down to the parameters under the group III, i.e. "*CRUSHERS*". In particular, the two studied parameters have been crusher type for the last crushing stage, i.e. cone crusher (Figure 2) or Vertical Shaft Impact crusher (VSI) (Figure 3), and influence of the VSI tip speed (Figure 3). This is natural, since these parameters are known to considerably affect the shape of coarse aggregates. Some of the general knowledge regarding this is illustrated in Figure 4, as proposed by Schouenborg et al. [3] during the ECO-Serve Seminar "*Challenges for Sustainable Construction: the "concrete" approach*" in 2006.

Figure 4 suggests that the crushers used for aggregate production today are generally designed to give the maximum quality for coarse aggregate [3]. On the other hand, those are also used for fine aggregate production with two key pieces of equipment being the same, i.e. cone crushers and VSI crushers. Impact crushers like VSI break the rock by hitting the material, thereby giving rock a sudden blow of high energy (Figure 3). While the cone crushers break the rock by compression (Figure 2) [2]. As the advantage of the cone crushers usually the ability of limiting

the amount of fine waste material produced is given, while the disadvantage is the poor shape in most fraction sizes [4-5]. The performance of VSI crushers is considerably different from cone crushers. They are capable of producing equidimensional particles in all size range, while the disadvantage is the large amount of fines generated [4-5]. However, as already mentioned, Figure 4 also indicates that it is still not clear how the particle shape of finer (≤ 2 mm) and especially the filler (≤ 125 µm) particles is affected as a result of different crushing techniques.

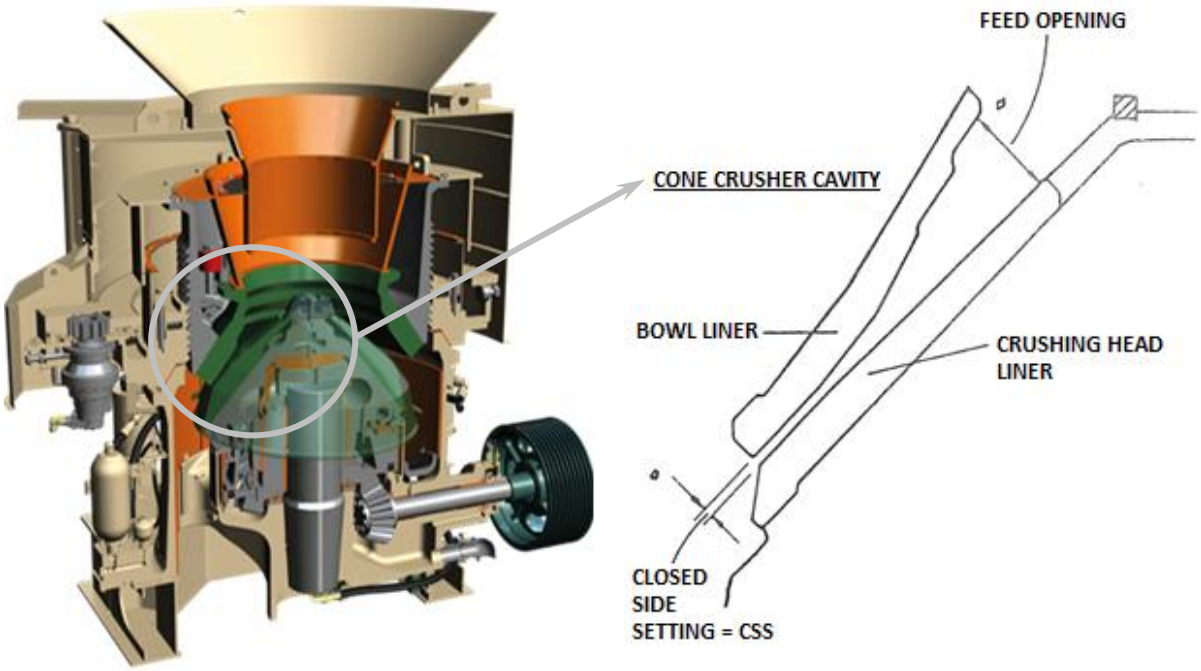

Figure 2 – Cross section of a cone crusher and the closed side setting (CSS) concept; CSS is the minimum distance between head liner and bowl (concave) liner at the discharged end of the cone crusher's crushing cavity [source: modified from Metso minerals; provided by T. Onnela]

Closed side setting or CSS, as indicated in Figure 2, is the minimum distance between liner and concave at the discharged end of the cone crusher's crushing cavity [1]. Particles with size near to CSS tend to be the most equidimensional of the crusher discharge product. In practice, 0.7 x CSS – 1.3 x CSS sizes have a good cubical shape (Figure 4) [2]. It is assumed, that greater CSS (20 mm) in the final stage leads to more equidimensional shape of fines, because material coarser than sand is crushed several times (particles not passing the sieve are re-crushed) and because more interparticle crushing occurs [2].

Recently two studies by Bengtsson and Evertsson [4, 6] have been carried out. They investigated the effect of crusher type and VSI tip speed also on particles smaller than 2 mm. Two types of crushers were used for the experiments: a cone crusher of type Hydrocone (Sandvik) with a medium chamber and a VSI crusher with rock box and no cascade flow, which was run at three different rotor speeds. The used tip speeds and the model of the VSI have not been specified. Both of the crushers operated in open circuit and the feed to the cone crusher was of a size 32-64 mm, while the VSI was fed with 11-16 mm and 11-12 mm fractions. The feed material used in the study was tonalite (igneous intrusive rock of a felsic composition). In addition, a reference natural fine aggregate was included in the study. After crushing, the 0.063-2 mm fractions and corresponding natural aggregate particles were analysed by determining the F-shape. As described by Bengtsson and Evertsson [6], F-shape is the aspect ratio F_{min}/F_{max} that is calculated by dividing the minimum Feret diameter (F_{min}) of the cross section of the particles

by their maximum Feret diameter (F_{max}). The results revealed that in the whole analysed range (0.063-2 mm) the F-shape of the natural gravel was considerably better than that of the crushed materials. Analysis of the crushed material results indicated that if the tip speed of a VSI is low, the fine aggregate will have poorer F-shape than the cone crusher's products; while the high VSI tip speed products will have a better shape than the products from the cone crusher. The given relationship was valid in all the range from 0.063-2 mm, what indicates that the crushing process can not only be crucial to the shape of the coarser sand fractions but can also determine shape of the filler (≤ 125 µm) fractions. However, it must also be noted that for the particle sizes below 250 µm, shape difference between natural gravel and crushed materials became greater. Bengtsson and Evertsson [6] have also studied the flow time and void content (loose packing) of the same fine natural gravel, cone crusher and VSI product particles with a New-Zealand's flow cone according to NZS 3111. When the mass flow (g/s) was plotted against different particle sizes, the high VSI tip speed material is then placed between natural gravel and cone crushed material. It can also be noted, that when the particles size is decreasing the VSI product material appears more similar to natural gravel than cone product fine aggregate. In general, the trend of void content results for the 0.063-2 mm fractions were similar as described for the mass flow.

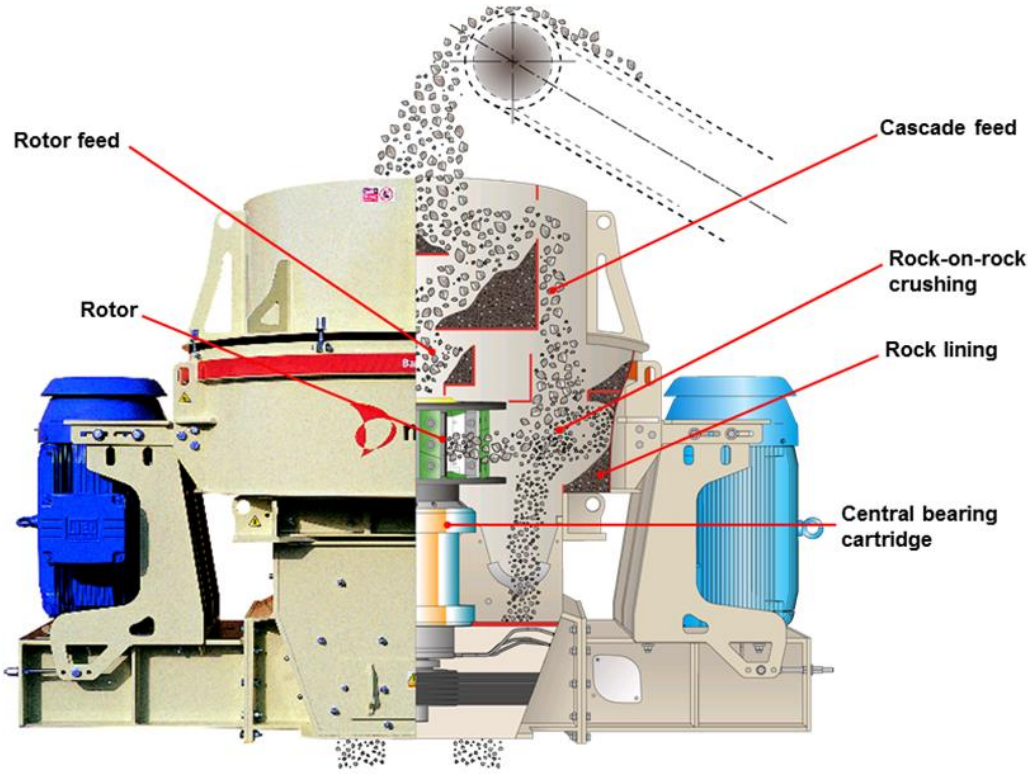

Figure 3 – Cross section of a vertical-shaft impactor (VSI) in operation and the VSI tip speed concept; VSI tip speed is to be understood as tangential velocity of the rotor in m/s [source: Metso minerals; provided by T. Onnela]

Analysis of 0/8 mm fine aggregate (granulite = medium to coarse grained metamorphic rock, composed mainly of feldspars) samples after different crushing processes have also been done by Gonçalvet et al. [7]. The rock was crushed by Hydrocones H4000 and H3000 (both Sandvik) and a BARMAC 3000 VSI (Metso Minerals). Some of the material was subjected to classification in order to partially remove the fines (≤ 75 µm). Gonçalvet et al. concluded that particles produced by impact crushing produced intermediate values of sphericity ($4 \cdot \pi \cdot projected\ area\ of\ particle / perimeter^2$) and F-aspect-ratio (inverted value of F-shape) when compared to natural fine aggregate and cone-crushed material, with the latter found to

produce the flakiest material. Particle shape was found to be varying depending on the particle size (size range between 0.1-2 mm was analysed). Flakiness increased as size decreased for the cone-crushed material, to lesser degree also the VSI crushed material, while being almost independent of size for a reference natural glaciofluvial aggregate. The unclassified impact crusher product presented the highest compacted packing density, while classified product from cone crusher had the lowest compacted packing density. It must also be noted here that the same trend with the increase in crushed particle flakiness in the filler fractions was observed in the study by Bengtsson and Evertsson [6].

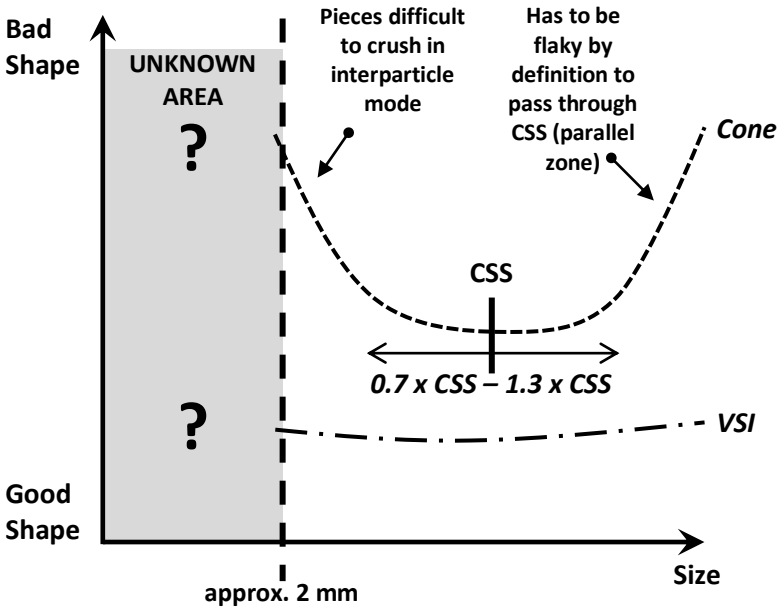

Figure 4 – Effect of cone crusher and VSI crusher on shape of different aggregate particle sizes (reproduced and modified from [3])

Gonçalves et al. [7] have also investigated the effect of fine natural and crushed (crushed by different crushers as described above) aggregate on workability of mortars. They concluded that for a w/c ratio of 0.50 all mortars present nearly the same workability (measured using a flow-table), regardless of the particle shape, grading or fines content. For a lower w/c of 0.40, mortars prepared with natural aggregate presented better workability than those prepared with manufactured fine aggregate. The most significant difference was found to be between mixture prepared with natural fine aggregate and mixture prepared with unclassified cone crusher product, the difference in flow being 14%. For the mortar with unclassified VSI product the consistency, when compared to natural sand, was only reduced by 6%.

Gram et al. [8] have presented results where the improvement of sand particle (0.063-4 mm) shape after VSI crushing has been investigated with the New Zealand's flow cone according to NZS 3111. They found that both the flow speed (g/s) and the void content (loose packing) improved considerably after the VSI crushing for all the particles sizes tested. However, the same as reported by Gonçalves et al. [7] and Bengtsson and Evertsson [6], the improvement was more pronounced in the coarser fractions, i.e. 0.5-4 mm in this case. Gram et al. [8] also investigated the effect of VSI crushing on the flow of mortars at w/c ratio of 0.6. The grading of the two 0/4 mm materials (before and after the VSI) was adjusted to be similar. Then a mini-cone (100 mm bottom diameter) test gave the following results: 118 mm for the material acquired before the VSI and 135 mm after the VSI crushing.

1.2. Effect of fine aggregate characteristics on concrete rheology

The effect of aggregates on the rheological properties of concrete have been studied rather extensively in the past decades, since they normally consume at least 75% of the total volume and thus it is natural to assume that aggregate characteristics will have a rather pronounced

effect on the flow of the mix. However, most of the research has been done with emphasis on the coarse aggregates and not the sand and filler fractions. This is probably since historically concrete has mostly been produced with natural glaciofluvial, fluvial and moraine fine aggregates, what means that the total amount of fines was low and the shape properties of different sands were fairly similar. Then the particle size distribution (PSD) of the natural sand and the presence of deleterious microfine particles, such as clay, silt or shale, were generally thought to be the main performance criterion. When the interest on using the co-generated leftovers from quarrying as crushed sand for concrete aroused, due to the lack of natural sand resources or simply due to economic and environmental issues, it was soon realised that the influence on the rheology of concrete of crushed sand is much more complicated than only the two mentioned parameters. This is because the shape of the crushed sand particles varies to a much greater extent, the amount of fines and their characteristics are different and so is the sand grading.

To some extent the knowledge from crushed coarse aggregates can be directly translated to crushed sand, however, one must remember that in practice the two particle size groups are quite different, i.e. while the coarse aggregate particle sizes range is in the order of 10, it is in the order of 10^3 for the sand size particles. This also suggests that most of the specific surface in the aggregate is concentrated in the sand and especially the filler fractions, since it is known that ratio of surface area to volume increases exponentially with decreasing particle size [9]. The assumption of the different effects from fine and coarse aggregates was confirmed already in 1967 by Wills [10] who studied nine different fine and coarse aggregates. He found that an equal change in shape characteristics caused fine aggregates to increase the water demand of the mix two to three times more than the coarse aggregates. This suggest that, when discussing the effects of any aggregates in concrete, one must also remember the fundamental findings by Krieger and Dougherty [11], who proved that the effect of solid particles on the flow in a concentrated suspension (such as concrete, mortar and cement paste) will firstly and mostly depend on their normalised solid concentration, i.e. the maximum packing fraction $\phi/\ \phi_m$ and only then on shape and other characteristics. In terms of concrete, this means that the found phenomena of the effect on the fine particle characteristics will depend on the concrete mix design parameters, such as w/c ratio, concrete type (conventional, SCC, high performance etc.) and the volume fractions of aggregates and cement paste.

A thorough study on the effect of different crushed and natural fine aggregate (0-4 mm) characteristics on the slump-flow value of concrete has been carried out by Järvenpää [12]. His studies followed the Particle-Matrix concrete workability model as introduced by Mørtsell [13], meaning that he treated the characteristics of 0.125-4 mm and 0-0.125 mm sand fractions separately. The Particle-Matrix concrete workability model for proportioning regards all particles > 0.125 mm as particle phase dispersed in lubricating matrix made up of all fluids (water, admixtures etc.) and particles (binder, filler etc.) ≤ 0.125 mm [13]. Concrete flow would then depend only on properties of the two phases and the volumetric relation between them. The method has been used in Scandinavian countries (especially Norway) by many practitioners for more than a decade and has proven to be very useful. Järvenpää [12] characterised both sand fractions (0.125-4 mm and 0-0.125 mm) with different methods and then used a statistical modelling approach to derive a model that related the characteristic properties of sand to the measured slump-flow values of two concrete qualities at w/c ratios of 0.65 and 0.58. Those had two different cement contents representing mixes with high (350 kg/m^3) and low (300 kg/m^3) paste volume, accordingly. Slump-flow measurements were preferred over slump values because Järvenpää [12] found the first to have a higher repeatability. The aggregate composition and grading of all the sands was normalised to be equal for all the concrete mixes. The acquired

flow model of Järvenpää [12] indicated that, when the aggregate grading was kept constant, the shape (flakiness, angularity and elongation) parameters and particle porosity of the 0.125-4 mm fraction were the two most important parameters affecting the fresh concrete flow. Even though the amount of paste was the decisive parameter in determining the general level of flow value, the fine aggregate characteristics could exceed the effect of paste difference in some extreme cases. The results also indicated that the influence of shape characteristics prevailed when the amount of paste was low, however, the differences could mostly be overcome when enough of paste was available. The presence of superplasticizer of a sulphonated naphthalene formaldehyde type enhanced the differences in the fine aggregate quality. Järvenpää [12] also assumed that the 0.125-4 mm fraction porosity was important because higher particle porosity will lead to higher water absorption and decreased amount of water available for concrete flow. However, porosity will only be an important parameter if concrete mix design is based on bone-dry fine aggregates, which is considered to be rather rare by the author of this paper.

Westerholm et al. [14] have also studied the effect of 14 (1 natural and 13 originating from crushed granitoid rocks) 0/2 mm fine aggregate characteristics on the rheological properties (yield stress τ_0 and plastic viscosity μ) of mortars at w/c ratio of 0.5. 635 kg/m^3 of cement and a polycarboxylate based superplasticiser were used for the mixes. The grading and thus also the fines content of the mixes was not normalised as in the study by Järvenpää [12]. In one of the experimental series Westerholm et al. [14] also worked with mortars containing an inert artificial paste. The paste volume of these mixes was successively increased in three steps from a paste volume of 57% to 68%, by adding more of the artificial matrix. Thus, the mixes can be considered to represent mortars which contain different amounts of cement at a given w/c-ratio. Their results [14] indicated that the higher yield stress of the crushed aggregate mixes (as compared to the natural sand) mainly originated due to the relatively high amounts of fines often found in crushed fine aggregate. They also report that the high amount of fines also contributed to the plastic viscosity by increasing the interparticle friction. However, the results also showed that the higher viscosity of the mortars with crushed fine aggregates is a particle shape effect. A change in the average F-aspect-ratio value of fraction 0.075-1 mm from 0.59 to 0.41 resulted in almost a three folded increase of the plastic viscosity. Their results also indicated that the effects of poorly graded and shaped fine aggregates could be eliminated or reduced by increasing the paste volume of the mortars.

In addition to the total fines content and shape of the crushed sand particles, the quality of the fines has also been reported to be a decisive parameter affecting on the fresh concrete workability. In particular, content of free mica particles in the fines has been demonstrated to be an important factor. This is since mica is flaky and laminated mineral which can considerably increase the water requirement of the mixes [15]. Apart from the presence of the free mica, PSD, as expressed through the specific surface, is considered to be strongly affecting the flow of filler modified cement pastes [13]. Finer filler (higher specific surface) is believed to result in reduced flow properties when compared to coarser reference filler having a lower specific surface area. Smeplass [16] has explained this by the adsorption of the free water on a larger total surface area.

1.3 Scope of the paper

The preliminary investigations on the effect from different crushing process variables have indicated that they have a detrimental influence on one of the most important properties of the sand particles, i.e. the shape, with a good chance to improve it in the whole range of sand size

particles, if the quarrying machinery is used to the best possible extent. However, a perfect model that can relate those improvements directly to concrete properties does not exist. Thus, it is not possible to judge if the improvements can be thought to be remarkable or not, or justify an investment into quarrying equipment, since the quarrying industry does not have a clear criteria. Or put it another way, as said by Baron William Thomson Kelvin [17]: "*I often say that when you can measure what you are speaking about, and express it in numbers, you know something about it; but when you cannot measure it, when you cannot express it in numbers, your knowledge is of a meagre and unsatisfactory kind …*"

The path from blasting the bedrock in a hard rock quarry, which in fact starts the aggregate crushing process, to mixing concrete in a batch plant and evaluating its performance at the building site is complicated and a huge amount of parameters are involved. Thus it is clear that in order to gain a substantial progress, on understanding which fine aggregate crushing processing process parameters are the most essential with respect to fresh concrete properties, a holistic approach is necessary. This paper is then an attempt of implementing such a holistic approach by investigating the given topic from a wider angle. Thus, developing a sophisticated concrete workability model is out of the scope and the given study has been mainly aimed at understanding the order of magnitude to which different crushed sand crushing processes can affect the fresh state properties (rheology) of concrete.

2. MATERIALS AND METHODS

2.1. Aggregate production plants and sand materials used for the study

Partly natural and crushed sand materials from five different plants have been included in the study. Four of the plants are hard rock quarries and one is a sandpit where the reference partly natural sand material was obtained from. The list of the plants along with the most essential information on the production process and the deposit type are summarised in Table 1. Layouts for some of the aggregate production plants can be found in the corresponding references as indicated in the last column of Table 1.

Table 1 – Description of the plants and the deposit types used for aggregate production

Plant No	Quarry name	Type	No of crushing stages	Crusher type used for the final stage	Settings for the final stage crushing	Rock type in the deposit	Crushability, %	Reference to plant layout
1	Årdal	Sandpit	-	-	-	Granite/ gneiss glaciofluvial and moraine deposit	-	-
2	Tau	Hard rock quarry	4	80% VSI/ 20% Cone	47 m/s (tip speed) 12-19 mm (CSS) 22-25 mm (stroke)	Mylonittic quartz diorite rock	23	[18]
3	Jelsa	Hard rock quarry	4	Cone	19-22 mm (CSS) 32 mm (stroke)	Granodiorite rock	34	[18]
4	Hokksund	Hard rock quarry	3	Cone	22 mm (CSS) 15 mm (stroke)	Gneiss diorite rock	41	[18-19]
5	Nord-Fosen	Hard rock quarry	3	Cone	20 mm (CSS) 20 mm (stroke)	Granite/ gneiss rock	61	-

As mentioned above and illustrated in Figure 1, the quality of crushed sand is thought to be affected by 4 groups of parameters, namely: *I Feed material properties*, *II Classification*, *III Crushers* and *IV Crushing process*. The present study aims at studying the effect of the parameters under the group III, i.e. *Crushers*. Thus, parameters from other three groups have been kept as constant as practically possible. With respect to group I, similar volcanic and metamorphic rock types have been chosen for the study. Even though, hardness of those is still quite variable (see Table 1), what will inevitably have some effect on the crusher performance and quality of the products. However, since hardness in terms of the crushability value is known, it can be accounted for when evaluating the results. Group II parameters are kept constant by normalising the filler (≤ 125 μm) content in the tested fine aggregates (see below). No particular means have been done to exclude the effect from group IV parameters; however, those are believed to some extent overlap with the group III and also to be of a much lower importance for the case than the first three groups.

In total, 21 different sand materials, obtained from the production processes in Table 1, have been used for the study. These are summarised in Table 2. As it can be seen from Table 2, all sand materials are divided into four groups:

- **Group I** (No 1-2) consists of partly natural sands (includes approx. 30% of crushed particles from crushing down oversize rock from the same deposit) obtained from the Årdal quarry. The crushed sand share particles are equidimensional [20]. The Årdal fine aggregate is a reference aggregate in most Norwegian concrete laboratories [21] and is usually denoted as NSBR sand. Concrete mixed with this type of sand normally has better workability, when compared to 100% crushed [21] and also most of 100% natural aggregates.

- **Group II** (No 3-8) consists of sands that are the commercial fine aggregate products in the quarries from Table 1. For some of those (see Table 2 for details) the D_{max} has been adjusted to 2 mm and the fines (≤125 μm) content normalised to 10%.

- **Group III** (No 9-14) consists of sands that have been produced by further re-crushing the final products from Tau, Jelsa and Hokksund quarries. This means that a 0/11 mm (for Tau) or 0/22 mm (for Jelsa and Hokksund) feed, as obtained after the final crushing stage, has been taken to a test plant and fed to a Metso minerals Barmac B5100SE VSI crusher, run at different tip speeds; followed by sieving to produce fraction with a D_{max} of 2 mm and normalisation of the crushed fines (≤ 125 μm) content to 10%. In this way the sands in this group have all been subjected to an additional impact crushing stage as compared to the corresponding materials in group II.

- **Group IV** (No 15-21) consists of sands obtained in the same way as in group III, the only difference being that in this case most of the crushed filler is removed, leaving only 1% passing the 125 μm sieve. An exception in this group is sand from Nord-Fosen quarry (N-CC-COM-0/2-1). It has not been subjected to the additional VSI crushing and is the commercial fine aggregate with D_{max} reduced to 2 mm and the initial crushed filler content reduced to the same 1% passing the 125 μm sieve.

PSD of sands No 1 to 14 are given in Figures 5 and 6. Sands No 15-21 are not included in order to make the chart easier to view, since these PSDs will be the same as for the corresponding materials from 1 to 14; with the only difference being the fines (≤ 125 μm) content. Results from flakiness index measurements of the fractions 2/2.5, 1.6/2.0 and 1.25/1.6 mm by using a

custom bar sieve set, flow time and loose packing (void content) results (obtained by the New Zealand's flow cone according to NZS 3111) are presented in Table 3.

Table 2 – Description and designations of the sands used for the study

Group of sands	Sand No	Type	Quarry	Fraction size, mm	Last step crusher type	VSI tip speed, m/s	Fines (≤ 125 μm) content, %	Designation	Description
I	1	Partly natural	Årdal	0/2	–	–	6.4	***NSBR**-0/2*	Commercial product after washing with adjusted D_{max}
	2	Partly natural	Årdal	0/8	–	–	5.1	***NSBR**-0/8*	Commercial product after washing
II	3	Crushed	Tau	0/2	20% cone/ 80% VSI	47	9.3	***T**-CC/IC-COM*	Commercial product after the last crushing stage and washing
	4	Crushed	Tau	0/2	20% cone/ 80% VSI	47	10	***T**-CC/IC-RAW*	The same as No 3 prior to washing and with adjusted filler content
	5	Crushed	Jelsa	0/2	Cone	–	10	***J**-CC-COM*	Commercial product after the last crushing stage and washing with adjusted filler content
	6	Crushed	Hokksund	0/2	Cone	–	10	***H**-CC-COM*	Commercial product after the last crushing stage with adjusted filler content and D_{max}
	7	Crushed	Nord-Fosen	0/2	Cone	–	10	***N**-CC-COM-0/2*	Commercial product after the last crushing stage with adjusted filler content and D_{max}
	8	Crushed	Nord-Fosen	0/8	Cone	–	9	***N**-CC-COM-0/8*	Commercial product after the last crushing stage
III	9	Crushed	Tau	0/2	VSI	45	10	***T**-IC-45-10*	Crushed/ sieved in the test plant
	10	Crushed	Tau	0/2	VSI	60	10	***T**-IC-60-10*	
	11	Crushed	Jelsa	0/2	VSI	50	10	***J**-IC-50-10*	
	12	Crushed	Jelsa	0/2	VSI	60	10	***J**-IC-60-10*	
	13	Crushed	Hokksund	0/2	VSI	45	10	***H**-IC-45-10*	
	14	Crushed	Hokksund	0/2	VSI	60	10	***H**-IC-60-10*	
IV	15	Crushed	Tau	0/2	VSI	45	1	***T**-IC-45-1*	
	16	Crushed	Tau	0/2	VSI	60	1	***T**-IC-60-1*	
	17	Crushed	Jelsa	0/2	VSI	50	1	***J**-IC-50-1*	
	18	Crushed	Jelsa	0/2	VSI	60	1	***J**-IC-60-1*	
	19	Crushed	Hokksund	0/2	VSI	45	1	***H**-IC-45-1*	
	20	Crushed	Hokksund	0/2	VSI	60	1	***H**-IC-60-1*	
	21	Crushed	Nord-Fosen	0/2	Cone	–	1	***N**-CC-COM-0/2-1*	Commercial product after the last crushing stage with adjusted filler content and D_{max}

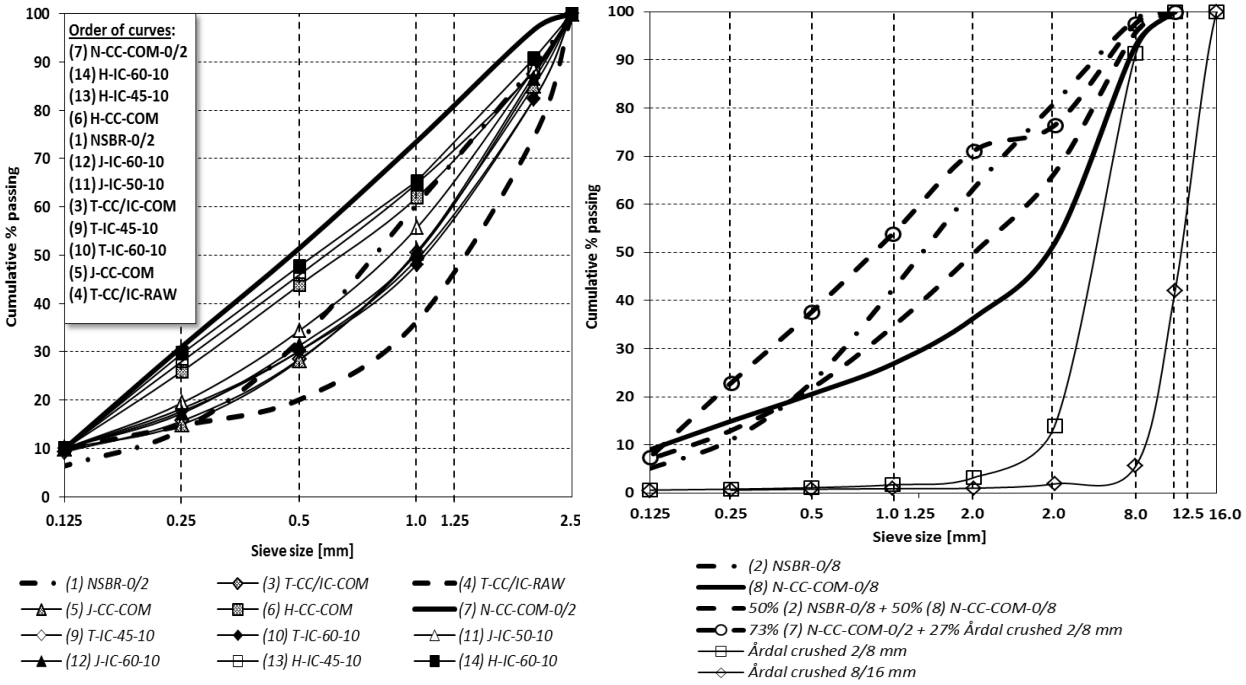

Table 3 – Results of sand characterisation

Group of sands	Sand No	Designation	Fineness modulus	Average flakiness index of 1.25-2.5 mm, %	Flow time in NZ flow cone, s	Loose packing
I	1	***NSBR**-0/2*	2.98	2.9	23.1	0.575
	2	***NSBR**-0/8*	3.76	-	-	-
II	3	***T**-CC/IC-COM*	3.09	24.1	31.2	0.561
	4	***T**-CC/IC-RAW*	3.44	20.2	28.69	0.556
	5	***J**-CC-COM*	2.11	20.2	29.96	0.544
	6	***H**-CC-COM*	2.70	32.0	28.12	0.539
	7	***N**-CC-COM-0/2*	1.37	22.0	28.97	0.517
	8	***N**-CC-COM-0/8*	4.47	-	-	-
III	9	***T**-IC-45-10*	3.10	16.6	30.8	0.563
	10	***T**-IC-60-10*	3.11	13.0	29.59	0.565
	11	***J**-IC-50-10*	2.92	13.9	27.76	0.571
	12	***J**-IC-60-10*	3.05	12.1	26.36	0.573
	13	***H**-IC-45-10*	2.63	18.8	27.63	0.545
	14	***H**-IC-60-10*	2.57	12.1	27.17	0.547
IV	15	***T**-IC-45-1*	3.10	16.6	30.15	0.566
	16	***T**-IC-60-1*	3.11	13.0	29.28	0.572
	17	***J**-IC-50-1*	2.92	13.9	28.3	0.566
	18	***J**-IC-60-1*	3.05	12.1	28.56	0.564
	19	***H**-IC-45-1*	2.63	18.8	30.18	0.541
	20	***H**-IC-60-1*	2.57	12.1	30.27	0.544
	21	***N**-CC-COM-0/2-1*	1.37	22.0	36.67	0.526

Since the effect of different crushed fines (≤ 125 μm) has also been investigated, PSD of the fines from all of the sands has been determined by a SediGraph (Figure 7).

2.2. Coarse aggregates and other concrete part materials

Crushed 2/8 mm and 8/16 mm coarse aggregates of a good shape from crushing down oversize rock in the Årdal sandpit (see Table 1) have been used for the concrete mix design. The grading curves of the coarse aggregate are provided in Figure 6.

The rest of the used materials include Norcem standard fly-ash cement (CEM II/ A-V 42.5 R) and a co-polymeric superplasticizer Dynamon SP-130 (long side-chains and dry solids content of 30%) from Rescon Mapei. Typical composition of the clinker for the cement is- C_3S: 60%, C_2S: 15%, C_3A: 8%, C_4AF: 10%; the cement normally includes approx. 4% of gypsum and 20% of fly ash, < 1.4% of Na_2O-eqv. and has a Blaine value of 450 m^2/kg (none of these values have been tested for the particular batch used).

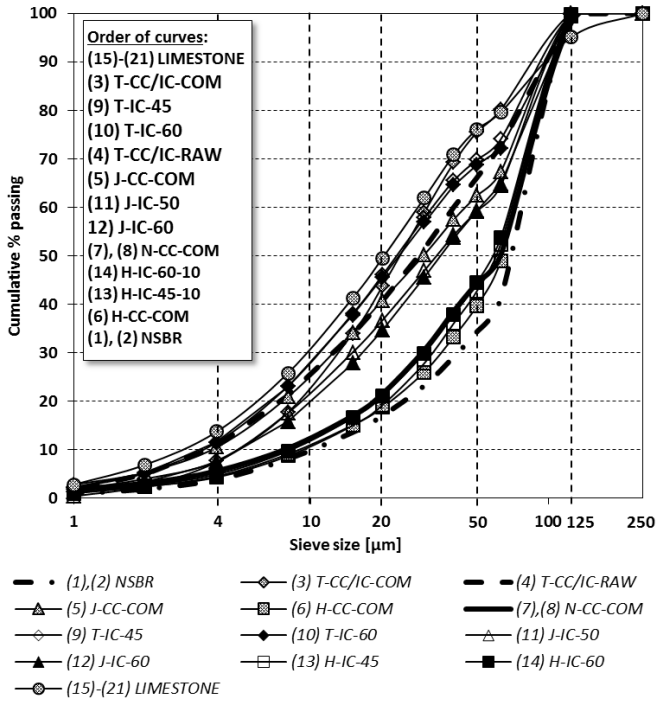

Figure 7 – PSD of fines (≤ 125 μm) from all the sands determined by a SediGraph

2.3 Concrete composition, mixing and testing

It is known from practical experience [21] (and also as indicated in the theoretical studies reviewed in Section 1.2), that the relative effect of aggregates in fresh concrete is dependent on the mix proportions, mainly including the paste (matrix) volume and w/c ratio. Since the amount of experimental work was limited, it was chosen to use a constant w/c ratio of 0.5 throughout the study. The value of 0.5 was suggested by a ready-mix concrete supplier (NorBetong AS, Norway) as being the most representative of the day-to-day production.

In total, 22 concrete mixes were prepared. This means one mix with each of the 21 sand materials (see Table 2) and a 22nd mix where sands No 2 (NSBR-0/8) and No 8 (N-CC-COM-0/8) were mixed together in a 50%/50% proportion on mass basis (densities of the materials are almost the same). For all the concrete mix designs 0/2 mm sand share was 45% of the total aggregate composition, while the semi-coarse and coarse fraction were divided 17% of 2/8 mm and 38% of 8/16 mm. In cases where the tested sand had a fraction size of 0/8 mm, the fine aggregate volume was increased to 45+17=62%, thus by the share of the 2/8 mm semi-coarse fraction (which was then omitted). For mixes with sands that had the intentionally reduced amount of initial crushed filler (sands No 15-21 in group IV), an additional amount of reference limestone filler was introduced in the mixes. PSD of the limestone filler is provided in Figure 7. The amount of the limestone filler used was such that the total filler content of the sands No 15-21 reached 10%, which is the same

as for the corresponding "parent" sands from groups II and III. This approach allowed studying the effect from different crushed fillers separately.

Particle-Matrix model proportioning approach (see Section 1.2) was utilised and matrix volume of 320 l/m^3 was chosen as suitable for the given aggregate combinations. The cement content of all the mixes was set constant at 342 kg/m^3; however, if the Particle-Matrix model is strictly applied then the content of the fines ($\leq$ 125 μm) in the sand fraction will affect the total matrix volume. Mixes with 10% of filler in the 0/2 mm fraction, i.e. mixes 4-7 and 9-21 were chosen as the reference for the given 320 l/m^3 of matrix at 342 kg/m^3 of cement. For the rest of the mixes (1-3, 8 and 22) it was chosen not to adjust the matrix content equal to the reference mixes in order to keep the cement content invariable. Thus, the total content of matrix for all of the mixes (see above) is as follows: (1) 310 l/m^3; (2) 311 l/m^3; (3) 318 l/m^3; (4-7) = 320 l/m^3; (8) 328 l/m^3; (9-21) 320 l/m^3; (22) 319 l/m^3.

With respect to the findings by Järvenpää [12], as discussed in Section 1.2, it must be noted that the water absorption of all the aggregates was measured and the mix composition was calculated on the saturated surface dry (SSD) basis, meaning that the given w/c ratio included only the effective water amount, i.e. water that is believed not to be absorbed by the aggregates. The water content of the mixes was then adjusted based on the aggregate water absorption values and moisture. Prior to mixing, the moisture content of all sands was normalized to 3% by rotating approximately 30 kg of sand and necessary amount of added water in a 50 litre plastic drum until a homogeneous moisture distribution was achieved. Then the sample was left still for at least 24 hours to be sure that the water absorption level of the aggregate has reached the saturation point. Before concrete mixing, moisture content of all the aggregates was measured once again. The concrete was mixed in a 60-litre Eirich laboratory paddle-pan mixer. The batch size was 33 litres. Mixing sequence according to Table 4 was utilised.

Table 4 – Concrete mixing sequence

Mixing step No.	Time line, min	Action
1	0.0-1.0	Dry mixing
2	1.0-1.2	Addition of water and admixture
3	1.2-3.0	Wet mixing
4	3.0-5.0	Rest*
5	5.0-6.0	Wet mixing

*During the rest it was assured that nothing was stuck at the bottom of the mixing pan.

The following fresh concrete properties were determined right away after the mixing: slump according to EN 12350-2, air void content according to EN 12350-7, density according to EN 12350-6 and Bingham parameters – τ_0 and μ. On average 15 minutes after mixing were used for measurement of fresh concrete slump, air void content and density before it was transferred to the viscometer. Concrete rheological measurements have been performed with a BML-Viscometer 3 by ConTec. BML-Viscometer 3 is a coaxial cylinders viscometer having a stationary inner cylinder and rotating outer cylinder with the following geometry: inner radius = 100 mm, outer radius = 145 mm and height = 199 mm. Standard rheological measurement set-up was used consisting of down flow-curve measurement (7 points from 0.49 to 0.09 rps). After the measurement, it was verified if the steady-state flow has been reached for all of the measurement points to assure correct determination of the Bingham parameters.

Repeatability of the measuring procedure was examined by repeated mixing and testing of a concrete mix (Table 5). The same procedure, materials and a similar mix design as for the given

study were used by the same operator; however, the mix is not part of the testing program presented here. Determined variation of the most relevant parameters is provided in Table 5.

Table 5 – Repeatability of the fresh concrete characterisation tests

Test No	Slump, mm	Air void content, volume-%	Density, kg/m^3	τ_0, Pa	μ, Pa·s
1	170	4.1	2321	168.3	9.3
2	180	4.1	2304	173.4	11.8
3	175	4.0	2305	168.3	9.9
Mean value	**175**	**4.1**	**2310**	**170.0**	**10.3**
Standard deviation	**5**	**0.1**	**10**	**2.9**	**1.3**
Variation coefficient, %	**2.9**	**1.4**	**0.4**	**1.7**	**12.3**

3. RESULTS AND DISCUSSION

Not all of the measured fresh concrete properties are reported. Density and air-content measurements were mainly made in order to assure that those values lie in the borders of acceptable variation. The density allows controlling if the weighting and mixing of the mix constituents have been performed correctly, while determining the air-content is important because an excessive amount of air is known to have an effect on concrete rheology. The air content of all the mixes varied between 1.3 to 3.2% with an average value of 2.7% which is by only 0.7% higher than the designed value of 2.0%. Also the variation between the measured and designed density was very low. Corrected concrete compositions of all the mixes were calculated according to the measured air void content and density. The results revealed that the average variation of the matrix volume of all the mixes has been only 0.5%. Based on this, it was estimated that the effect of density and air-void content variations on measured concrete rheology is negligible. In addition, all of the mixes can be classified as very stable based on visual observations.

Three different parameters describing fresh concrete rheology have been determined, namely slump and two Bingham parameters, as measured with the BML-Viscometer, i.e. yield stress (τ_0) and plastic viscosity (μ). However, only the slump and the plastic viscosity results are reported here. This is because a strong relationship between the yield stress and the slump value is anticipated; due to the nearly invariable matrix content (320 l/m^3) of the mixes. Such a relationship and its dependency on the matrix content is reported in [18; 22-23] and is not surprising assuming that the concrete flow after lifting the slump cone continues until the stress induced by the gravity is higher than the yield stress (τ_0). This is confirmed also for the given study, since the squared linear correlation coefficient between yield stress and slump values was calculated to be R^2=0.9075. Thus, for the current work, reporting both of these values would basically provide the same information. The most important difference is, however, that yield stress gives a result in fundamental physical quantities that can then be further used in, for example, fluid dynamics calculations [24]. However, since the purpose of the study was to investigate relative differences between the effects of various parameters, the slump value was preferred over the yield stress due to its greater practical relevance.

The results have been presented in three different sets: Figures 8-11 for the first, 12 and 13 for the second and 14 and 15 for the third set. The first set of results includes mixes No 1, 3-7 and 9-14 with 0/2 mm party natural reference sand (NSBR-0/2) and 0/2 mm crushed sands with normalised amount (10%) of the original crushed filler. It can be seen from the results, that the

reference partly natural sand has shown the most favourable rheological results, i.e. the highest slump value and the lowest plastic viscosity. When the comparison of the natural and crushed sands is based only on the slump test, the differences between the natural and the best of the crushed sands seem rather limited, i.e. in the range of only 20-50 mm of slump. In practice this difference could be overcome by adding a small additional amount of water reducing admixture. However, the plastic viscosity measurements, as presented on Figure 9, reveal that, while the difference in the slump (Figure 8) between the partly natural sand and the crushed sands in some cases is rather negligible, at the same time the discrepancy in the plastic viscosity values can be much larger. For example, mixes with crushed sands T-CC/IC-RAW and J-CC-COM have slump values of 180 mm as compared to the reference value of 235 mm determined for the mix having the partly natural sand NSBR-0/2. However, when the plastic viscosity of the same sands are compared, the plastic viscosities of the crushed sands are found to be 140 [Pa·s] / 40 [Pa·s] = 3.5 times higher. This is a quite considerable difference. In practice, if such a concrete would be delivered to a construction site with a desired slump value determined based on the experience with natural sand concrete, the workers would most likely describe the mix as "harsh" and hard to work with. This is since due to the higher plastic viscosity, the same muscle force has to be applied for a longer period of time, in order to move the fresh mix for the same distance, as compared to concrete with a lower plastic viscosity. The same will apply to the required compaction energy, i.e. time for working with a poker vibrator at a given spot. The described reveals the importance of using the rheological two parameter (yield stress/ slump/ slump-flow or other "stoppage test" and plastic viscosity) approach when the performance of crushed sand in fresh concrete is to be evaluated.

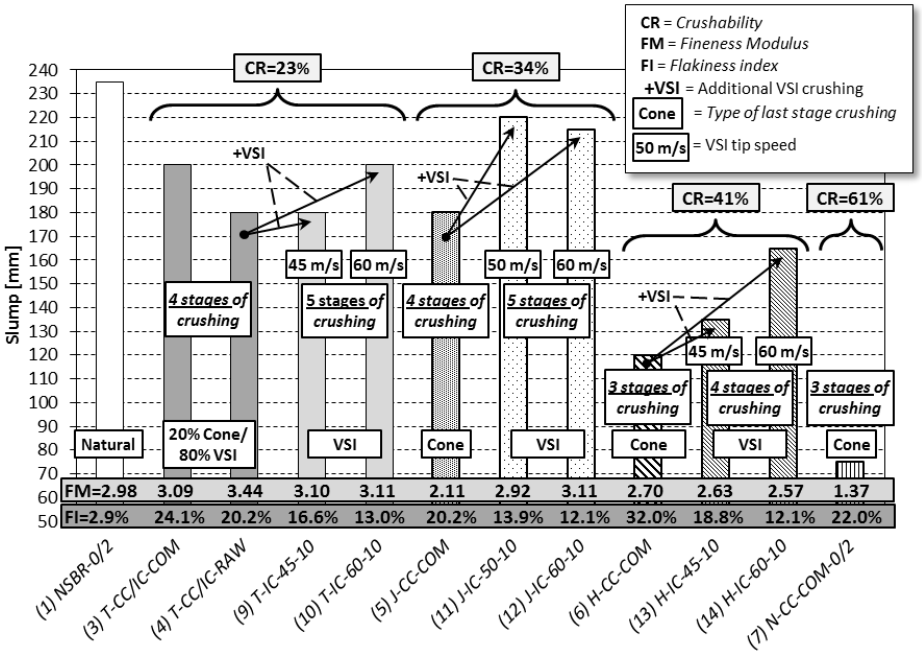

Figure 8 – Slump values for the first set of results

When it comes to the effect of different crushing process parameters on the performance of the mixes from the first data set (Figures 8 and 9), a couple of interesting trends can be observed. The results indicate that materials subjected to 4 and 5 stages of crushing performed better than materials crushed only in 3 steps. While the 5th step, where applicable, can be attributed to the improvements believed to arise from the VSI shaping, the better performance of the materials subjected to 4 stages of only gyratory and cone crushing it at least partly a result of lower reduction ratio of the cone crushers. In the coarse aggregate production technology reduction ratio is a well-known criterion that allows improving shape of the cone crusher products [1, 25]. Reduction ratio (also crushing ratio) is the ratio between the size of feed and outcoming product [1]. When more crushing stages are present, the maximum feed size to the cone crushers can be reduced resulting in a better shape, since reduced reduction ratio will allow for more interpaticle crushing in the crushing chamber.

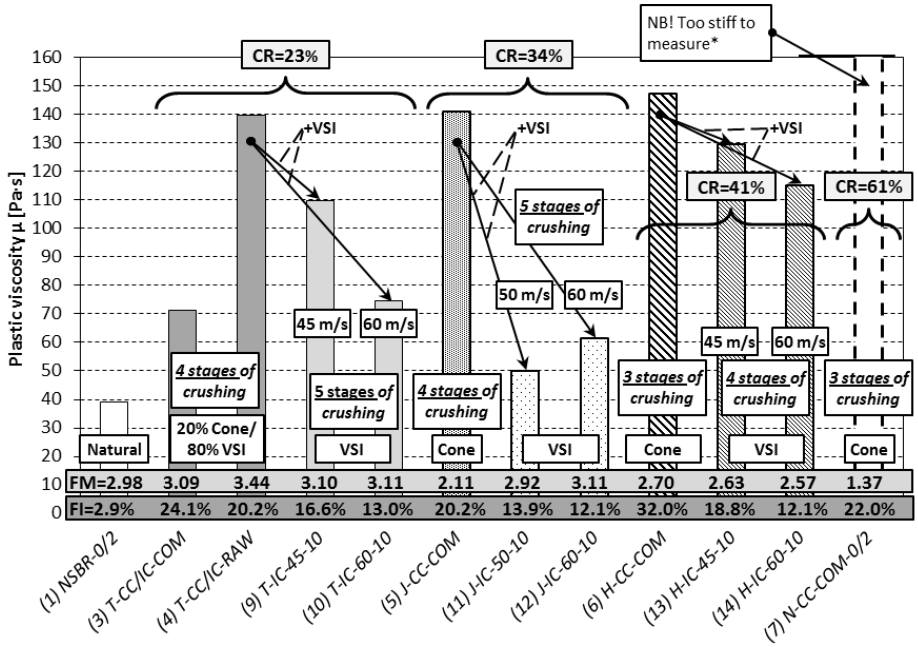

*Figure 9 – Plastic viscosity values for the first set of results; *mix was too stiff for measurements in the BML-vicometer*

The results presented in Figues 8 and 9 also indicate that differences in the 0/2 mm material properties, as a result of crusher type for the last crushing stage (cone or VSI) or the VSI tip speed used, can cause measureable changes to the fresh concrete rheological properties. Slump increase due to additional step of VSI crushing (20-45 mm of slump) seems to be somewhat higher than changes due to VSI tip speed increase (5-30 mm of slump). However, the influence of the additional VSI crushing and the utilised VSI tip speed seem much more pronounced in the case of plastic viscosity measurements. It also seems that the VSI tip speed increase from 45 m/s to 60 m/s gives a bigger benefit that increase from 50 m/s to 60 m/s. This means that for crushed sand production running VSI at a very low rotor speed in order to increase the capacity or reduce the filler content/ wear costs is generally not recommended, if the material is intended for use in concrete. In this case a cone crusher that generates fewer fines is probably preferable.

The results also indicate that some of the effects cannot be observed in terms of change in the slump value, but are rather noticeable in the plastic viscosity measurements. For example, 80% of the T-IC-D-45-10 sand has first been crushed with a Rotopactor BM 300 (Kemco) at tip speed of 47 m/s and then re-crushed at the test plant with a Barmac 5100SE VSI at tip speed of 45 m/s; while 80% of the T-CC/IC-RAW fine aggregate is processed only with a Kemco Rotopactor BM 300 at tip speed of 47 m/s. The results indicate that even though the shape of T-IC-D-45-10 particles is slightly better than the shape of the T-CC/IC-RAW material, there is no measurable difference between them in terms of the slump value, while the decreased plastic viscosity due to additional VSI crushing can be observed on Figure 9.

Modelling crushed sand characteristics-concrete rheology relationship was not the main goal of this paper, though some efforts were put into trying to relate the determined sand characteristics (Table 3 = fineness modulus, average flakiness index of 1.25-2.5 mm fraction, flow time and loose packing) to the observed rheological behaviour for the first set of result. The determined squared linear correlation coefficients are summarised in Table 6. Two of the relations are also presented as plots on Figures 10 and 11. The results in Table 6 indicate that for the given sands and the used mix design, the fineness modulus (FM) has a limited influence on both slump value and plastic viscosity, flakiness of the 1.25-2.5 mm fraction can only to some extent be attributed to the effect on the slump value, while the flow time does not seem to be able to predict any of the two rheological properties. On the other hand, loose packing or the loose state voids content

of the sand fractions has a much better correlation to the rheological properties of concrete. This is, however, not surprising since the volume of sand in the total aggregate composition was considerable and thus could have dominated also the packing values or void content of the total 0/16 mm aggregate composition. The latter parameter has been reported to have a remarkable influence on the rheology of fresh concrete [26].

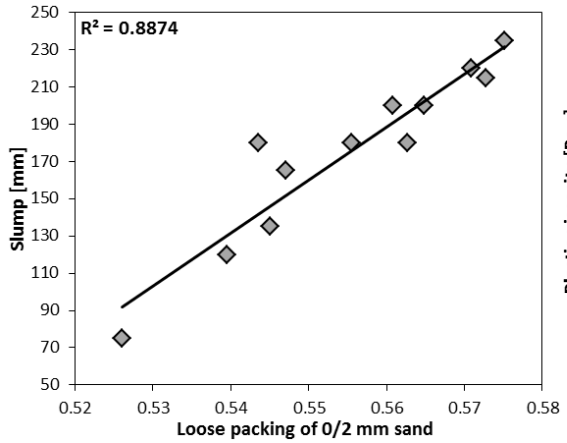

Figure 10 – Slump vs. loose packing of 0/2 mm sand fraction for the first set of results

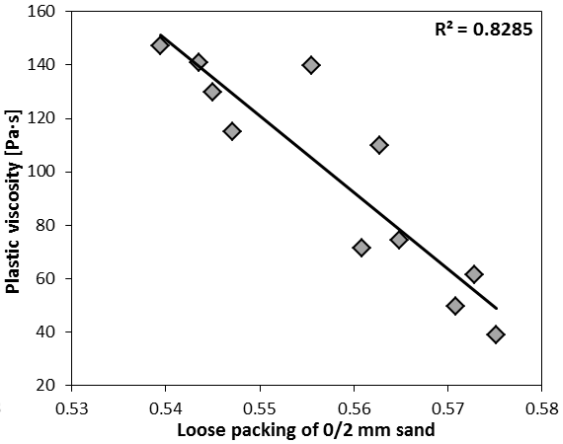

Figure 11 – Plastic viscosity vs. loose packing of 0/2 mm sand fraction for the first set of results

Table 6 – Squared linear correlation coefficients of 0/2 mm sand fraction characteristics-concrete rheology relations for the first set of results

Concrete rheological parameter and 0/2 mm sand characteristic	Fineness modulus (FM)	Flakiness index of 1.25-2.5 mm fraction	Flow time in NZ flow cone	Loose packing
Slump	0.4228	0.6418	0.0826	0.8874
Plastic viscosity	0.4600	0.1224	0.1613	0.8285

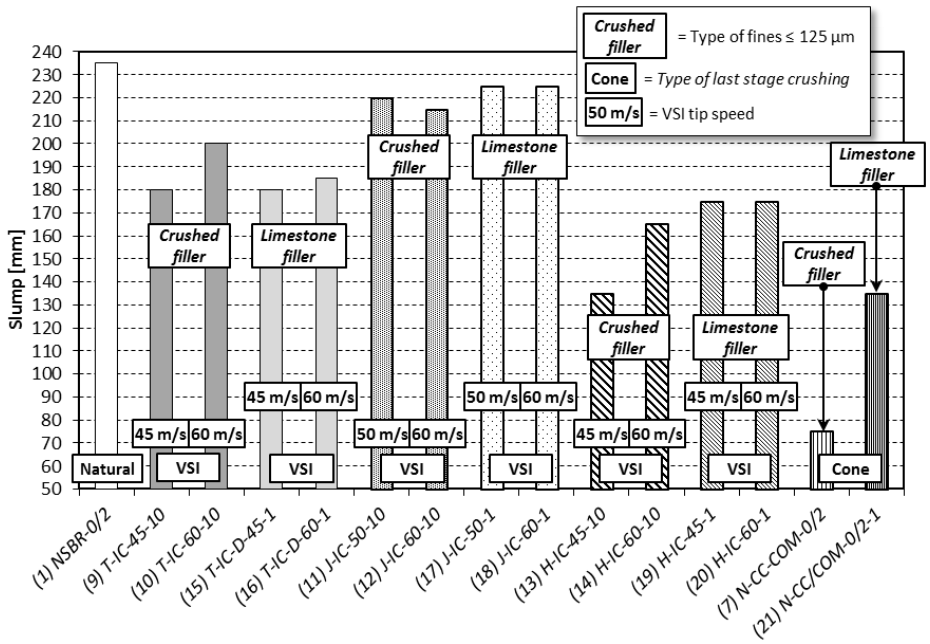

Figure 12 – Slump values for the second set of results

The second set of results includes concrete mixes with crushed sands that had reduced (from 10% to 1%) crushed filler content, i.e. mixes No 15-21. The missing 9% of crushed filler were replaced by industrially produced limestone reference filler on volume basis. This allows investigating if the effect from different crushing process variables (VSI tip speed in this case) can affect the properties of the filler (≤125 µm) fraction to the extent measurable in concrete rheology experiments. Results of these investigations are presented in Figures 12 and 13. It must

also be noted that previously reported investigations [6] have indicated that VSI tip speed can have an effect on particle shape also in the filler particle size range. The results from the given study reveal (Figures 12 and 13) that in general changes in the filler type did not have a great effect on the rheological parameters, with an exception of the N-CC-COM-0/2 sand. The results also show that when the reference filler is used, the difference due to varying VSI tip speeds is eliminated in the case of the slump value measurements. The effect on the plastic viscosity is similar since for 2 out of 3 materials the difference due to VSI tip speed variations is reduced. So in general, the results support the observations by Bengtsson and Evertsson [6], that also the filler fraction properties can be affected by the crushing process. The most relevant effect is believed to arise from the changes in shape of the filler particles as reported by Bengtsson and Evertsson [6], since the grading of the fines is not affected considerably due to different VSI tip speeds (Figure 7).

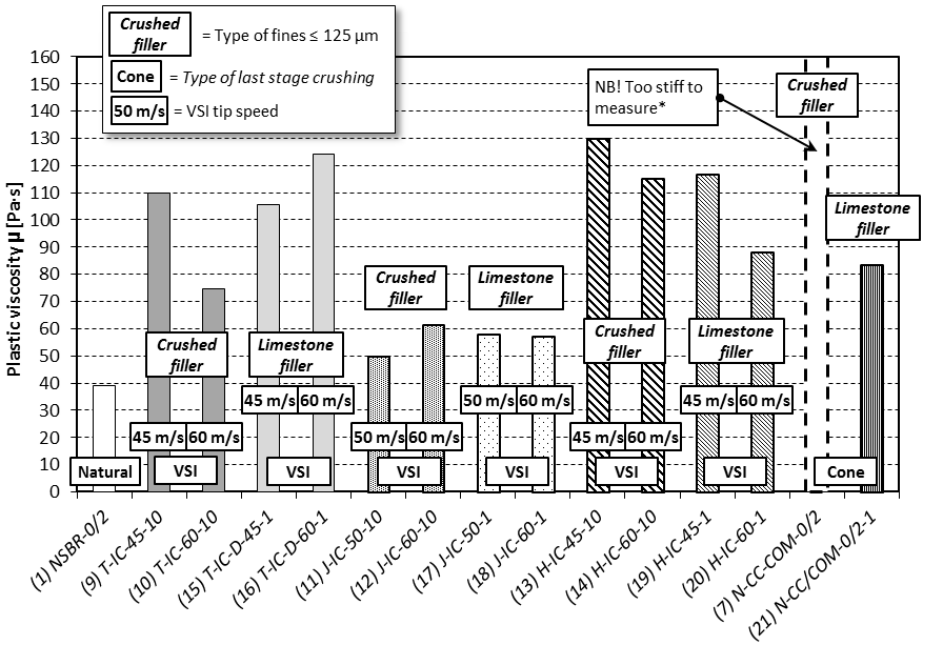

*Figure 13 – Plastic viscosity values for the second set of results; *mix was too stiff for measurements in the BML-vicometer*

The third set of results aims at investigating the reasons why the sand N-CC-COM-0/2 from the Nord-Fosen quarry showed by far the worst rheological parameters (Figures 8 and 9), i.e. the lowest slump value and was in fact too stiff to measure the plastic viscosity (which is therefore assumed to be much higher than for the rest of the tested mixes). For this reason, three additional mixes apart from those presented on Figures 8-13 were prepared. Those are mixes No 2, 8 and 22. Mixes No 2 and No 8 were mimes of the mixes with 0/2 mm NSBR-0/2 partly natural sand and N-CC/COM-0/2 crushed sand from the Nord-Fossen quarry. The difference was that the 0/2 mm sand fractions were replaced with 0/8 mm sands from the same quarries, i.e. NSBR-0/8 and N-CC/COM-0/8 accordingly, which then caused a change in the total grading of the 0/8 mm part of the aggregate composition (see Figure 6) and to the total matrix content of the mixes (see Section 2.3). In mix No 22 the sands from mixes No 2 and No 8 were mixed together in 50%/50% proportions on mass basis (densities of the materials are almost the same). Results from the third set of results are presented on Figures 14 and 15. The results indicate that the bad performance of the N-CC-COM-0/2 sand was mainly due to combination of two things. One is unfavourable properties of the filler fraction, since replacing the original crushed fines with the reference limestone filler allowed considerably increase the slump value and reduce the plastic viscosity. From the presented results it is hard to assess why the specific fines from the N-CC-COM-0/2 seem to be unfavourable. It is generally known that finer filler will increase the flow resistance of the matrix phase due to higher specific surface that has to be covered with water [16]. However, it does not seem to be the case, since from the filler grading measurement results it appears to be one of the coarsest. Then the reason most likely lies in the shape of the very fine particles or

perhaps due to presence of high free mica content [15]. N-CC-COM-0/2 sand was also by far the finest of all the 0/2 mm sands tested, having a fineness modulus of only 1.37 in contrast to 2.8-3.0 for most of the other crushed sands (see Table 3). As it can be seen in Figure 6, the fine 0/2 mm part in combination with the rather low amount of 2/8 mm crushed Årdal semi-coarse fraction (73% (7) N-CC-COM-0/2 + 27% Årdal crushed 2/8 mm) results in an unfavourable "open" grading with a small gap between 2-4 mm. If the grading is changed to a more equally distributed and "dense" such as in the N-CC-COM-0/8 sand, this gives a considerably improved slump value. Though, the plastic viscosity is still very high when compared to the reference mixes with the partly natural sands (NSBR-0/2 mm and NSBR-0/8 mm). Finally, when further half of the 0/8 mm crushed sand from Nord-Fosen (N-CC-COM-0/8) is replaced by the reference party natural sand from the Årdal quarry (NSBR-0/8), the difference between the reference sand and the crushed sand seem to be almost eliminated, both in terms of slump value and plastic viscosity.

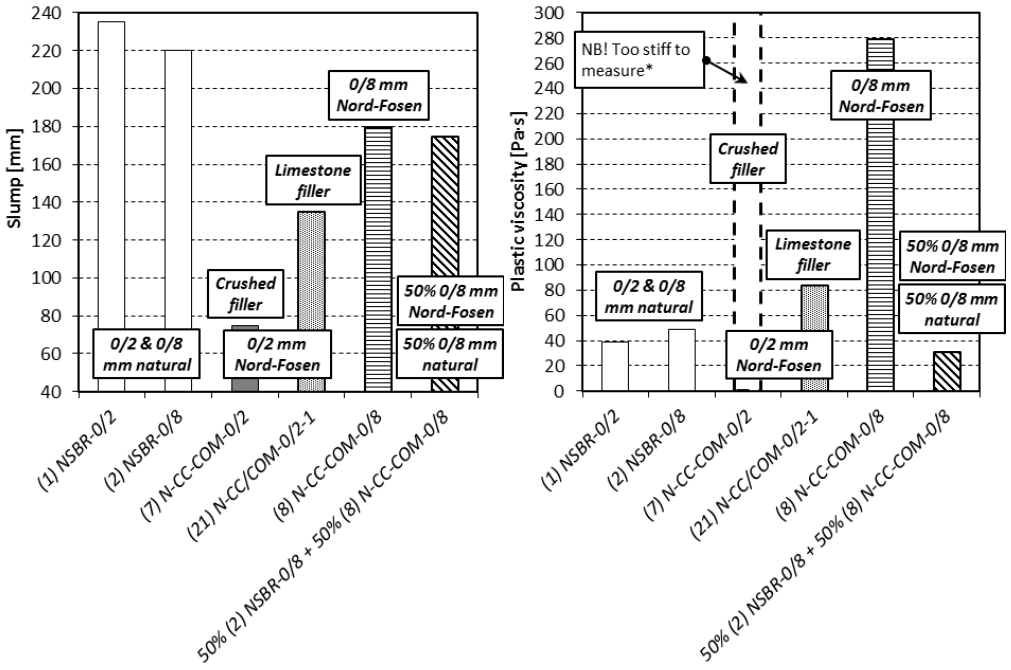

4. CONCLUSIONS

Results of the study demonstrate that, within the limitations of the current study, the crushing process parameters that are important for the coarse aggregate quality (with respect to their performance in fresh concrete) seem to be important also for the fine aggregate (0/2 mm) characteristics. The two most important parameters are the number of crushing stages used (reflecting the reduction ratio of the cone crushers) and crusher type (cone or VSI) used for the last stage. The VSI tip speed itself seems to be of a second order of importance. However, measurable changes in fresh mix properties were observed when materials processed at different tip speeds were tested in concrete. Both the coarser particles 0.125-2 mm and the filler fractions 0-0.125 mm seem to be affected by adjusting the tip speed. It was also observed that increase

from 45 m/s to 60 m/s had a greater influence on fresh concrete rheology than an increase from 50 m/s to 60 m/s.

Grading (as described by the fineness modulus) and flakiness index of the 1.25-2.5 mm fractions seem to be parameters that can indicate the performance of 0/2 mm crushed sands in concrete to some extent. Though, loose packing or loose state void content showed a much better relation to fresh concrete rheology. This is, however, not surprising since the packing of particles will be affected by both: their size distribution and shape (includes not only the flakiness index, but also parameters like angularity, elongation and surface texture as suggested by Järvenpää [12]). Thus, the loose packing or loose void content test can be recommended as a simple, fast and cheap test for crushed sand quality control at a hard rock quarry. For the concrete composition used in the given study, void content reduction by 1% in the 0/2 mm fraction resulted in a roughly 3 cm increase in the slump value and a 28.7 Pa·s reduction of plastic viscosity.

The study revealed that the reason for the worst performance in concrete by one of 0/2 mm crushed sands seems to be a combination of an unfavourable grading and the fine fraction properties. Fine fraction properties affected more on the plastic viscosity, while grading affected more on the slump value. The most effective way of improving the crushed sand concrete properties was a partial (50%) replacement of the given crushed sand by high quality partly natural sand, which is known to perform very well in fresh concrete. The replacement approach allowed for fully eliminating any difference in the slump value and the plastic viscosity. This means that if such a concrete would be delivered to a construction site, it would be hard to easily distinguish the mix from a 100% natural sand based concrete. So in practice this seems to be one of the easiest and most effective solutions of utilising the fine leftovers from quarrying as they are, though the solution is by no means sustainable.

The final conclusion is that a good and optimised coarse aggregate production process is more likely to generate a better quality co-generated fine sand fractions than a simple 3 three stage crushing layout. However, some other crushed sand properties, which are important for performance in fresh concrete, such as for example the mineralogical composition, will always remain rock dependant. New and novel techniques, above those discussed in this paper, must be developed in order to overcome problems arising from the unfavourable mineralogical composition resulting in intrinsically unfavourable PSD or enrichments of free mica or other flaky mineral content in the filler fractions.

ACKNOWLEDGEMENTS

The results presented here are based on work performed in COIN – Concrete Innovation Centre (www.coinweb.no) – which is a Centre for Research based Innovation, initiated by the Research Council of Norway (RCN) in 2006. The author would also like to especially acknowledge the in-kind contributions by Metso Minerals to the COIN project and to this work, what made it possible. The supervision contribution to major parts of this work by Stefan Jacobsen, Bård Pedersen and Tero Onnela is also greatly appreciated.

REFERENCES

1. Eloranta, J., 1995. *Influence of crushing process variables on the product quality of crushed rock.* Ph.D. Tampere University of Technology.

2. Mahonen, J., 1999. *SAND: Applications, Manufacturing, Classification, Requirements – Nordberg Way of Sand Making*. Nordberg-Lokomo: Tampere.
3. Schouenborg, B. et al., 2006. Resources for Concrete Production. In: *Proceedings of ECO-SERVE SEMINAR "Challenges for Sustainable Construction: the "concrete" approach"*, Warsaw, Poland, May 18th and 19th 2006.
4. Bengtsson, M. and Evertsson, C., 2006. An empirical model for predicting flakiness in cone crushing. *International Journal of Mineral Processing*, 79(1), pp. 49-60.
5. Morrow, D., 2011. Why manufactured sand? *Metsos's customer magazine for the mining and construction industries – results: minerals&aggregates*, 1, pp. 26-27.
6. Bengtsson, M. and Evertsson, C., 2006. Measuring characteristics of aggregate material from vertical shaft impact crushers. *Minerals Engineering*, 19(15), pp. 1479-1486.
7. Gonçalves, J.P. et al., 2007. Comparison of natural and manufactured fine aggregate in cement mortars. *Cement and Concrete Research*, 37, pp. 924-932.
8. Gram, H-E., et al., 2008. Characterisation of crushed rock sands in Sweden. In: *Proceedings of manufactured sand workshop*, Stavanger, Norway, October 30th and 31st 2008.
9. Esping, O., 2008. Effect of limestone filler BET(H_2O)-area on the fresh and hardened properties of self-compacting concrete. *Cement and Concrete Research*, V. 38, Issue 7, pp. 938-944.
10. Wills, M. H. Jr, 1967. How aggregate particle shape influences concrete mixing water requirement and strength. *Journal of Materials*, V. 2, 4, pp. 843-865.
11. Barnes, H.A, Hutton, J.F. and Walters, K., 1989. *An Introduction to Rheology*. Amsterdam: Elsevier Science.
12. Järvenpää, H., 2001. *Quality characteristics of fine aggregate and controlling their effects on concrete*. Ph.D. Helsinki University of Technology.
13. Mørtsell, E., 1996. *Modelling the effect of concrete part materials on concrete consistency*. Ph. D. Norwegian University of Science and Technology (In Norwegian).
14. Westerholm, M. et al., 2006. Influence of fine aggregate characteristics on the rheological properties of mortars. *Cement & Concrete Composites*, 30, pp. 274-282.
15. Danielsen, S.W. and Rueslåtten, H.G., 1984. Feldspar and mica. Key minerals for fine aggregate quality. *Bulletin of the International Association of engineering geology*, Vol. 30, Issue 1, pp. 215-219.
16. Smeplass, S., 2004. Fresh concrete – proportioning. In: Jacobsen S., ed. et al, 2012. *TKT 4215 Concrete Technology 1. Course compendium*. Norwegian University of Science and Technology. Ch. 4.
17. Thomson, W., 1889. *Popular lectures and addresses. Vol. I. Constitution of matter.* London: Macmillan and Co.
18. Cepuritis, R., 2011. *Effects of Concrete Aggregate Crushing on Rheological Properties of Concrete and Matrix*. Master thesis. Norwegian University of Science and Technology.
19. Wigum, B. J., 2011. *Hokksund Quarry – Review of the aggregate production. COIN Project report 33 – 2011*. Trondheim: SINTEF.
20. Wigum, B. J, 2010. *Classification and particle properties of fine aggregates*. Trondheim: NTNU.
21. Pedersen, B., 2011. *Manufactured sand in concrete – effect of particle shape on workability. COIN Project report 34 – 2011*. Trondheim: SINTEF.
22. Wallevik, J.E., 2006. Relationship between the Bingham parameters and slump. *Cement and Concrete Research.* V. 41, pp. 1214-1221.

23. Ferraris, C.F., de Larrard, F. and Martys, N., 2001. Fresh concrete rheology: recent developments. In: American Ceramics Society, Mindes, S. and Skalny, J., eds., *Material science of concrete VI*, pp. 215-241.
24. Roussel, N. et al., 2007. Computational modelling of concrete flow: General overview. *Cement and Concrete Research*, 37, pp. 1298-1307.
25. Eloranta, J., ed., 2008. *Crushing and Screening Handbook. 4th edition.* Metso Minerals: Tampere.
26. Ferraris, C.F. and de Larrard, F., 1998. *Modified Slump Test to Measure Rheological Parameters of Fresh Concrete.* Cement, Concrete and Aggregates, 20 (2), pp. 241-247.

Crack development and deformation behaviour of CFRP-reinforced mortars

Katalin Orosz
M.Sc., Ph.D. student
Luleå University of Technology
971 87 Luleå, Sweden
katalin.orosz@ltu.se

Thomas Blanksvärd
Ph.D., Senior Assistant Lecturer
Luleå University of Technology
971 87 Luleå, Sweden
thomas.blanksvärd@ltu.se

Björn Täljsten
Ph.D., Professor
Luleå University of Technology
971 87 Luleå, Sweden
bjorn.taljsten@ltu.se

Gregor Fischer
Ph.D., Associate Professor
Technical University of Denmark
2800 Kgs. Lyngby
gf@byg.dtu.dk

ABSTRACT

This paper reports on a research study investigating CFRP-reinforced mortars in uniaxial tension, as a strengthening material for concrete structures. The bare strengthening material was tested on dogbone specimens. Crack formation, crack development and the interaction between the grid and the mortar phase with varying geometrical parameters and mortar compositions have been investigated and evaluated. The use of engineered cementitious composites, exhibiting multiple cracking and enhanced pseudo-ductility in uniaxial tension, was found to result in an improved overall performance.

Keywords: concrete, strengthening, carbon fibre reinforced polymers (CFRP), mortar, mineral based composites (MBC), strain-hardening cementitious composites (SHCC), tensile tests, strain hardening, cracking, pseudo-ductility

1. INTRODUCTION

Fibre-reinforced polymers (FRP) have become a popular material for strengthening and/or retrofitting of existing concrete structures. Externally epoxy-bonded FRP systems have been proven to be an effective strengthening method in repairing or strengthening structures and there has been a large amount of literature published on the topic; see for example [1-4].

Despite their advantages over traditional strengthening methods, the use of epoxy-bonded systems is not entirely problem-free [2]. The epoxy resin creates sealed surfaces. Furthermore, it has poor thermal compatibility with the concrete substrate, it is sensitive to moisture at the time of application, and it creates a hazardous working environment. In cold climates, the use of epoxy is limited because of the minimum temperature of application (typically, 10°C or 50°F) [2]. Therefore, it is of interest to develop alternative strengthening systems where the epoxy bonding agent can be replaced with cementitious materials, for example a polymer-modified or purely cementitious mortar with similar properties to those of the concrete substrate and applicable in a more environmentally friendly and possibly also cost-effective way.

Mortars can be combined with FRP textiles or 2D grids to form an effective strengthening system. This kind of strengthening system has already been tested by [5, 6] on flexural and shear beams.

In the research presented, conventional, quasi-brittle, and “ductile” binders have been combined with CFRP grids. The quasi-brittle binders used are commercially available, pre-mixed, polymer-modified mortars. The ductile binder is strain-hardening cementitious composite (SHCC), namely, a polyvinyl alcohol-reinforced engineered cementitious composite (PVA-ECC), that exhibits strain hardening along with enhanced tensile ductility. The uniaxial tensile tests aimed at obtaining better understanding of the tensional behaviour of the FRP grid-reinforced cementitious composite material.

Only the bare strengthening material is tested here, not considering the interaction with the concrete structure to be strengthened. The main reasons for replacing the conventional mortar with strain-hardening mortars, in a few specimens, were to 1) enhance the loading capacity, 2) enhance the deformation capacity, and 3) prevent brittle failure in the FRP.

2. RESEARCH SIGNIFICANCE

By substituting the traditionally quasi-brittle mortar with a strain-hardening cementitious mortar in an externally bonded strengthening system, the interaction between the cementitious mortar and the FRP reinforcement can be significantly altered and improved, (potentially) leading to a more effective use of the FRP reinforcement. Such cement-based systems may in certain conditions, replace the conventional epoxy-based systems. It is also shown how the behaviour of a strain-hardening cementitious mortar can improve the mechanical properties of a mineral-based strengthening system.

3. RESEARCH QUESTIONS

The study aimed to answer the following questions:

1. Which is the best material combination/orientation leading to the optimal utilization of the FRP?
2. How do the failure modes and the load- and deformation capacity compare, depending on the mortar type? Can a strain-hardening effect be shown in specimens cast with tensile strain-hardening mortars?
3. Can the brittle and/or premature failure of the FRP grid be prevented by applying a ductile matrix?
4. Prove whether the dogbone test setup is a suitable test method for testing MBC in tension.

4. STRENGTHENING WITH CEMENTITIOUS COMPOSITES

The mechanics and design of different FRP reinforcements together with cementitious bonding agents have been extensively researched. The short overview here is selective to applications, which have led to strengthening with grid-reinforced mortars. A more detailed "state-of-the-art" can be found in [7].

Embedded continuous (dry) fibres, fibre reinforced cementitious mortars, textile-reinforced mortar (TRM) or textile-reinforced concrete (TRC) make use of the tensile strength of the FRP reinforcement which is significantly higher than that of the mortar phase. The FRP component in these applications is intentionally aligned accordingly to the principal stresses expected during the lifespan of the structure. In TRC, the load capacity is heavily dependent on the proper penetration of the textile by the mortar, as emphasized by e.g. [8]. If instead of a textile, the FRP is a grid, it offers the advantage of an improved mechanical anchorage due to the rigid joints of FRP in fine-grain mortars and it ensures that all fibre filaments will work together. The pre-cut grid, available with different grid spacing and thickness, can be embedded between two layers of polymer-modified mortar, resulting in a strengthening layer of about 5-10 mm of total thickness [5].

In a cementitious strengthening system, the bond between base concrete (structure to be strengthened) and first layer of polymeric mortar is enhanced by a primer. Several tests have been carried out with grid-reinforced mortars, mainly focusing on flexural [5, 9], and shear strengthening [5, 10]. These tests have shown that that it is possible to achieve a near-perfect bond between the grid and the cementitious matrix so that the composite material will fail with FRP rupture. However, failure of the grid is often premature because of local stress concentrations.

In the mortar phase, mix designs that introduce fly ash and/or silica fume partly replacing the cement in order to densify the microstructure result in higher bond strength between FRP (textiles) and matrix [11]. Mortars can also contain chopped or milled fibres of different kinds. If such a mortar is used together with an embedded reinforcement, improved bond is expected because of the fibre interlock mechanism.

In recent years, micromechanically designed strain-hardening materials have been developed, in which a tensile stress-strain behaviour analogous to that of metals has been achieved. Strain-hardening cementitious composites (SHCC) are defined by an ultimate strength higher than their first cracking strength and the formation of multiple cracking during the inelastic deformation process [12]. However, the inelastic deformation behaviour of SHCC is based on the sequential development of matrix multiple cracking while undergoing strain-hardening [13]. It is more

accurate to refer to the mechanism as *pseudo* strain hardening in order to differentiate it from the "real" strain hardening observed in metals, that is based on dislocation micromechanics in the plastic deformation regime.

The most typically used SHCC, the engineered composite (ECC) utilizes short, randomly oriented polymeric fibres (e.g. polyethylene, polyvinyl alcohol) at moderate volume fractions - typically less than 2% [13, 14]. ECC has been used in standalone and strengthening applications where ductility is an important criterion. The pseudo strain-hardening behaviour of ECC has been utilized as a mechanism to redistribute concentrated loading and thus prevent sudden failure at critical structural connections where steel and concrete come into contact, i.e., shear studs, fasteners or joints, where a steel beam meets an RC column in a hybrid structure [15]. The high damage tolerance of ECC is valuable to the performance of a structure in terms of collapse resistance, extension of service life, and minimization of repair after an extreme event [15] or strengthening purposes. When used in combination with (steel) reinforcement, the tensile ductility of the ECC matrix can on a macro scale, eliminate the strain difference between reinforcement and matrix material [13].

5. LOAD-DEFORMATION RESPONSE OF CEMENTITIOUS COMPOSITES

5.1. Tensile response of cementitious materials

Cement-based composites can be conveniently classified according to their tensile response [12]. The authors have compared the tensile behaviour of steel fibre reinforced concrete, textile reinforced concrete (TRC), engineered cementitious composites (ECC), and steel-reinforced ECC more in detail, based on the existing literature. Only a comparative figure is being presented here (Figure 1) with brief explanations. The different stages are named in a way that they mean the same for the different materials, so not all stages exist for all materials.

Quasi-brittle and ECC mortars used in the tests behave identical to the mortar components shown in Figures 1a and 1c, respectively. During the formation of multiple, evenly distributed, closely spaced, small cracks (Figure 1c), the ECC matrix shows an overall strain-hardening behaviour, without definitely distinctive parts in the curve from σ_{cc} to σ_{pc}. After localization, there is a gradually decreasing, softening range due to the fibre pullout mechanism.

ECC works well with regular steel reinforcement [16]. The hardening part of the load-deformation curve of the steel reinforced ECC (R/ECC) is not as uniform as in plain ECC but has a steeper and a gradually raising part, in accordance with the elastic stage/yielding of the steel. In the inelastic deformation regime, where both components are yielding, cracking of the ECC and yielding of the reinforcement are uniformly distributed over the length of the specimen, until rupture of the steel. The hatched area in Figure 1d represents the contribution of the ductile matrix compared to steel.

Finally, in TRC [17] where the FRP is linear elastic up to failure and the mortar (typically) is quasi-brittle, the hardening part can be divided in two distinct parts as shown in Figure 1e. After first crack formation, the load-deformation curve shows a small increase in loading capacity due to the formation of additional transverse cracking. The member is softened by the formation of additional crack(s) and the load increase per deformation increment is decreasing with each crack until the stabilized crack pattern (II/b) is reached which is nearly linear.

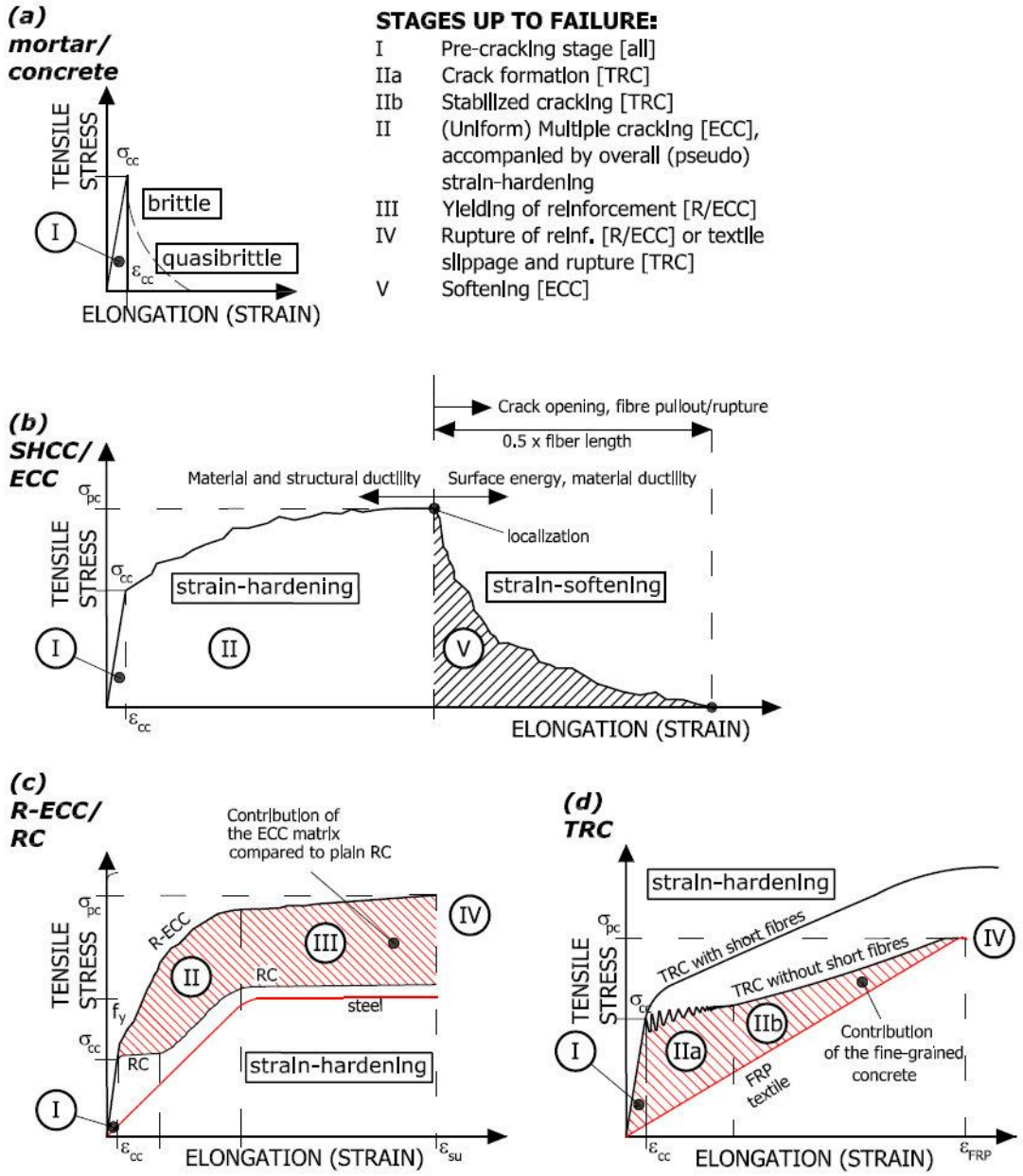

Figure 1 – Tensile response of cementitious materials, based on and [12, 13, 18, 19]. (a) Conventional mortar and concrete, (b) strain-hardening cementitious composites, (c) steel vs. reinforced concrete vs. steel-reinforced engineered cementitious composite, (d) textile-reinforced concrete.

Crack widths here are governed by the FRP reinforcement and the bond characteristics to the surrounding concrete matrix, and *mainly* the FRP determines the stiffness of the member. However, the uncracked segments between the cracks still increase the stiffness of the member, as long as they are not debonded from the FRP reinforcement. Since the FRP reinforcement has no inelastic deformation capacity, failure of a TRC is characterized either by slippage in the fibre tows or by linear elastic deformations until the FRP ruptures in a brittle manner upon reaching its tensile failure strain [17]. In practice, final failure normally is a combination of both fibre slippage and rupture [19].

If the TRC matrix contains short fibres, after first cracking the hardening part becomes uniform, similar to that of the ECC [18].

5.2. Tension stiffening effect

The contribution of a cementitious matrix to the load–deformation response in uniaxial tension is generally described as tension-stiffening effect [20]. The response of the reinforced cementitious composite is compared to that of the bare strengthening material (steel or FRP) and the difference in load capacity is attributed to the tensile load carried by the cementitious matrix between transverse cracks. The matrix contribution is most emphasized in steel reinforced ECC (Figure1d), but also significant in textile reinforced concretes (Figure 1e).

6. EXPERIMENTAL PROGRAM

6.1. Materials

In the experimental program, two different CFRP grids and three types of mortars were used. Material properties are listed in Table 1 (grids) and Table 2 (mortars).

Table 1 – Material properties of the grids used

FRP *tested* values	Spacing L x T [mm]	E_{Lt} [GPa]	E_{Tt} [GPa]	f_{Lt} [GPa]	f_{Tt} [MPa]	ε_{Lt} [‰]	ε_{Tt} [‰]
small	24 x 25	79	51	988	740	12.5	14.0
medium	42 x 43	85.4	45	944	500	11.1	11.1
FRP *supplier* data	Spacing L x T [mm]	E_{Lm} [GPa]	E_{Tm} [GPa]	f_{Lm} [GPa]	f_{Tm} [MPa]	ε_{Lt} [‰]	ε_{Tt} [‰]
small	24 x 25	262	289	4300	3950	15.0	14.9
medium	42 x 43	284	253	3800	3800	13.4	15.0

Table 2 – Material properties of the mortars used

Material	E_c [GPa]	f_{cc} [MPa]	f_{ct} [MPa]	w/c	notes
M1 (from supplier)	26.5	53.2	9	0.16	-
M2 (from supplier)	35	77	2.8		-
ECC (from earlier tests)	19	60	3	0.88	Fly ash 45 mass %; PVA 0.01 mass %

The utilized grids are the C3000 A X1 grid (referred to as “medium grid”) and the C5500 A X1 grid (“small grid”) from Chomarat, U.S. Both grids are epoxy-coated with a fibre volume percentage of 20-25%. We used two pre-mixed, commercially available mortars; StoCrete GM1 (M1) and StoCrete TS100 (M2), from Sto Scandinavia AB. These mortars are one-component, high-strength, polymer-modified, quasi-brittle mortars with tensile strengths of 53.2 MPa (M1) and 77.0 MPa (M2). M1 also has low fibre reinforcement content. The exact mortar compositions or information on the fibrous component is not provided by the manufacturer.

The used primer (Table 3) is a one-component, cement-based and polymer-reinforced powder mixed with water. It is used as a silt-up product on the roughened (sandblasted) concrete surface. Its function is to enhance the bond in the transition zone.

Table 3 *– Material properties and mixing ratio for the primer*

	Density [kg/m^3]	d_{max} [mm]	Mixing ratio, primer:water
Primer	2020	2	1:0.22

The third mortar tested is an ECC mix ("DTU ECO-3 M9 Melflux") containing PVA fibres (1% by weight, or 2% by volume) and a large portion (44% by weight) fly ash. Its tensile strength is 60 MPa. The exact mix composition is given in Table 4.

Table 4 – Mix composition of the ECC used

Material	Fraction [mass %]
Cement (basic Portland)	22
Fly ash	44
Sand (<0.15mm)	8
Quartz powder 100/22	8
Water	18
Superplasticizer (Melflux)	0.02
PVA fibre (oiled)	1

6.2. Test matrix

With the three different mortars (M1, M2, ECC), two different grids (medium and small) and three chosen grid configurations (0°, 90°, and 15° with respect to the applied tensile force), the final test matrix consists of 13 different combinations, 3 specimens per each series, in total 44 specimens. The first five are dummies (2 x M1 without reinforcement, 2 x M1 with medium grid longitudinal direction, and 1 x ECC medium grid longitudinal direction), followed by the 3x13 reinforced specimens. The tested combinations are summarized in Table 5.

Table 5 – Test matrix

Series nr.	Mortar	Grid spacing	Grid config.	Test specimen	No. of specimens
1	M1	---	---	Dummy	2
2	M1	medium	0°	Dummy	2
3	ECC	medium	0°	Dummy	1
4	M1	---	---	M1 reference	3
5	M2	---	---	M2 reference	3
6	M1	medium	0°	M1-0-M	3
7	M1	small	0°	M1-0-S	3
8	ECC	medium	0°	ECC-0-M	3
9	ECC	small	0°	ECC-0-S	3
10	M2	medium	0°	M2-0-M	3
11	M1	medium	15°	M1-15-M	3
12	M2	medium	15°	M2-15-M	3
13	M2	small	15°	M2-15-S	3
14	M1	medium	90°	M1-90-M	3
15	M1	small	90°	M1-90-S	3
16	M2	small	90°	M2-90-S	3

6.3. Specimens

Earlier "dogbone" tests with textile reinforced concrete and a large-scale experiment were described by [21], on 900 x 100 x 60 mm specimens with a 10mm thick web. Based on those sizes, but considering that a typical MBC strengthening layer consists of two 10 mm thick layers and a grid, new specimens were designed, as illustrated in Figure 2.

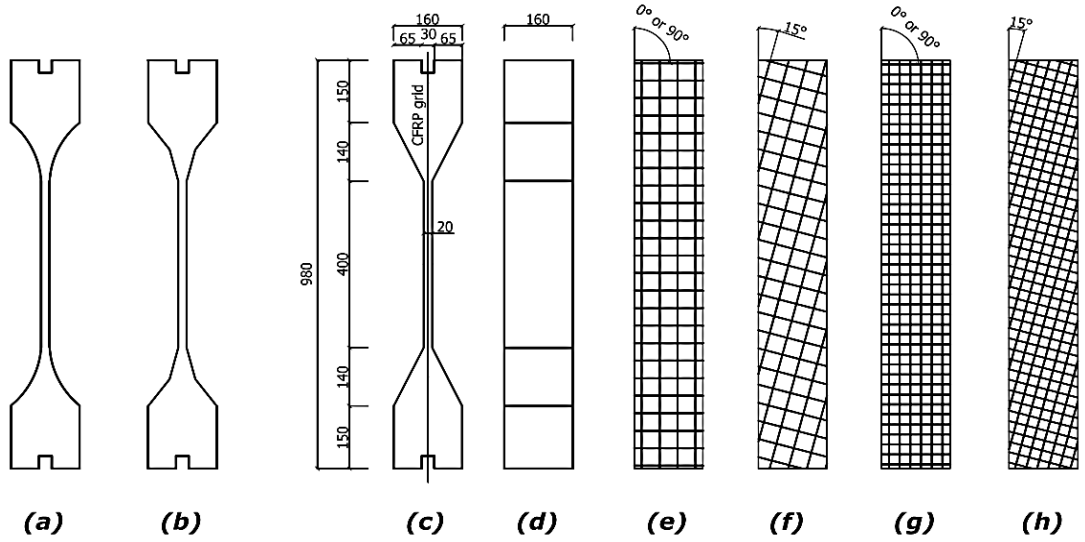

Figure 2 – Test specimen and reinforcement configuration

For brittle or quasi-brittle materials, the uniaxial tests are very sensitive, as an uncontrolled deformation at cracking occurs despite the displacement control. In addition to that, the dogbone geometry is very sensitive to cracks initiating towards the ends of the test field, where the thin web meets the bulk end of the specimen. To prevent cracking in these areas, the optimal solution would be a concave slant surface (a) or a specimen with 2-step slant surface (b) to minimize this risk. Due to resources, simpler dogbone geometry was decided upon (c and d), with a total length of 980 mm, and a web thickness of 20 mm.

The length of the test field was set to the longest possible so that it has a high crack potential; yet short enough to be able to de-mould and handle the specimens without breaking them apart. The final dimensions were set to 160 x 160 x 980 mm in order to meet the geometry of the existing moulds, with a representative test section of 400 x 160 x 20 mm. The CFRP grid was placed in the mid-plane of the specimen (Figure 2b) into the slits at the ends. Figure2e through Figure 2h shows the different reinforcement orientations. The 30 x 30 mm wedged slits at the end of each bulk can be used to glue some additional CFRP material to the reinforcement with epoxy as extra anchorage in the case that bond slippage occurs prematurely. The end slits were wedged, to ease the de-molding process. All specimens were de-molded after 24 hours except for the unreinforced reference specimens and the ECC specimens, which were de-molded after 48 hours. All specimens were water cured for at least 28 days prior to testing.

6.4. Anchor clamp

The uniaxial test requires special devices for loading. The anchor clamp is the fixating mechanism between the test machine and the test specimen. Its main purpose is to hold the specimen fixed and centred, and to transfer the tensile force form the test machine evenly into the specimen. It has joints in both planes parallel to the tensile force, to avoid any shear forces in the specimens.

The clamps were designed based on combining multiple clamp designs detailed in [22], shown in Figure 3. A combination of (b) and (d) has been chosen and custom-welded for this experiment. From (b), the concept of two crossbars, transferring the force through a slant surface, and from (d), the double joints were taken, in order to nullify any shear forces in the web. However, in order to save space, the custom device had both joints working in the same plane.

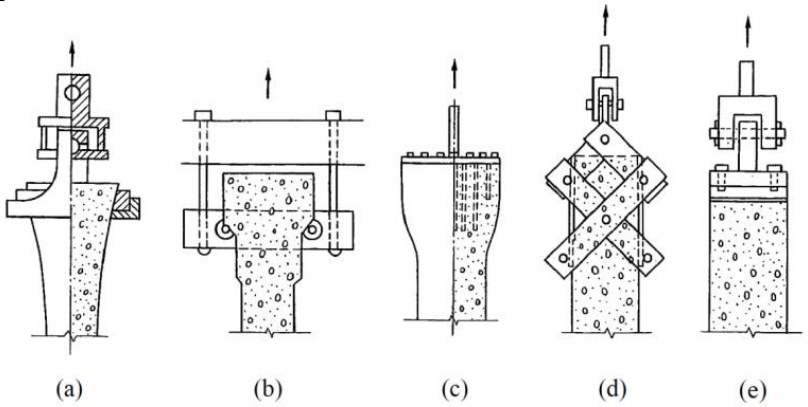

Figure 3 – Various tensile clamps for direct tensile testing [22]

Between the crossbars and the specimen, neoprene was used to distribute the forces evenly. The main bulk of the specimen is in compression at all times during testing, which means that the

connection between the clamp and the specimen is less vulnerable to fracture. The clamp is self-centring, since the crossbars are rotate-able and automatically wedge the specimen into the right position. The side plates are also able to rotate, to help the easy mounting and demounting of the specimens. The anchor clamps are shown in Figure 4.

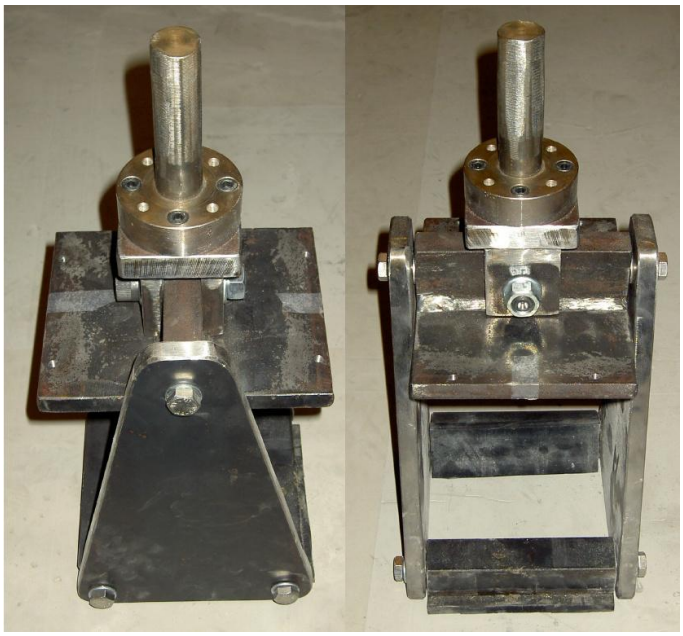

Figure 4 – Custom-welded self-centring anchor clamps

6.5. Measurements and monitoring

The dogbone tests were run under displacement control at a rate of 0.6 mm/s. The load-deformation behaviour was monitored within the representative test section, and recorded by a data logger connected to the test machine. A digital image correlation system (ARAMIS from GOM Optical Measuring Techniques, Germany) was also used to monitor deformations in the test field. ARAMIS is a non-contact and material independent 3D optical measuring system, which analyzes, calculates, and documents material deformations by means of recording and calculating relative displacements of discrete points on a patterned surface. The ARAMIS measurements were conducted primarily to monitor and analyze crack development and crack widths. In addition, strain overlay photos were taken for illustrating crack development within the test field.

7. EXPERIMENTAL RESULTS

7.1. Evaluation and presentation of test data

The specimens were compared by their load-deformation behaviour, first cracking strength, failure load, mean number of cracks developed within the test field and average crack width. The ARAMIS documentation consists of plots illustrating crack development (crack widths, crack density) and elongations within the test field.

7.2. Load-deformation response

The un-strengthened mortar specimens failed in a brittle manner as expected for plain mortar. Average failure loads were 8.7 kN and 8.3 kN for M1 and M2, respectively.

Three quasi-brittle specimens had small cracks on them close to the end of the test field after de-molding; these are excluded from the results. For the remaining specimens, the tensile response is plotted in Figures 5-15. Here we did not include the plain mortar specimens to save space (the response was linear elastic). Additionally, part of the curves we plotted against the *measured* properties of the bare grid on Figures 5-9, and 13 [23], which is the straight line starting at first cracking.

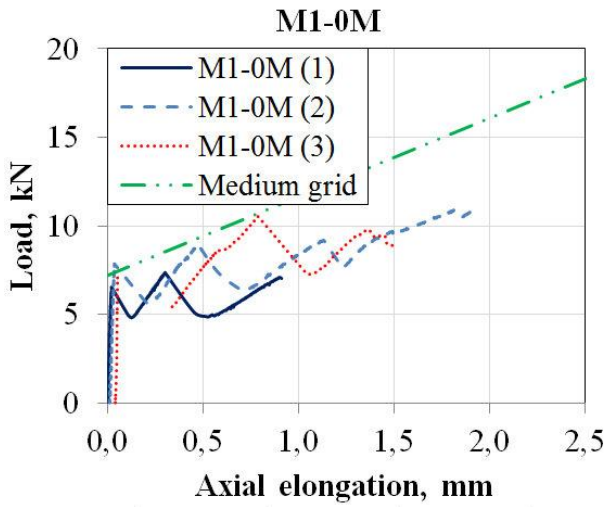

Figure 5 – M1-0-M

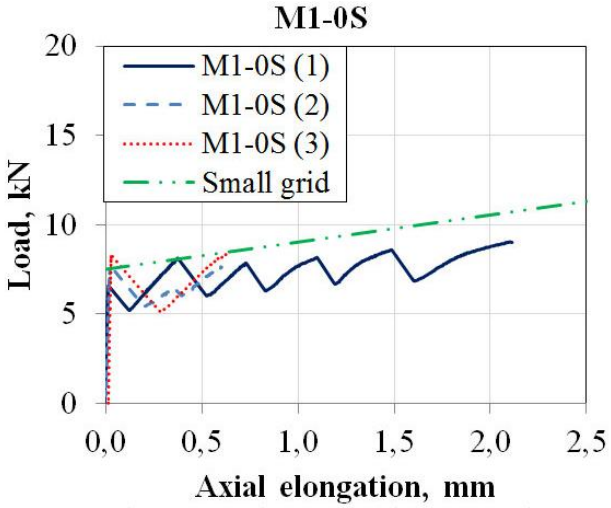

Figure 6 – M1-0-S

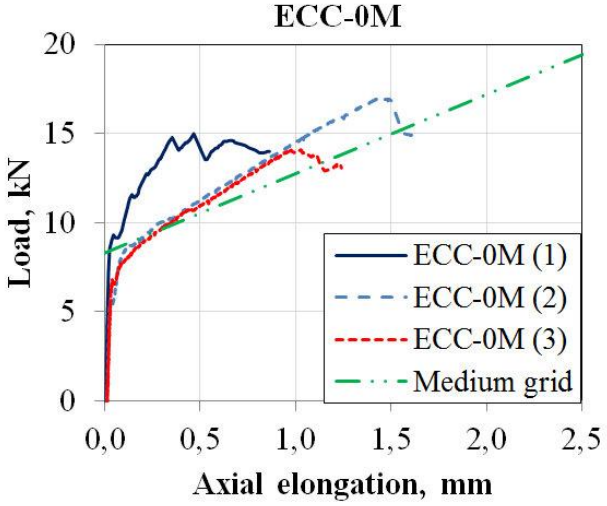

Figure 7 – ECC-0-M

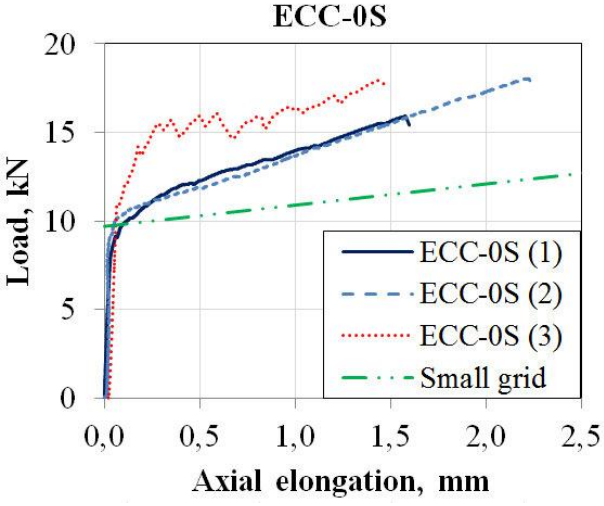

Figure 8 – ECC-0-S

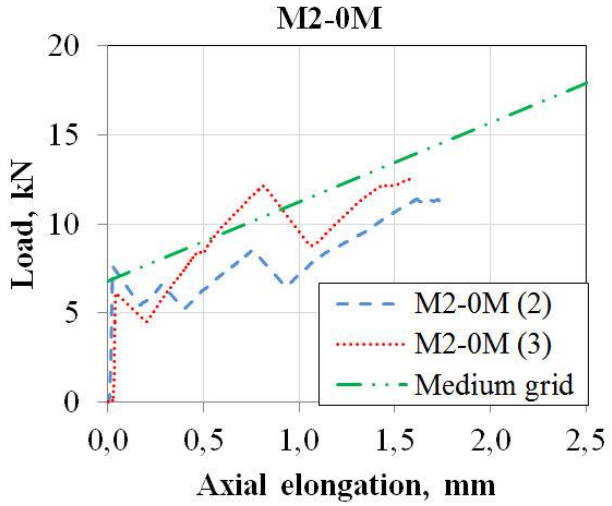

Figure 9 – M2-0-M

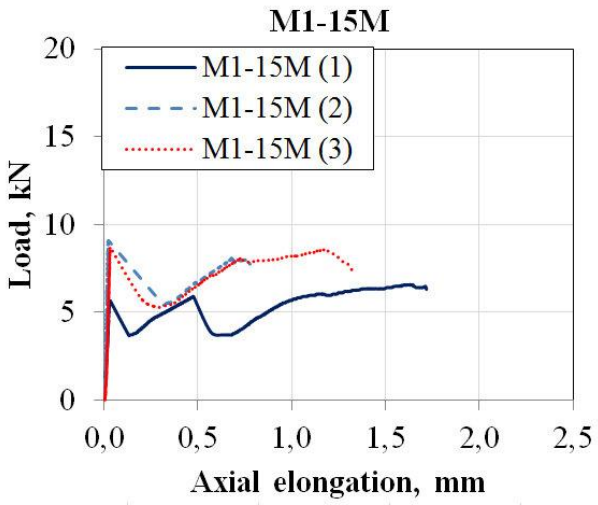

Figure 10 – M1-15-M

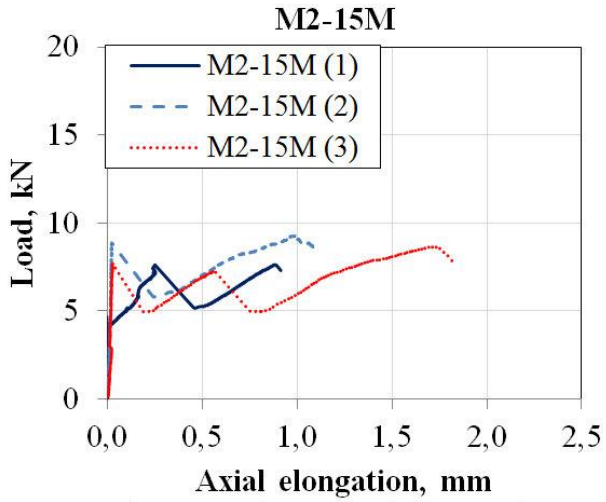

Figure 11 – M2-15-M

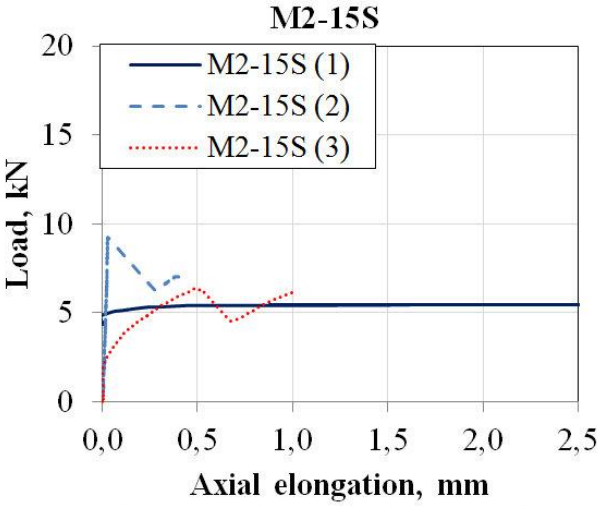

Figure 12 – M2-15-S

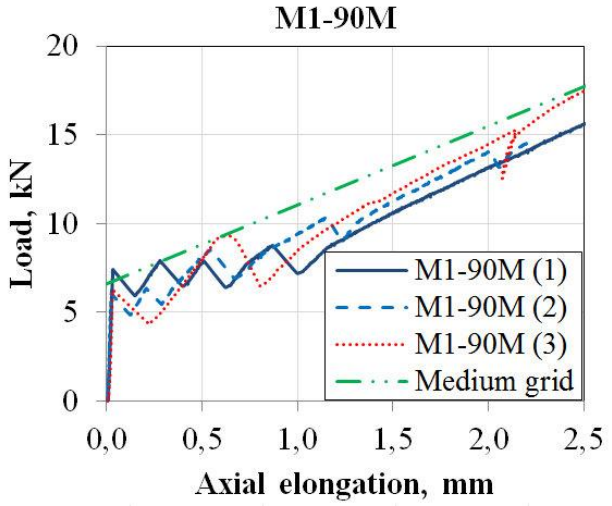

Figure 13 – M1-90-M

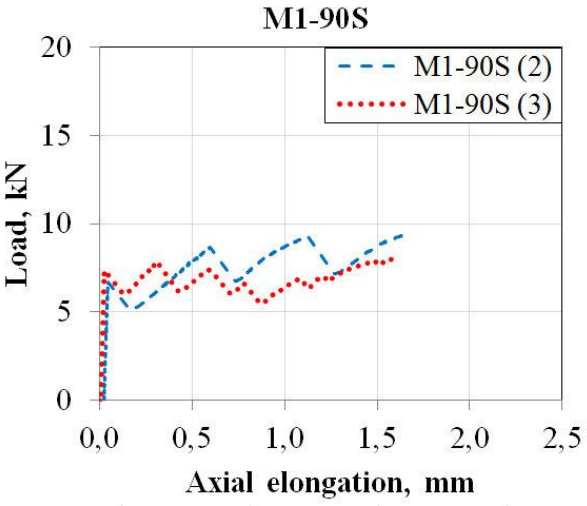

Figure 14 – M1-90-S

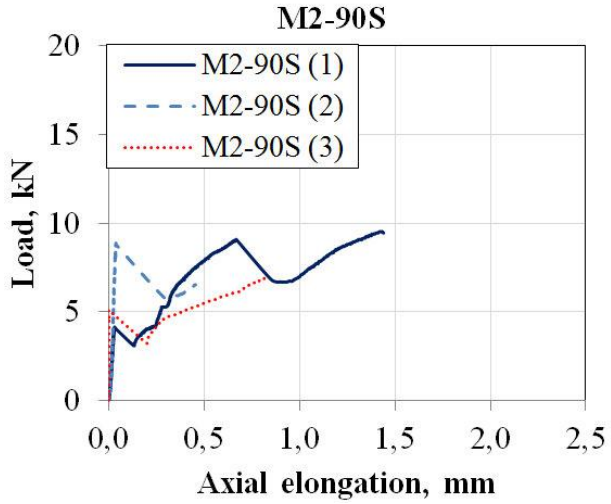

Figure 15 – M2-90-S

Parallel to the plots, Table 6 summarizes first cracking and failure loads, also including the plain mortar specimens.

Table 6 – Results

Test specimen	Failure load [kN]	First cracking load [kN]	Mean nr. of cracks	Average crack width [mm]	Min. expected load capacity (grid only) [kN] theoretical/measured
M1 reference	8.7	8.7	1	N/A	N/A
M2 reference	8.3	8.3	1	N/A	N/A
M1-0-M	9.2	7.2	2.3	N/A	14/22
M1-0-S	8.3	7.5	2.7	0.7	7/8.8
ECC-0-M	15.0	8.3	6.7	0.3	14/22
ECC-0-S	17.3	9.7	7.0	0.2	7/8.8
M2-0-M	11.9	6.8	2.3	0.7	14/22
M1-15-M	7.7	5.7	1.3	N/A	N/A
M2-15-M	8.5	7.1	1.7	N/A	N/A
M2-15-S	6.6	N/A	N/A	N/A	N/A
M1-90-M	15.9	6.6	4.0	N/A	14/22
M1-90-S	8.9	7.4	4.3	0.6	9.8/8.1
M2-90-S	9.0	5.9	6.0	N/A	9.8/8.1

As a general remark, we can conclude that the there is a significant difference in the behaviour of the quasi-brittle and “ductile” specimens after first cracking. Curves of quasi-brittle mortars M1 and M2 are jagged and have a significant drop in load carrying capacity right after the first crack (and after every further crack developing). Contrary to the quasi-brittle ones, the ECC specimens after the first crack show a further load increase until the peak load. These curves are smooth due to the fibre-bridging characteristics of the ECC. However, it has to be noted that only a total number of six ECC specimens were tested, so our results are not conclusive.

First cracking strengths are slightly higher in the ECC specimens (8.3-9.7 kN) compared to the quasi-brittle specimens (5.7-7.5 kN). In case of the ECC, it was difficult to determine, even from the test data, when exactly the actual cracks form, because of the smooth transition between the un-cracked and the cracked stage. Studying the load-deformation graphs of the ECC specimens and applying tendency lines between the pre- and post-cracking stages, we approximated the first cracking loads. It revealed that the initial cracking of the ECC does in fact occur at a later stage than for the M1 and M2 specimens.

The most consistent behaviour we could observe in the M1-90-medium and M1-90-small specimens. Interestingly, in both of the ECC series, we had one specimen behaving very differently both in terms of first cracking load and stiffness (see discussion).

7.3. Comparative load-deformation plots

Specimens with similar grid size, and/or orientation have been paired and plotted in Figures. 16-19. Figure 16 shows all medium grids when placed longitudinally, in different mortars. Figure 17 compares all transversally placed grids. Figure 18 shows the small grid placed longitudinally. Finally, Figure 19 illustrates the effects of the (medium) grid orientation from 0° to 90° for one quasi-brittle mortar (M1).

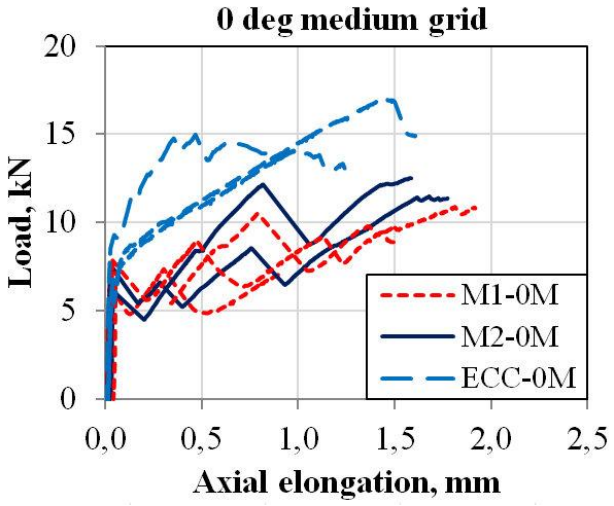

Figure 16 – Medium grid 0°

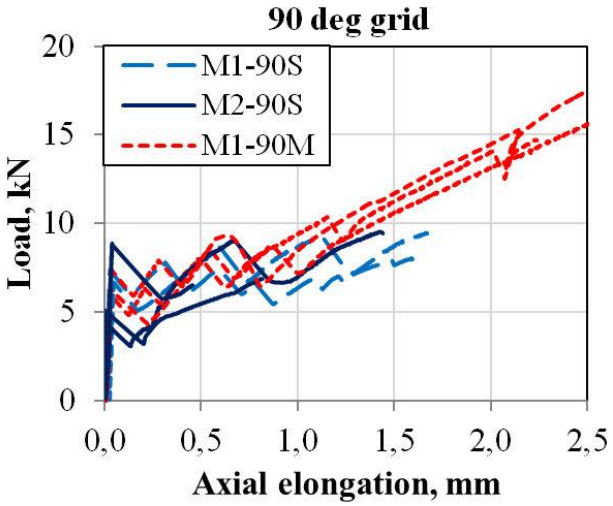

Figure 17 – All 90° grids

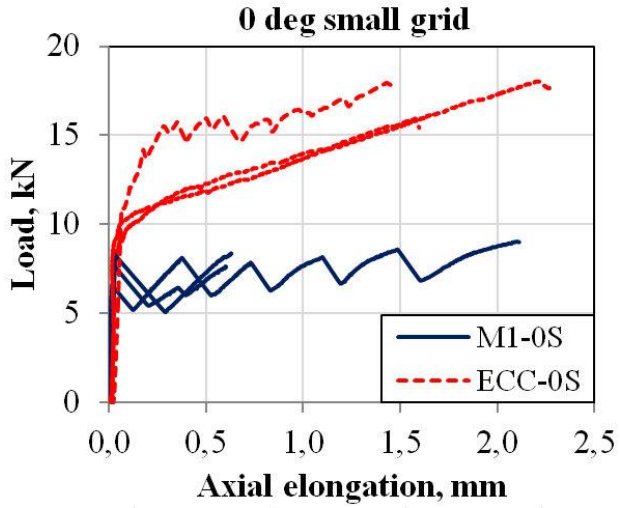

Figure 18 – Small grid 0°

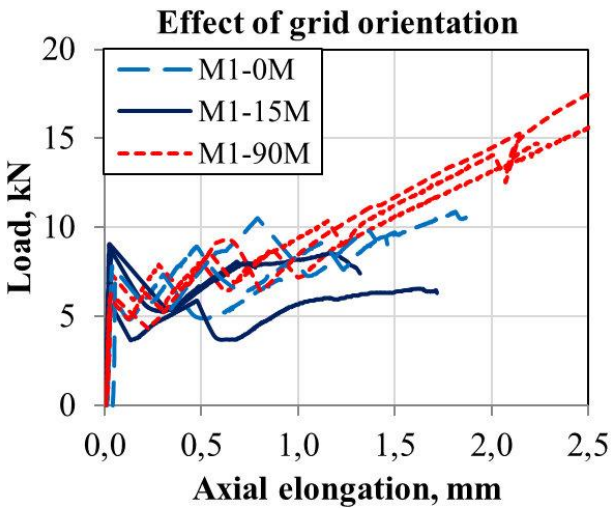

Figure 19 – Medium grid 0°-15°-90°

From Figures 16-19 along with the individual plots against the bare grid (Figures 5-9) it can be concluded that a significant and consistent tension-stiffening effect can only be shown for the ECC, while there is only a slight to moderate increase in load capacity with the quasi-brittle mortars. First cracking in ECC happens slightly later than in M1 and M2. In case of the small grid (Figure 18), after first cracking, the load capacity does not increase significantly if we use quasi-brittle mortars, while it does in the ECC-based specimens.

All 90° grids are plotted in Figure 17. The M1 mortar gave the most concise results, highest failure loads, and largest deformations, while the most brittle mortar, M2 yielded the most jagged and least concise results allowing very little deformations compared to any other combinations.

Finally, Figure 19 illustrates the changes in stiffness and load capacity with the grid orientation for the medium grid with the M1 mortar. Unexpectedly (and against the material data given in Table 1), the transversally rotated grid showed to be the strongest, while the 15° grid the weakest. In addition, the 90° medium grid combinations accommodated the largest elongations.

7.4. Crack widths, crack patterns

Figures 20-21 show two ARAMIS plots for the specimens M1-90-small and ECC-0-small. The crack widths of the ECC specimens are very small, ranging from 0.20 mm to 0.40 mm of the medium grid, and 0.08 mm to 0.50 mm for the small grid and they are not fully developed. In addition to that, the cracks are more evenly distributed in the ECC. In contrast, the crack widths determined by ARAMIS are ranging from 0.20 mm to 0.80 mm of the M1-90-small and between 0.75mm and 1 mm for the M2-0-medium. “Average crack widths”, defined as the sum of crack widths divided by the number of the cracks within the test field, are also given in Table 6, where available.

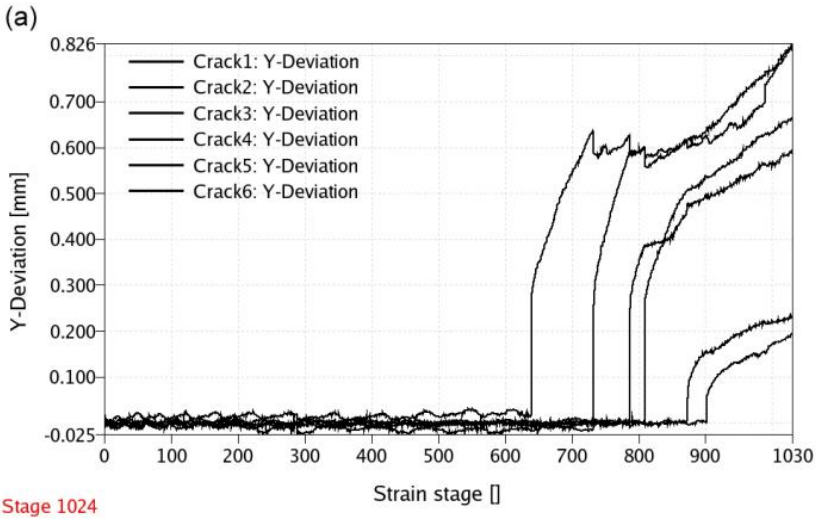

Figure 20 – Crack widths recorded by ARAMIS, M1-90-small

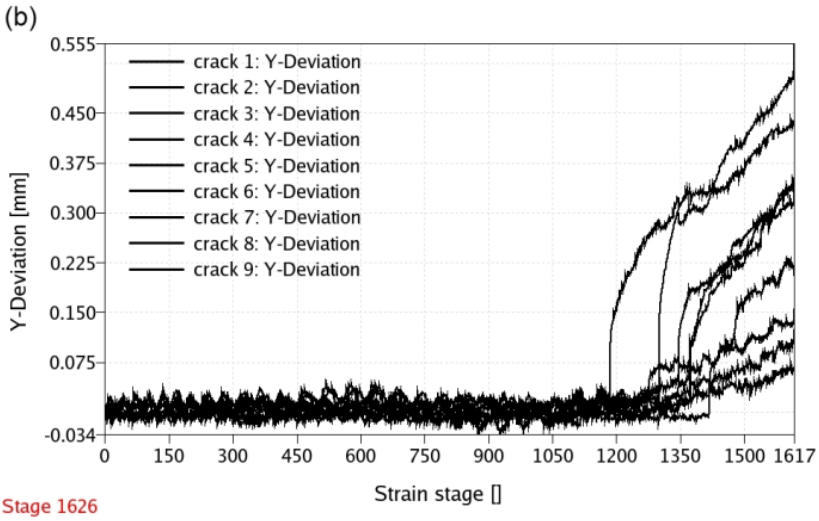

Figure 21 – Crack widths recorded by ARAMIS, ECC-0-small

7.5. ARAMIS "strain images"

The crack development was monitored by ARAMIS. The strain overlay images taken at the moment of failure confirm the characteristic ductile behaviour of the ECC as it shows more numerous, finer and more evenly distributed crack patterns compared to the quasi-brittle (M1 and M2) mortars. Where no strain images were available (Figure 22a, f, g and h), failure photos are given. The cracks in all specimens developed in line with the grid tows.

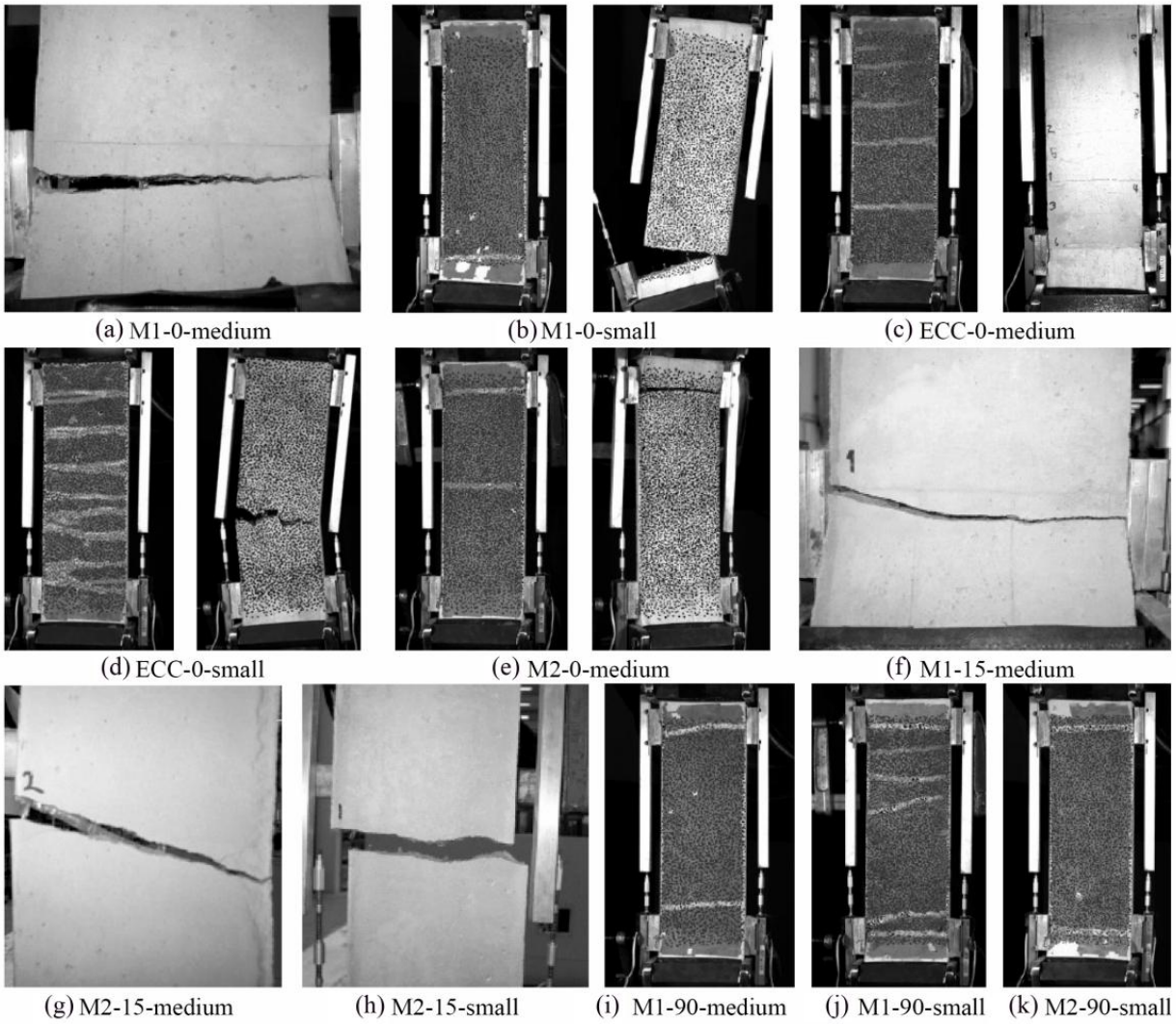

Figure 22 – Crack development as documented by ARAMIS.

8. DISCUSSION

We can compare the behaviour of the composite with the tensile properties of the bare grid. The specimens with the medium or small grid have 4 or 7 tows in the test section, respectively. The load capacity of the bare grid can be calculated based on manufacturer data. For the medium grid, it is 3.5 kN/tow in both directions, while for the small grid it is 1.4 kN/tow and 1.0 kN/tow in longitudinal and transversal direction, respectively. Test data from Blanksvärd gave much higher values [23]. Compared to these, the failure loads of the composite should be higher. Examining the failure loads, however, we can conclude that with quasi-brittle mortars we get significantly lower values (we do not even reach the nominal capacity of the grid) in all cases except for the transversally placed medium grid. The ECC specimens exceed the manufacturer-given grid failure loads, but still fall behind the tested values, suggesting premature failure of the grid.

The most concise, and homogenous test series were M1-90-medium and M1-90-small, with quasi-brittle, but fibre-reinforced mortars while the most scattered ones are the M2-series. The significant differences within the same test series (in particular, M2-15-small and M2-90-small)

are attributed to micro-cracks developing during the de-molding process, due to the very fragile geometry.

In case of the ECC, there is one specimen in both series showing a very different behaviour. One possible explanation to this could be the way we mixed the mortars. We could only mix a very small quantity in one batch because we used a dedicated mortar mixer with a limited capacity. It is possible that there were some very slight changes in the fibre content (2 vol. %) and/or water-to-cement ratios in the two separate mixes. Based on the known behaviour of the bare ECC (Figure 1), we believe that ECC-0-medium (3) and ECC-0-small (3) should be cancelled out of the results. The remaining specimens show a similar behaviour in terms of first cracking strength and stiffness.

It was observed that the medium grid performs very differently depending on its orientation. Two possible reasons for the "over-performance" of the medium grid when transversally placed are (1) that the joints can deform more without fibre breakage in that direction. The grid joints look and behave differently depending on the grid orientation; this is due to the "woven" nature of the grid. (2) Another possible explanation is the additional anchorage provided by the epoxy surplus, which for some reason is only present on the transversal fibre tows. In earlier tests by [5] however, it was shown that sanding the grid (giving increased bond) creates stress concentrations and premature rupture, therefore it cannot be stated that the additional anchorage equals to increased load capacity. Further research is needed in this regard.

The 15° orientated specimens, compared to the longitudinally placed reinforcement, do not develop as many cracks, and have a slightly reduced tensile strength. Cracks developing here tend to follow the grid tows. Finally, the behaviour of the small is less direction-dependent than that of the medium grid.

Some specimens initiated cracks near the ends of the test field. We attributed this to the fact that the dogbone geometry is prone to initiating cracks near sharp changes in cross section because of possible local stress concentrations. Using improved (curved) dogbone geometry, however, would have made the testing procedure far more time consuming and expensive. The test setup showed to be particularly sensitive to de-moulding, handling, and testing because of the very thin test field.

In addition to the possibly too low curing time before de-molding, there is an initial curvature in the grid strips because of the factory shape (roll). The grids were tensioned in the slits at both ends before casting in order to reduce the curvature. Yet in such a thin cross-section, the effect of the slightest curvature may be significant, and it might result in reduced performance. This effect has not been investigated more in detail.

9. CONCLUSIONS

The goals of the experimental program have been fulfilled in great part. A wide scale of material combinations has been tested, yet not all possible combinations. Adaptation of the dogbone geometry to testing large MBC-specimens has been successful with some limitations. Most of the specimens have been able to initiate cracks within the pre-defined test field, but an improved geometry would yield results that are more concise.

Multiple cracking and a significant tension stiffening behaviour were observed when applying a ductile, PVA-reinforced ECC as bonding agent, which, based on the two only test series, has

proven to be superior to quasi-brittle mortars. ECC has given significantly higher failure loads and prevented pronounced drops in load capacity by its increased ductility. Recorded peak values in the load-displacement curves show a more balanced behaviour for the ECC specimens. The same plots for the quasi-brittle mortars are jagged indicating a more uneven stress distribution and possible local failures in the grid joints. Typical brittle failure and corresponding crack patterns were recorded in case of the quasi-brittle M1 and M2 mortars.

10. FURTHER RESEARCH

Quasi-brittle mortars rely on high bond strength between CFRP reinforcement and the mortar, to accommodate the high internal stresses. Therefore, bond slip or local high stress concentrations may result in failure of the grid joints. Using a mortar with improved ductile deformation capabilities, where the CFRP reinforcement and the cementitious matrix deform close to identically, results in a composite material where apparently high mechanical bond stresses in local areas, as the grid intersections between the longitudinal and transversal tows are significantly reduced, thereby preventing bond slip damage to the CFRP-reinforcement.

The high fly ash content of ECC results in a refined and densified grain structure. This may improve the bond strength between the grid and the mortar, as confirmed by [11] for yarns/textiles embedded in cementitious matrices. The apparently better bond characteristics of ECC are also partly due to the compatible deformation behaviour between FRP reinforcement and ECC, which makes ECC very attractive for further investigation in combination with FRP grids.

Due to its pseudo strain hardening and fibre bridging properties, and for the additional mechanical anchorage it provides for the FRP grid, ECC will be tested further as a bonding agent for mineral-based strengthening. The different geometry (and associated rigidity, and deformation capacity) of the grid joints in the two perpendicular directions could also be further investigated, as this may have caused the significant “over-performance” of the medium grid in transversal direction.

Finite element modelling of the interaction between grid and mortar would give a better understanding of structural applications where mineral-based strengthening systems are subject to tensional/splitting forces, or axial forces combined with bending.

ACKNOWLEDGEMENTS

The research work presented in this paper was performed at the Technical University of Denmark and financed by the Norwegian Research Council through the strategic institute program RECON at Norut Narvik Ltd. The ARAMIS equipment was acquired with support from the Villum Kann Rasmussen Foundation. Sto Scandinavia should also be acknowledged for supplying most of the strengthening material.

REFERENCES

1. Carolin, A., Carbon Fibre Reinforced Polymers for Strengthening of Structural Elements, in Department of Civil and Mining Engineering2003, Luleå University of Technology: Luleå, Sweden.

2. Täljsten, B., FRP Strengthening of Existing Concrete Structures. Design Guideline, 4th Edition. 3rd Edition ed. 2006, Luleå, Sweden.
3. Triantafillou, T.C., Shear strengthening of reinforced concrete beams using epoxy-bonded FRP composites. ACI Structural Journal, 1998. 95(2): p. 107-115.
4. Ohuchi, H., et al., Seismic strengthening design technique for existing bridge columns with CFRP, in Proceedings of the Second International Workshop on Seismic Design and Retrofitting of Reinforced Concrete Bridges1994: Queenstown, Nerw Zealand. p. 495-514.
5. Blanksvärd, T., Strengthening of concrete structures by the use of mineral based composites, in Department of Civil and Environmental Engineering2007, Luleå University of Technology: Luleå, Sweden.
6. Blanksvärd, T., B. Täljsten, and A. Carolin, Shear Strengthening of Concrete Structures with the Use of Mineral-Based Composites. Journal of Composites for Construction, 2009. 13(1): p. 25-34.
7. Orosz, K., et al., From material level to structural use of mineral based composites – An overview. Advances in Civil Engineering, 2010. 2010.
8. Hegger, J., et al., Load–bearing behaviour and simulation of textile reinforced concrete. Materials and Structures, 2006. 39(8): p. 765-776.
9. Becker, D., Betongplattor förstärkta med kolfibrekomposit (in Swedish), in Division of Structural Engineering2003, Luleå University of Technology: Luleå, Sweden.
10. Blanksvärd, T. and B. Täljsten, Strengthening of concrete structures with cement based bonded composites. Journal of Nordic Concrete Research, 2008. 38: p. 133-153.
11. Soranakom, C. and B. Mobasher, Geometrical and mechanical aspects of fabric bonding and pullout in cement composites. Materials and Structures, 2008. 42(6): p. 765-777.
12. Naaman, A.E. and H.W. Reinhardt, Characterization of high performance fiber reinforced cement composites-HPFRCC, in Proceedings of High Performance Fiber Reinforced Cement Composites 2 [HPFRCC 2]1995. p. 1-23.
13. Li, V.C. and G. Fischer. Reinforced ECC - An Evolution from Materials to Structures. in Proceedings of the 1st FIB Congress. 2002. Osaka, Japan.
14. Kim, Y.Y., B.Y. Lee, and J.K. Kim, Evaluation of fiber dispersion of PVA-ECC, 2008, ICCES. p. 167-172.
15. Stang, H. and V.C. Li, Classification of fibre reinforced cementitious materials for structural applications, in 6th RILEM Symposium on Fibre-Reinforced Concretes (FRC) - BEFIB 20042004: Varenna, Italy. p. 197-218.
16. Fischer, G. and V.C. Li, Influence of matrix ductility on tension-stiffening behavior of steel reinforced engineered cementitious composites (ECC). ACI Structural Journal, 2002. 99(1): p. 104-111.
17. Brameshuber, W., Textile Reinforced Concrete: State-of-the-art report of RILEM technical committee 201-TC, 2006, RILEM Publications.
18. Hinzen, M. and W. Brameshuber, Improvement of Serviceability and Strength of Textile Reinforced Concrete by using Short Fibres, in 4th Colloquium on Textile Reinforced Structures (CTRS4)2009: Dresden, Germany. p. 261-272.
19. Hegger, J. and S. Voss, Textile reinforced concrete under biaxial loading, in 6th Rilem Symposium on Fibre Reinforced Concrete (FRC), BEFIB 20042004: Varenna, Italy. p. 1463-1472.
20. ACI 224.2R-92, 1992, American Concrete Institute.
21. Hegger, J., et al., Decentralized Wastewater Treatment Plants Made of Textile Reinforced Concrete, in 12th International Techtextil Symposium for Technical Textiles, Nonwovens and Textile Reinforced Materials 2003: Frankfurt, Germany. p. CD-ROM nr. 4.28, 38pp.

22. Kanakubo, T., Tensile Characteristics Evaluation Method for Ductile Fibre-Reinforced Cementitious Composites. Journal of Advanced Concrete Technology, 2006. 4(1): p. 3-17.
23. Blanksvärd, T., Mechanical properties of different geometries of CFRP grid: tensile evaluation of material properties, 2006, Luleå University of Technology: Luleå, Sweden.

Research Council and Editorial Board for Nordic Concrete Research

Prof. Dr. Olafur H. Wallevik, Chairman for the Research Council
Dr. Dirch H. Bager, Editor of Nordic Concrete Research

18 November 2013

Active reviewers for Nordic Concrete Research as per December 2013

DENMARK	
Dr.	Dirch H. Bager
Dr.	Mette Glavind
Prof., Dr.	Per Goltermann
Mr.	Oscar Klinghoffer
Prof., Dr.	John Forbes Olesen
Mr	Claus Pade
Prof., Dr.	Eigil V. Sørensen
Prof., Dr.	Jens Peder Ulfkjær
FINLAND	
Dr.	Klaus Juvas
Dr.	Matti V. Leskala
Prof., Dr.	Jussi Mattila
Dr.	Jouni Punkki
Mr	Juha Valjus
ICELAND	
Mr.	Einar Einarsson
Mr.	Haukur J. Eiriksson
Dr.	Gisli Gudmundsson
Mr.	Karsten Iversen
Mr.	Torfi G. Sigurdsson
Mr.	Sveinbjörn Sveinbjörnsson
Dr.	Jon E. Wallevik
Prof., Dr.	Òlafur H. Wallevik
Prof., Dr.	Børge J. Wigum
NORWAY	
Dr.	Helge Brå
Ms.	Danielle Bosnjak
Mr.	Anton Gjørven
Mr.	Steinar Helland
Dr.	Bernt Jacobsen
Prof., Dr.	Terje Kanstad
Dr.	Terje F. Rønning
Mr.	Tor Kristian Sandaker
Mr.	Sverre Smeplass
Mr.	Hans Stemland
SWEDEN	
Prof., Dr.	Anders Ansell
Dr.	Thomas Blanksvärd
Prof.	Lennart Elfgren
Prof., Dr.	Mats Emborg
Prof., Dr.	Kent Gylltoft
Prof., Dr.	Mikael Hallgren
Prof., Dr.	Jan-Erik Jonasson
Prof., Dr.	Björn Lagerblad
Prof., Dr.	Karin Lundgren
Prof., Dr.	Tang Luping
Prof., Dr.	Per-Erik Petersson
Prof., Dr.	Johan Silfwerbrand
Dr.	Peter Utgenannt